FOG

Freiberg Online Geology

FOG is an electronic journal registered under **ISSN 1434-7512**

2012, VOL 32

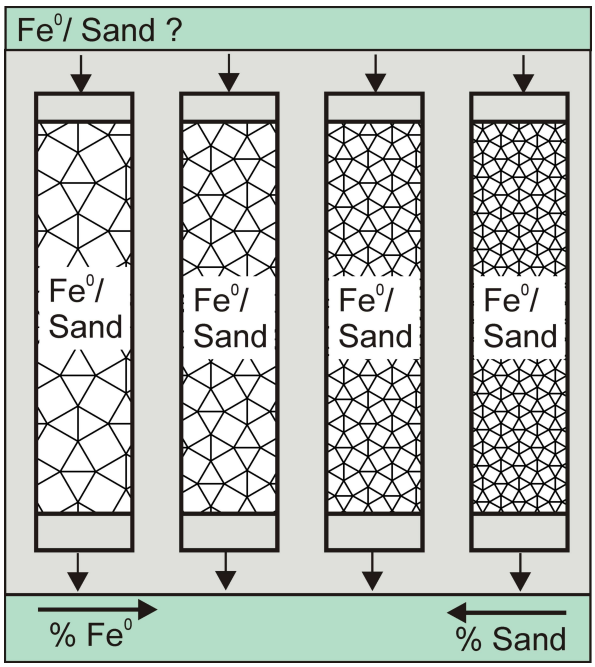

Kumiko Miyajima

Optimizing the Design of Metallic Iron Filters for WaterTreatment

60 pages, 22 figures, 13 tables, 124 references

Acknowledgments

I would like to express my appreciation to my supervisors Prof. Dr. Thomas Ptak for his support, and Dr. Chicgoua Noubactep for his countless advice and kind support. Their guidance was invaluable for the completion of my thesis. Further, I would like to thank Dr. Mohammad Azizur Rahman for his advice. I would also like to thank Stefan Glatz for proofreading the manuscript and many helpful discussions, ongoing encouragement and last but not least buying food and dinner preparation. Special thanks to my family, Stefan's family and all of my friends for their support and warm encouragement when I let it get me down. Gerhard Max Hundertmark from the Geosciences Center (University of Göttingen) is acknowledged for technical support.

Abstract

Elemental iron (Fe^0), is a versatile reactive agent for various water treatment. Due to the inexpensiveness while wide-ranging removal capabilities, the technology of Fe^0-based filtration is used in permeable reactive barriers and in safe drinking water provision.

Because of the expansive iron corrosion, mixing Fe^0 with an non expansive material (e.g. activated carbon, sand, etc) is a prerequisite for long term efficiency. The design of Fe^0 filtration was theoretically addressed recently to contain less than 52 vol % Fe^0.

This work is the first attempt to experimentally validate the concept, the impact of various Fe^0/sand mixtures on the contaminant removal efficiency, using Methylene Blue (MB) as a model contaminant. For the sake of that, batch experiments in Fe^0/sand and Fe^0/sand/MnO_2 systems and column experiments using various volumetric Fe^0/sand ratios were performed.

Results from batch studies indicate that sand impairs MB discoloration by Fe^0. Three mechanisms are considered: (i) limiting the accessibility to the vicinity of Fe^0, (ii) delaying the availability of 'free' corrosion products for MB co-precipitation, and (iii) forming iron oxide coated sand which becomes a poorer MB adsorbent.
In the column tests, a disturbance of MB adsorption on sand by iron oxides coating was observed (early MB breakthrough). Results indicated that the most efficient filter must contain about 30% Fe^0 (v/v). However mechanically pumping caused an increment of transport of colloidal corrosion products and pore flux due to porosity reduction in the columns, therefore it is necessary to confirm the optimal Fe^0/sand ratio under variable flow conditions.

Keywords: Elemental iron, Iron-amended sand filtration, Methylene Blue, Iron corrosion, Water treatment, Fe^0/MnO_2,

Table of Contents

List of Tables

List of Figures:

Fig.16: Photograph of the ten test columns after 90 days of running.

Fig.17: (a) Extent of $[MB]/[MB]_0$ (%), (b) amount of discolored MB (mg) over time, (c) the evolution of flow velocity (mL/h).

Fig18: (a) Cumulative mass of adsorbed MB before and after BT, (b) Total MB removal rate (Σdiscolored MB/ Σinlet MB) for each layer.

Fig.19: Concentration of dissolved iron in the effluent of columns of Fe^0 loadings 10-100%.

Fig.20: Diameter expansion (a) and fraction of volume expansion (b) over time calculated for different corrosion densities.

Fig.21: Porosity evolution over time of Fe^0 loadings 10-100%.

Fig.22: Evolution of pore flow velocities (expressed as flux) and the extent of the unfiltered MB outflow [MB]/[MB]0 at several time steps (27th-76th day).

1. Introduction

1.1 Motivation and background

"The world has met the Millennium Development Goal (MDG) target of reducing the number of halving the proportion of people without sustainable access to safe drinking water. Between 1990 and 2010, over two billion people gained access to improved drinking water sources, however according to 'Progress on drinking water and sanitation 2012', at least 11% of the world's population of 783 million people are still without access to safe drinking water." (WHO/UNICEF 2012). The report of the previous citation was borrowed from elaborates on the huge regional disparities in development, for example, when comparing Europe to China or India, where 2 billion people gained access to drinking water as late as 1990, in sub-Saharan Africa, more than 40% of the total population still lacks access to drinking water. The report further mentions the huge differences of modernization between urban and rural areas. In Sierra Leone, for example, the wealthy elites of the urban population have almost universal access to decent water supply in contrast to only 10% of the poorest population in rural areas (WHO/UNICEF 2012).

In this scope, Elemental iron (Fe^0) amended Bio-Sand-Filtration (BSF) has proven its efficiency for the removal of a wide range of contaminants including organic and inorganic substances, microorganisms and viruses in the application of safe drinking water provision (Noubactep, 2013). Furthermore it is very advantageous because of its simple operation, low maintenance, locally available labor and materials, no power requirements and low cost (Hussam et al., 2007; Hussam, 2009). Due to the robustness of this universal filtration system, its use should be fostered further, to increase the overall accessibility to safe drinking water in rural and outback areas of developing countries. It has been shown that for the method to work reliable the pH value of the water should be at least 4.5 or higher, which is usually the case for natural resource water (Noubactep et al., 2012aa).

1.2 Current stand in designing Fe^0 filtration systems

In numerous studies Metallic iron (Fe^0) has also been demonstrated to be the best available material for subsurface permeable reactive barriers (Bartzas and Komnistas, 2010; Comba et al., 2011; Gheju, 2011; Crane and Noubactep 2012; Togue-Kamga et al., 2012a). However porosity reduction due to expansive iron corrosion and subsequent filter clogging is one of the major problems in this application. In order to improve the filter durability and to prevent premature filter clogging, i.e. clogging occurs before all iron is used up, non-pure reactive zones with iron loadings less than 100% but typically over 50% are used by mixing Fe^0 with some inert substance (Noubactep, 2012b; Noubactep and Caré, 2011). For its cost-effectiveness and high availability, sand is a commonly used additive for this purpose. Increasing the filter efficiency by reducing the amount of comparatively expensive iron and substituting it by low-cost additives like sand renders the Fe^0/sand filtration-systems particularly interesting, as cost-efficiency is the key to further dissemination of Fe^0 amended BSF technology at household level in remote areas. Despite Fe^0 has been studied for several decades, there is still a lot of contradiction between the theoretically suggested working mechanisms and efficiencies and the experimental results. Also the literature contains little basic information on Fe^0/sand mixtures (Devlin and Patchen, 2004; Bi et al., 2009; Ruhl et al., 2012b; Biliardi et al., 2013), and conclusive experimental evidence for Fe^0/sand mixtures being better or worse than a pure Fe^0 systems is yet to be obtained (Ulsamer, 2011). However recent theoretical studies from Noubactep (Noubactep, 2010a; Noubactep et al., 2012a; Caré et al., 2013) indicate that Fe^0/sand mixtures perform better than pure Fe^0-systems while they studied the relationship between the Fe^0/sand ratio, filter efficiency and filter lifetime. According to the authors, filter clogging occurs at volume percentages (vol%) of Fe^0>51% due to uniform porosity decrease for all Fe^0-containing systems, thus constraining Fe^0 volume fractions in the reactive to less than 50 %(Togue-Kamga et al., 2012b).

1.3 Objectives of the thesis

The aim of the present study is to characterize the impact of sand admixture on the discoloration performance of Fe^0 for Methylene Blue (MB) in batch and column experiments. Particular attention was directed at: (i) characterizing the impact of particle cementation in batch experiments, (§ 5.2.1) (ii)

characterizing the evolution of the permeability and the extent MB discoloration of individual systems as a function of the Fe^0/sand ratio in column experiments (§ 5.2.2). Preliminary works were directed at characterizing the intrinsic reactivity of the used material and comparing it to those of seven other commercial materials (§ 5.1). The results were discussed and conclusions driven in terms of the optimal volumetric proportion of Fe^0/sand ratio for a sustainable Fe^0/sand filtration system.

1.4 Outline of the thesis

The large number of potential natural and anthropogenic water contaminants make a conclusive evaluation of the applicability of Fe^0 filtration systems for all classes of compounds virtually impossible for a master thesis. However, previous research in the research group of Dr. Noubactep has demonstrated that contaminant removal in Fe^0/H_2O systems is primary a characteristic of aqueous iron corrosion yielding non-specific enmeshment of trace contaminants (micropollutants). The presented work is a consequent continuation of ongoing research activities for a science-based design of Fe^0 filters. This efforts started with the development of tools to characterize the intrinsic reactivity of Fe^0 materials: Ethylenediaminetetraacetic acid (EDTA) test, MB test (Noubactep et al., 2005). The next step was to elucidate the mechanism of contaminant removal in Fe^0/H_2O systems (Noubactep, 2007; 2008a; Scott et al., 2011). The resulted concept was validated by extensively characterizing the extent of methylene blue (MB) discoloration. MB has low adsorptive affinity for iron corrosion products, can not be significantly discoloured by any redox process but is quantitatively removed by co-precipitation with in situ generated iron corrosion products. The present thesis was intended at a better characterization of the Fe^0/H_2O system as influenced by the presence and the amount of sand in batch and column experiments. A more detailed outline is presented in the following.

Chapter 2 describes theoretical mechanisms of iron corrosion and of contaminant removal in Fe^0/H_2O systems. Mathematical model for column design and expansive iron corrosion are presented in this chapter. Chapter 3 presents the used materials and methods. In Chapter 4 the procedure of performed experiments are explained and their results are presented in Chapter 5. Chapter 6 summarizes the conclusions regarding the focus of the thesis and provides suggestions for following research. In the Appendix the actual measured values in all tests are given.

2. Theoretical Background

The effectiveness of Fe^0 for contaminant removal can be assessed using the method of Methylene Blue (MB) discoloration as an indicator, i.e. monitoring the change in concentration of dissolved MB in water passing through a filter system using Fe^0 as the reactive material. Three mechanisms for MB removal by Fe^0 have been identified in batch systems: adsorption, co-precipitation and adsorptive size-exclusion (Noubactep, 2008a; 2008b). The importance of the kinetics of mass transfer for the evidence of co-precipitation has been delineated (Kurth, 2008; Noubactep et al., 2009a). It can be anticipated that in column experiments the importance of co-precipitation will depends on the intrinsic reactivity of Fe^0 and the water velocity. This chapter summarizes the main features for the rationalization of MB discoloration by aqueous iron corrosion under tested experimental conditions.

2.1 Mass transport

Two mass transport mechanisms need to be considered in this study: Diffusion due to concentration gradients and advection due to fluid flow (Honrath, 1995). In a stationary fluid (non-disturbed batch experiments), diffusion is the only mechanism for contaminant transport from the bulk solution to the surface of the tested material. In order to reach thermodynamic equilibrium, spatial concentration differences of the contaminant cause a flux from regions higher in concentration to those with lower concentration (molecular diffusion) (Kurth, 2008). As the tested material reduces the contaminant concentration in its vicinity, a concentration gradient is established, that subsequently drives the contaminant towards the wall and does not vanish unless either the contaminant itself is eradicated or the tested material becomes saturated or non reactive.
Under shaken or flow condition advection becomes the predominant mass transport mechanism, where the flow intensifies migration of contaminant molecules toward removal materials (e.g. sand, Fe^0, MnO_2) much faster than only by diffusion.

2.2 Aqueous Iron Corrosion

Corrosion can be defined as "the destructive attack of a metal by chemical reaction with its surroundings. Corrosion is an oxidation reaction characterized by a donation of electrons. Aqueous iron corrosion is in essence an electrochemical process (Faraday, 1961). Fe^0 oxidation releases electron in an anodic area. The released electrons migrate through a metallic path and are consumed by a different chemical reaction in a cathodic area. In the present study, relevant cathodic reactions (coupled to Fe^0 oxidation) included water reduction (H_2 evolution), and oxygen (O_2) reduction.

2.2.1 Aqueous Iron Corrosion Process

A reactive Fe^0 material starts to corrode immediately after immersion into aqueous solutions. Starting from the fluid/metal interface, the iron gets consumed by corrosion, where the corrosion products form an oxide film covering the underlying Fe^0 surface. The fact that the Fe^0 surface is permanently covered with an oxide film does not depend on size or composition of the Fe^0 material. Due to its porous nature, the film remains permeable to the oxidizing agents, namely dissolved oxigen (DO) and water (Noubactep, 2010b). The oxide film does only slow down the kinetics of iron corrosion. It has been reported, that immersed Fe^0 may reach a pseudo-equilibrium stage at which further corrosion proceeds at a constant rate of around 25.4 µm/year (DOE, 1993).
It has been shown that the dynamic processes of iron corrosion and formation of oxide films play a major role in contaminant removal from aqueous solutions (Stratmann and Müller, 1994; Ghauch et al., 2010; Nesic, 2007; Noubactep, 2009a; 2010b; 2010c). As the oxide film develops, it becomes a sponge-like structure which is thought to non-selectively entrap the contaminant species. The captured contaminant may be further transformed chemically by oxidation or reduction. The process of iron corrosion is strongly influenced (inhibited or sustained) by temperature, flow velocity and solution characteristics (pH, Eh, alkalinity, DO, contaminant, microbiological activity, etc.) (Sarin, et al., 2004a). Thus it is reasonable to assume that composition and structure of the iron oxide films has unique features strongly depending on the details of the setup. However similarities exist with respect to the common corrosion products: Goethite (α-FeOOH), Lepidocrocite (γ-FeOOH), Magnetite (Fe_3O_4), Maghemite (α-Fe_2O_3), Ferrous Oxide (FeO), Siderite ($FeCO_3$), Ferrous Hydroxide ($Fe(OH)_2$), Ferric Hydroxide ($Fe(OH)_3$) and green rusts are frequently

found in various oxide film samples from different experimental sites (Benjamin et al., 1996). The corrosion process occurs due to different electrical potentials at anodic and cathodic sites on the Fe surface. In the remainder of this section we shall explain the chemical process in greater detail.
An oxidation reaction at the anodic site occurs following.

$$Fe^0 \Leftrightarrow Fe^{2+} + 2e^- \quad (1)$$

One of a the most common reductive reactions at the cathodic site are oxygen reduction as well as hydrogen reduction:

$$O_2 + 4e^- + 2H_2O \Leftrightarrow 4OH^- \quad (2)$$

$$2H^+ + 2e^- \Leftrightarrow H_2 \quad (3)$$

In aqueous solution electron acceptors such as oxygen and hydrogen ions (eqs. 2 and 3) serve to complete the reaction.

Another reductive reaction at the cathodic site is due to aqueous chlorine which is a disinfectant in drinking water and acts as an electron acceptor:

$$HOCl + H^+ + 2e^- \Leftrightarrow Cl^- + H_2O \quad (4)$$

$$NH_2Cl + 2H^+ + 2e^- \Leftrightarrow Cl^- + NH_4^+ \quad (5)$$

Generated ferrous iron (Fe^{2+}) may either dissolve in the solution, or deposit as an oxide film. Dissolved Fe^{2+} is further oxidized to ferric iron (Fe^{3+}) in contact with oxidants, which then again acts as an oxidant for Fe^0:

$$Fe^{2+} \Leftrightarrow Fe^{3+} + e^- \quad (6)$$

$$Fe^0 + 2Fe^{3+} \Leftrightarrow 3Fe^{2+} \quad (7)$$

The generated iron ions Fe^{2+} and Fe^{3+} react with water to form hydroxides, which become dehydrated and transform into either amorphous or crystalline oxides as following:

$$Fe^{2+} + 2H_2O \Leftrightarrow Fe(OH)_2 + 2H^+ \quad (8)$$

$$Fe^{3+} + 3H_2O \Leftrightarrow Fe(OH)_3 + 3H^+ \quad (9)$$

$$Fe(OH)_2 \Leftrightarrow FeO + H_2O \quad (10)$$

$$Fe(OH)_3 \Leftrightarrow FeO(OH) + H_2O \quad (11)$$

$$2FeO(OH) \Leftrightarrow Fe_2O_3 + H_2O \quad (12)$$

$$3Fe_2O_3 + H_2 \Leftrightarrow 2Fe_3O_4 + H_2O \quad (13)$$

The whole iron corrosion cycle can be described as follows (Noubactep, 2010b):

$$Fe^0 \Rightarrow Fe^{2+}/Fe^{3+}(H_2O)_6 \Rightarrow Fe^{2+}/Fe^{3+}(OH)_n \Rightarrow FeOOH \Rightarrow Fe_2O_3 \Rightarrow Fe_3O_4 \quad (14)$$

In the case of only insoluble species, the corresponding cycle reads (Noubactep, 2010b):

$$Fe^0 \Rightarrow Fe(OH)_2/Fe(OH)_3 \Rightarrow FeOOH \Rightarrow Fe_2O_3 \Rightarrow Fe_3O_4 \quad (15)$$

This transformation leads to the material surface area and density to change, which results in volumetric expansion/compression given by the fraction V_{oxide}/V_{Fe} (Table 1). The volume expansion is considered the main reason for filter clogging and consequently loss of hydraulic conductivity (permeability loss) in Fe^0/H_2O system.

Table 1: Characteristics of iron oxides.(a) Cornell and Schwertmann (2003); n.a.=not available

Solid phase	Name	SSA [m^2/g]	Density [g/cm^3]	Molar vol. [cm^3/mol]	Color [(a)] [-]	V_{oxide}/V_{Fe} [-]	Reference
Fe^0	ZVI	1	7.3	7.6	-	-	Henderson 2011
$Fe(OH)_2$	-	n.a.	3.4	26.4	-	3.75	Noubactep 2009b
$Fe(OH)_3$	-	n.a.	n.a.	n.a.	-	4.2	Noubactep 2009b
$Fe(OH)_3 \cdot H2O$	-	n.a.	n.a.	n.a.	-	6.4	Noubactep 2009b
γ-FeOOH	Lepidocrocite	59	3	29.6	orange	3.03	Hanna 2007b
α-FeOOH	Goethite	50	4.3	20.3	red-brown	2.91	Hanna 2007b
$1/2Fe_2O_3$	Hematite	11	5.5	29.1	red	2.12	Henderson 2011
$1/3Fe_3O_4$	Magnetite	2	5.2	45	black	2.08	Henderson 2011

Considering the process of the iron evolution, it is reasonable to assume that the resulting oxide film is a multi-layer structure. Centering around a Fe^0 core, the film continues to grow outward (into the direction of the free surface) while its chemical properties change and as time advances, the outer layer of the oxyhydroxides may be dehydrated, forming a less porous shell. Therefore the density as well as the porosity increases from the outer layer towards the center (Noubactep, 2008a; 2008b).
Sarin et al. (2004a; 2004b) identified four characteristic layers of oxide films: (1) a corroded floor, (2) a porous core where both fluid and solid exist, (3) a relatively dense shell-like layer that covers the porous core, and (4) a surface layer, present on the top of the shell-like layer at the film-water interface (Sarin et al., 2004a). A schematic of the film structure is presented in Fig. 1, which was proposed by Koelle and Rosch (1980) and Sontheimer et al. (1981). The corroded floor is the iron surface covered by the oxide film and the source of the iron corrosion products. Above it, in the porous core α-FeOOH, Fe_3O_4, α-Fe_2O_3 and $FeCO_3$ are often found among high concentrations of Fe(II) either as dissolved iron or in solid state (Sarin et al., 2004b). Green rusts, ferrihydrites and ferric hydroxides exist in the upper part of the porous core. Inside the structure cavities and voids form out naturally. The shell-like structure around the porous core is denser than the core and the top surface layer and separates the bulk solution from the readily oxidizable Fe(II) ions and solids present inside the porous core. The layer consists mainly of α-FeOOH and Fe_3O_4. The top surface layer is in contact with solution (water) and greatly influenced by the solution quality (i.e. the oxidation rate, pH-value, ferrous ion concentration and concentration of other soluble species) (Sarin et al., 2004a).

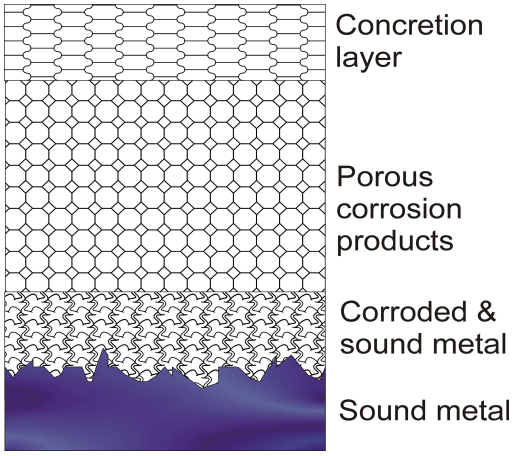

Fig. 1: Schematic diagram showing the micro-environment in the vicinity of immersed metallic iron (Modified after MacLeod, 1989). The layer of porous corrosion products is primarily the domain of hydroxide precipitation and contaminant co-precipitation. The density of secondary reductants (Fe^{II}, H/H_2) in this layer is significant such that reductive species crossing the concretion layer, will be chemically reduced. Electrochemical reduction (electrons from the metal body) is only favourable in the 'corroded & sound metal' layer. This layer is only accessible to species which can cross the porous corrosion products layer (Noubactep, 2007; 2008a).

In aqueous solutions, the solution migrates through the oxide film layers towards the Fe^0 surface. Under flow conditions (e.g. common groundwater situation), near the outer layer of the oxide film, the advection is the major transport process, however near the Fe^0 surface in the porous core, large scale flow is restricted by the tubercle structure (Sarin et al., 2004a), consequently no turbulence occurs in the vicinity of the Fe^0 surface (Noubactep, 2009a). Contaminant migration across the oxide film is governed by molecular diffusion and electromigration. It depends on the pore structure and tortuosity, e.g. the film permeability (van der Kamp et al., 1996; Nordsveen et al., 2003). Due to the electrochemical processes described in eq. 1 to 5, certain dissolved species such like Fe^{2+} are produced in the vicinity of the Fe^0 surface while others are depleted (e.g. contaminant, O_2, H^+). This causes concentration gradients of these species across the oxide film and leads to molecular diffusion of these species, including contaminant molecules, toward or away from the Fe^0 surface (molecular diffusion) (Noubactep, 2008b; Gunawardana et al., 2011). Any diffusion will tend to separate the charges, however the separation will be resisted by short- range but strong attraction forces between opposing charges. This small separation leads movement of electrons (electromigration) (Nordsveen et al., 2003). In other words, the oxide film mediates electron transfer from Fe^0 to the bulk solution and to the contaminant, acting like as an electron conductor (Fig. 2) (Scherer et al., 2000; Huang et al., 2007).

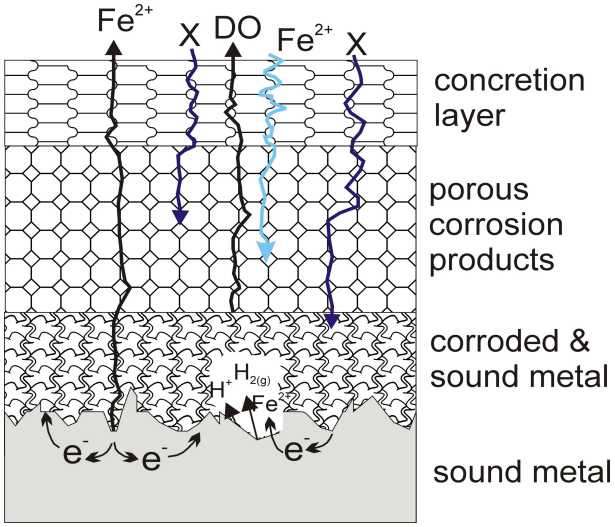

Fig 2: Schematic diagram showing the migration of (i) contaminants (X), (ii) dissolved oxygen (DO), (iii) electron (e-), (iv) ferrous iron (Fe^{2+}) and (v) hydrogen in the vicinity of immersed metallic iron (modified after Sarin et al., 2004b). It is important to keep in mind that the migration of DO and X depends on their relative size and the porosity and toutuosity of the individal layers.

2.2.2 Effects of Water Quality

Dissolved Oxygen

Increasing the concentration of dissolved oxygen (DO) in water decreases iron release and promotes precipitation by: (1) oxidizing the readily soluble Fe(II) to less soluble Fe(III) species, (2) making the film denser and less permeable for Fe(II) diffusion by precipitation of Fe(III) species within the oxide films (Sarin et al., 2004b). High flow rates cause more DO to be transported from the bulk solution to the the oxide film and consequently decrease the iron release.

Alkalinity

Alkalinity causes precipitation of iron-carbonates (e.g. $FeCO_3$) leading to a decreased iron release (Sarin et al., 2004a).

pH-Value

As mentioned earlier, the characteristics of iron corrosion depend strongly on the pH-value of the surrounding solution. At pH<4 (acid), iron corrosion rate becomes extremely high (see Fig. 3) while the iron is dissolved without forming out an oxide layer. At natural pH-values about 4.5 and up to 10 corrosion dynamics as described in chapter 2.2.1 are observed and ferric (hydr)oxides, which are less likely to dissolve

than ferrous solids precipitate at the iron surface, hindering ion transport and slow down the corrosion rate. The abrupt change in linearity of this behavior for pH-values higher than 10 is believed to be related to changes in the reaction kinetics of the oxide layer eventually leading to the formation of Fe_2O_3 which is hardly dissolved (DOE, 1993).

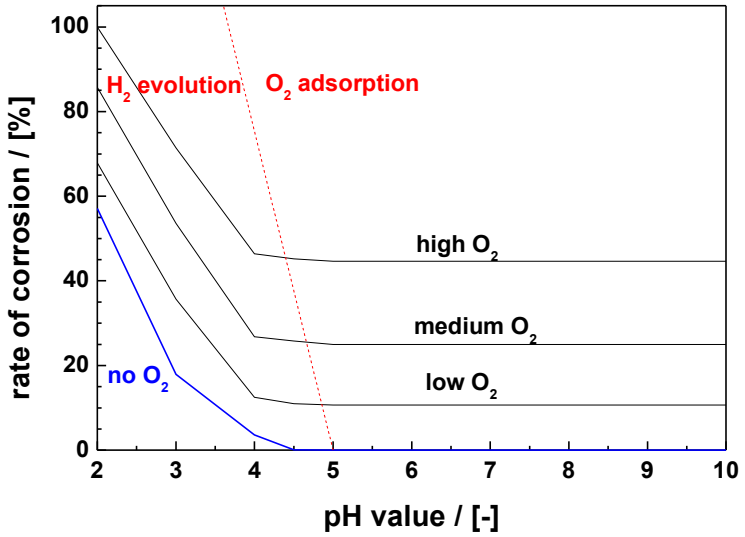

Fig.3: The relationship between iron corrosion rate, pH value and dissolved oxygen availability (adapted from Wilson 1923). It is clearly seen that at pH < 5.0, H_2 evolution may be quantitative. For the pH range of natural waters (6.0 to 9.0), the rate of iron corrosion depends on the availability of oxidizing agents (here O_2).

2.3 Contaminant Removal Mechanisms in Fe^0/H_2O Systems

It has been shown in many studies, that a wide range of contaminant species - ionic, neutral, organic, inorganic and microorganisms - can be successfully removed from aqueous solutions in Fe^0/H_2O systems (Noubactep, 2010c; 2010d; Noubactep and Schöner, 2009). It is therefore reasonable to conclude that the mechanism which leads to the removal of contaminants does not very much depend on specific properties of the contaminant itself but rather is a characteristic feature of the iron corrosion process. As has been explained in the previous chapter, the evolution of iron corrosion is accompanied by a cycle of volume expansion/contraction due to the various volume fractions in the corrosion states (see Noubactep, 2010d). The primary state of Fe^0 with specific surface areas (SSA) smaller than $1 m^2/g$ is rapidly converted into iron hydroxides, with much greater SSA ($>500 m^2/g$) before it turns into amorphous oxides which again features a comparably small SSA of about $10 m^2/g$. In the course of this process, contaminants are entrapped by voluminous colloids of iron (hydr)oxides and undergo chemical conversion. The iron corrosion expansion will stop when all pore space is completely used up (Noubactep, 2010b).
Contaminant removal by means of iron corrosion in the Fe^0/H_2O system can be described with the following three mechanisms in mind (Noubactep, 2007):

1) Adsorption: Accumulation of the contaminant molecules on Fe oxides/hydroxides (corrosion products)
2) Co-precipitation: Entrapment in the matrix of precipitating or recrystallizing Fe oxides/hydroxides on the Fe^0 surface (Gunawardana et al., 2011)
3) Adsorptive size-exclusion: In Fe^0 beds, contaminants are physically retained because generated iron corrosion products reduce the porosity.

Possible reaction pathways of the contaminant removal in the aqueous phase of the Fe^0/H_2O system are given in Table 2.

Table2: Reaction pathways for contaminant removal in the Fe^0/H_2O system. (cited from Noubactep, 2009a)

Mechanism	Reaction	Eq.
Precipitation	$Ox_{(aq)} + nOH^- \leftrightarrow Ox(HO)_{n(s)}$	(16)
Adsorption	$S_{(sorption\ site)} + Ox \leftrightarrow S\text{-}Ox$	(17)
Co-precipitation	$Ox + nFe_x(OH)_y^{(3x-y)} \leftrightarrow Ox\text{-}[Fe_x(OH)_y^{(3x-y)}]_n$	(18)

There is no clear distinction between adsorption, co-precipitation and precipitation, because they are related to each other. When Fe^0 is immersed into solutions with pH>4.5, it immediately oxidizes to Fe^{2+}, some of which is released into the bulk solution while the remainder is further oxidized and precipitated as Fe(III). In case the Fe(III) precipitation occurs in the presence of contaminants, co-precipitation may also occur as follows: The contaminant may be adsorbed either on nascent iron oxyhydroxides inside the oxide film, where it is entrapped in the growing matrix of the corrosion products or on aged corrosion products on its surface, which has a high adsorption ability.
It has been argued that the main difference between adsorption and co-precipitation lies in the geometry of the adsorbents' surface; co-precipitation should be considered a three-dimensional process leading to a greater effective removal capacity than plain adsorption (Crawford et al., 1993). Adsorbed or co-precipitated contaminants are reduced further by Fe^0 itself (direct reduction) or by Fe(II) (indirect reduction) (Table 2), while the direct contaminant reduction is not always the most favorable reduction pathway (Noubactep, 2010b; Noubactep et al., 2010). In the past reduction was widely accepted to be the most significant reaction in the contaminant removal mechanism, however recently several researchers advocate that adsorption and co-precipitation are the fundamental processes for contaminant removal. According to Noubactep, a huge amount of experimental evidence show that not for all classes of contaminants in Fe^0/H_2O systems the removal can be observed, which would be necessary to explain the mechanism by mere chemical reduction. On the other hand, assuming contaminants are fundamentally adsorbed and co-precipitated by dynamic iron corrosion processes seems to give a satisfactory explanation to the observed evidence (Noubactep, 2011a). Therefore Co-precipitation and adsorption are assumed to be the underlying processes of the contaminant removal mechanism in Fe^0/H_2O systems.

2.3.1 Adsorption

Adsorption is the process in which one chemical species, the adsorbate, in form of insoluble rigid particles is preferably accumulated (adsorbed) at the liquid-solid interface. The process can occur at an interface between any two phases such as liquid-liquid, gas-liquid, gas-solid, or liquid-solid interfaces. The interface of interest in water and waste water treatment is the liquid-solid interface (Vasireddy, 2005).
The adsorption behavior of contaminants is affected by their affinity for the available surface, solution pH value, physical and chemical characteristics (pKa, pKs) of the adsorbent (surface) and adsorbate (contaminant) and the point of zero charge (pH_{pzc}) of solid surfaces (Nesic, 2007; Ghosemi and Asadpour, 2007). Contaminants are adsorbed by either chemical or physical adsorption, where the former is a reaction between adsorbent and adsorbate (Ghosemi and Asadpour, 2007), while the latter is an attraction due to electrostatic forces and the comparatively weak Van der Waals forces (Kurth, 2008). In case the adsorbent and adsorbate are oppositely charged, adsorption proceeds effectively by means of the electrostatic forces (Janos et al., 2005).

2.3.2 Co-precipitation

Co-precipitation is a process in which a soluble species is removed from solution by sequestration in a precipitating phase. It can be defined as “the transfer of impurities to a precipitate concurrently with the deposition of some primary substances (macroscopic constituent) from a solution, melt, or vapor containing several substances” (The Great Soviet Encyclopedia). While the corrosion products are formed continuously from Fe^0 and precipitate in the oxide-film, the contaminants, even hardly adsorbable species, are entrapped in the matrix of aging corrosion products and removed from the aqueous solution (Crawford et al., 1993). The precipitation of corrosion products proceeds by nucleation and growth, aggregation or stabilization and aging

of iron corrosion products. The co-precipitation occurs whenever iron oxides are precipitated in the presence of foreign species (Kurth, 2008). There are three mechanism of co-precipitation (Crawford et al., 1993; Karthikeyan et al., 1997):

1. "Contaminant adsorption onto freshly formed hydrous ferric oxides (surface adsorption)"
2. "Solid solution formation by contaminant incorporation into the hydrous ferric oxide lattice (mixed-crystal formation)"
3. "Enclosure of contaminant-containing solution by the precipitate (mechanical entrapment)"

Contaminants are entrapped and removed from aqueous solution regardless of the contaminant being ionic, organic, inorganic or redox sensitive. Therefore a wide range of foreign species even living bacteria (Hussam et al., 2007; Diao and Yao, 2009), viruses (You et al., 2005) and non reducible organic (e.g. Methylene Blue) and inorganics can be successfully removed (Crawford et al., 1993). Furthermore the co-precipitated contaminants can not be released into the environment, unless the iron oxide is dissolved (Stipp et al.,2002; Noubactep et al., 2009a; 2009b; Ghauch et al., 2010; 2011). Even though structural reformation of the iron oxides may lead to random contaminant release, newly generated corrosion products on the reformed surfaces will entrap these contaminants within the oxide-film. The entrapped contaminants may then be reduced either directly or indirectly. Otherwise, even if they are not reduced, they are tightly bound inside the matrix of the iron oxide-film. According to Crawford, "co-precipitation will enhance the removal profile to an even greater extent than that of direct adsorption" (Crawford et al., 1993).

2.3.3 Adsorptive size-exclusion or straining

Straining is a major removal mechanisms for filtration system which is related to size of particles in pre-treated water and pore size of filters. when the particles are larger than the void spaces in the filter, they are excluded from aqueous solution and remain on the void space, so called size exclusion. With greater than 0.15 of the ratio of particle diamter comparing to grain diameter, packed filter with spherical granular media will remove particles (Crittenden et al., 2005). When the concentration of the particles are high enough, the particles form layer (so-called cake) over the entrance of the filter medium (Holdich, 2002). The cake filtration may contribute to strain out particles which are smaller than the filter pore size (USAPHC, 2011).
It is still widely considered that contaminant removal in Fe^0/H_2O systems results from the interaction of oxidizing species which reduction is coupled to the oxidative dissolution of Fe^0. However, several studies (partly available before the advent of 'Fe^0 technology') indicate that ferrous iron can act as a reducing agent for soil components and contaminants (Postma, 1985; Fendorf et al., 1996; Liger et al., 1999; Postma and Appelo, 2000). From comparisons of the electrode potentials E^0 of $Fe^{III}_{(s)}/Fe^{II}_{(s)}$ (E^0= -0.36 to -0.65V) and Fe^{II}/Fe^0 (E^0 = -0.44V) (see Table3), it can easily be seen that structural Fe^{II} (Fe^{II}(s)) can reduce contaminants more powerfully than the inaccessible surface of Fe^0 (Noubactep, 2008a; 2008b).

Table 3: Standard electrode potentials of iron species. (cited from Noubactep, 2008a)

Redox couple	E^0(V)(SHE)	Eq.
$Fe^0 \Leftrightarrow Fe^{2+} + 2e^-$	-0.44	(1)
$Fe^{2+}_{(S)} \Leftrightarrow Fe^{3+}_{(s)} + e^-$	-0.36 to -0.65	(6)
$Fe^{2+}_{(aq)} \Leftrightarrow Fe^{3+}_{(aq)} + e^-$	0.77	(6)

2.4 Methylene Blue Discoloration Process in Fe^0/H_2O Systems

Methylene Blue (MB) ($C_{16}H_{18}N_3SCl$) is a cationic thiazine dye and a well-known redox indicator. In the oxidized state, it features a deep blue color, while it is colorless in its reduced form (so-called leukomethylene blue-LMB) (Li et al., 2012). MB discoloration in Fe^0/H_2O systems can be described by three mechanisms (Noubactep, 2009a):

1. MB adsorption onto Fe^0 and iron corrosion products
2. MB co-precipitation in the structure of nascent corrosion products
3. Reduction from MB to LMB either by oxidation of Fe^0/Fe^{2+} or Fe^{2+}/Fe^{3+}

In the following we shall expand briefly on the process of MB adsorption.
As MB is water soluble, in aqueous solution it dissociates positive cations.

$$C_{16}H_{18}N_3SCl \Leftrightarrow [C_{16}H_{18}N_3S]^+ + Cl^- \tag{19}$$

When the positively charged MB functional group gets into contact with the deprotonated surface of the corrosion products, MB adsorption occurs as following (Nassar and Ringsred, 2012):

$$[C_{16}H_{18}N_3S]^+ + Fe-OH \Leftrightarrow Fe-O[C_{16}H_{18}N_3S] + H^+ \tag{20}$$

As the isotherm of MB adsorption in the Fe^0/H_2O system, the Langmuir isotherm is commonly used. However, as explained above, in Fe^0/H_2O systems, MB is removed via three mechanisms. Besides, iron corrosion products are continually generated and remove MB, therefore removal equilibrium will not be attained. Under these condition, the interpretation of MB removal with the adsorption isotherm alone is not justified (Burris et al., 1995; Noubactep, 2009a).
As mentioned in chapter 2.3, quantitative MB discoloration is contributed mostly by co-precipitation and adsorption with in situ generated corrosion products. MB is discolored quantitatively only at pH>4.5, where Fe-oxides can precipitate and the oxide film can be formed, owing to the low solubility of Fe(II) or Fe(III) species. The co-precipitated or adsorbed MB will be reduced to LMB within the oxide film driven either by Fe^0 or Fe(II) species. However, as MB discoloration is quantified by measuring the MB concentration (sorption of light wave by blue color) using UV-Vis spectrophotometers at a wavelength of 664.5nm, this reduction does not contribute to the measurable MB discoloration, (Noubactep, 2008a; 2008b).

2.5 Column Design (Fe amended sand Filter with Sand+Fe Mixture)

For water treatment with Fe^0-amended filtration systems, the main concern is the relatively short filter service time due to porosity loss and filter clogging. Conceivable factors which cause filter clogging are: (1) adsorption of fouling substances, (2) biocorrosion, (3) cake formation (particle cementation), and (4) volumetric expansion of iron corrosion (Noubactep, 2010d). Among these (4) has been shown to be the one factor that most of the filter clogging can be accounted for. In order to tackle this problem and extend filter service life, using mixtures of Fe^0 and sand has been proposed, where the chemically inert sand increases the inter-particle space (void volume) for long term iron corrosion expansion in the reactive zone of the filter. Fe^0+sand filters are regarded as iron amended slow sand filtration systems (Neku and Tandlker, 2003; Lea, 2008; Pokhrel et al., 2009; Noubactep, 2010d). In such systems, the main contaminant removal mechanism is adsorptive size exclusion, which takes place in the Fe^0-containing zone (so-called the reactive zone) by (1) the cycle of iron corrosion expansion/contraction and (2) an ultrafiltration system yielded by filling the pore space with in situ corrosion products (Noubactep, 2010d). Thus the pore space in the Fe^0-amended filtration system should be kept large enough for long time to accomodate the expansion/contraction cycle of iron corrosion. Past works by Noubactep (Noubactep, 2010b and Noubactep and Caré, 2011; Noubactep et al., 2011) elaborated on optimal Fe^0/sand proportions for long filter lifetime. According to their studies, filter clogging at Fe^0 depletion has been found to occur at a volumetric proportion (vol%) of Fe^0=51%, which has been accounted for by a uniform porosity decrease inside the reactive zone, concluding the volumetric proportion of Fe^0 in the reactive zone must not be larger than 52%. Otherwise the filter will be clogged

before the Fe^0 is completely depleted, resulting in material wastage and a shorter filter service time (Noubactep and Schöner, 2010). Due to the common theme of our studies, many of the quantities needed here have been previously named and defined by Noubactep, thus we find it most appropriate to adopt their mathematical notation. In the following we shall list the names and definitions of common quantities involved in the column studies.

The total volume of a cylindrical reactive zone V_{RZ} which can be written as the sum of the occupied volume V_{solid} and the excluded volume V_{pore}, is given by

$$V_{\mathrm{RZ}} = \frac{\pi D^2 h_{\mathrm{RZ}}}{4} = V_{\mathrm{solid}} + V_{\mathrm{pore}} \tag{21}$$

where D is the diameter and h_{RZ} the height of the reactive zone. The height of the reactive zone can be expressed as

$$h_{\mathrm{RZ}} = \frac{4 \cdot (V_{\mathrm{solid}} + V_{\mathrm{pore}})}{\pi D^2} \tag{22}$$

Introducing the compaction factor C, which is defined as the volume fraction of occupied volume and available volume, V_{solid} and V_{pore} relate to V_{RZ} as

$$V_{\mathrm{solid}} = C\, V_{\mathrm{RZ}} \tag{23}$$

$$V_{\mathrm{pore}} = (1 - C) V_{\mathrm{RZ}} \tag{24}$$

For monodisperse randomly close packed spheres (RCP) C is 0.64 (Radin, 2008). The Volume is generally calculated using the formula

$$V_{\mathrm{i}} = \frac{m_{\mathrm{i}}}{\rho_{\mathrm{i}}} \tag{25}$$

where m_i is the mass and ρ_i the density, which is either the materials bulk density (crystal) or RCP density, depending on the circumstances. Reorganization of eq. 22 leads to

$$h_{\mathrm{rz}} = \frac{4 V_{\mathrm{rz}}}{\pi D^2} = \frac{4 V_{\mathrm{solid}}}{C \pi D^2} \tag{26}$$

In our column study we use the above equations to calculate the volumes and masses of the iron material. It has been shown, that in order to obtain a homogeneous mixture of Fe^0 and sand, the height of the reactive zone should be at least 5cm (i.e. h_{RZ}>5cm) (Noubactep and Caré, 2011).

Regarding the design of Fe^0+sand filtration system, sandwich-like structures of at least three layers have been proposed, such that the reactive zone containing the Fe^0+sand mixture is located in between two sand layers on top and below (Noubactep and Caré, 2011). The bottom sand layer is essential for removal of dissolved O_2 from water before it reaches the reactive zone while the top layer prevents dissolved iron coming from the reactive zone to exit the filter and to mix with the treated water (Pachocka, 2010).

Employing Fe^0+sand mixtures can be beneficial in a number of ways, namely (i) avoid Fe0 compaction (Leupin and Hug, 2005; Gottinger et al., 2010), (ii) increase the hydraulic conductivity (O'Hannessin et al., 2004; Westerhoff and James, 2003; Moraci and Calabro, 2010) and (iii) decrease the cost of the filter (Bi et al., 2009).

2.6 Iron Corrosion Induced Rust Expansion Model

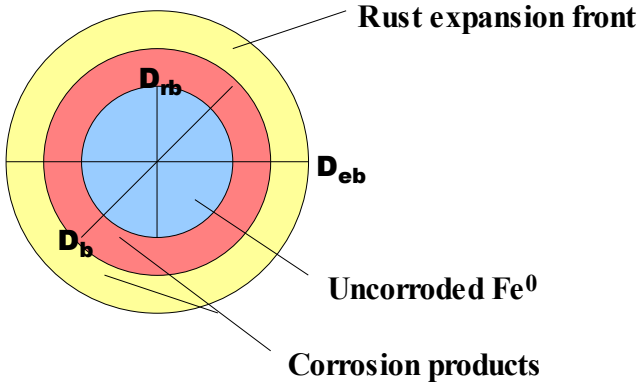

Fig.4: Schematic image of iron corrosion (Chen and Mahadevan, 2006): Cut through plane of a corroded spherical iron colloid.

In order to quantitatively assess the impact of iron corrosion expansion on filter clogging we employ a mathematical model for iron corrosion expansion originally developed by Chen and Mahadevan (2006) to be used for iron rods in soil. To apply the model to our target system, the reactive zone of the Fe^0+sand filtration system, which we consider to be a monodisperse, homogeneous mixture of sand and Fe^0 colloids, we adapt the model to this new geometry, assuming the reaction kinetics to be independent of the system size.
Iron corrosion expansion is described using a concentric three-shell model, as shown in figure 4. In its center lies a core of uncorroded Fe^0 (diameter D_{rb}). As the iron undergoes corrosion, corrosion products expand and the corrosion front moves outward (diameter D_{eb}) while the core shrinks and leaves a layer of corrosion products (diameter D_b) behind. In the following we shall derive a formula to predict the volume expansion as a function of time following closely the derivation by Chen and Mahadevan (2006).
Iron corrosion is a function of the corrosion current, I_{corr} (A). The mass of consumed iron M_s (g) for corrosion can be described using the following rate equation

$$\frac{d M_s}{dt} = \frac{I_{corr} A}{nF} = 2.315 \times 10^{-4} \cdot I_{corr} \quad \text{(g/s)} \quad , \tag{27}$$

where A=55.85g/mol and F=96,500 C/mol are the atomic weight of elemental iron and the Faraday constant and "n" is the valency of the iron corrosion products. As there are a number of possible corrosion products we chose to set n=2.5 which is the mean value of the valencies of the most dominant corrosion products $Fe(OH)_2$ (n=2) and $Fe(OH)_3$ (n=3). The corrosion current density I_{corr} (A/m^2) is defined as the corrosion current per unit surface of iron, hence relates to the corrosion current via the iron surface at all times as

$$I_{corr} = \begin{cases} \pi i_{corr} \cdot D_b^{\,2} & (t=0) \\ \pi i_{corr} \cdot D_{rb}^{\,2} & (t>0) \end{cases} \tag{28}$$

For simplicity we assumed the iron colloids to be spherical in shape.
The volume of uncorroded iron is given by

$$V_{rb} = \frac{4}{3}\pi \left(\frac{D_{rb}}{2}\right)^3 \quad \Rightarrow \quad D_{rb} = \left(\frac{6 V_{rb}}{\pi}\right)^{1/3} \tag{29}$$

However V_{rb} itself is related to the volume of consumed iron $V_s(t)$ as follows

$$V_{rb} = V_b - V_s(t) = V_b - \frac{M_s(t)}{\rho_s} \quad . \tag{30}$$

Combining all of the above equations (30, 29, 28 and 27) yields the ordinary differential equation

$$\frac{dM_s}{dt} = \frac{I_{corr} A}{nF} = 2.315 \times 10^{-4} \cdot \pi \cdot i_{corr} \cdot D_{rb}^2 = 2.315 \times 10^{-4} \cdot \pi \cdot i_{corr} \cdot \left(\frac{6}{\pi} \left\{ V_b - \frac{M_s(t)}{\rho_s} \right\} \right)^{2/3} \tag{31}$$

which may be solved by separation of variables. Upon integration we obtain the desired functional form for the mass of consumed iron $M_s(t)$:

$$M_s(t) = V_b \rho_s - \rho_s \left(\frac{-1.1 \cdot \sqrt[3]{\pi} \cdot 2.315 \times 10^{-4} \cdot i_{corr} \cdot t}{\rho_s} + V_b^{1/3} \right)^3 \tag{32}$$

M_s and its density ρ_s are directly proportional to the mass and density of the corrosion products M_r and ρ_r via

$$M_r = M_s / r_m \quad , \quad \rho_r = \rho_s / \gamma \quad , \tag{33}$$

where r_m is the fraction of mass of consumed iron and generated corrosion products, where again we use the mean value of the main corrosion products $Fe(OH)_3$ (r_m=0.523) and $Fe(OH)_2$ (r_m=0.622), that is r_m=0.5685. ρ_s is the iron bulk density ρ_s=7850(kg/m^3) and γ is the fraction of density of consumed iron and generated corrosion products. We assume γ=2.17, which is the case if the corrosion products consists to equal parts of $Fe(OH)_3$ and $Fe(OH)_2$ (Chen and Mahadevan, 2006).
Consequently the volume of the corrosion products V_r can be expressed as

$$V_r = \frac{M_r(t)}{\rho_r} = \frac{M_s(t)}{r_m \cdot \rho_s / \gamma} \tag{34}$$

and

$$V_r = V_{eb} - V_b \quad \Rightarrow \quad V_{eb} = \frac{M_s(t)}{r_m \cdot \rho_s / \gamma} + V_b \quad , \tag{35}$$

by relating it to the volume of expanded iron V_{eb}. Using the geometric relation

$$V_{eb} = \frac{4}{3} \pi \left(\frac{D_{eb}}{2} \right)^3 \quad \Rightarrow \quad D_{eb} = \left(\frac{6 V_{eb}}{\pi} \right)^{1/3} \tag{36}$$

and inserting equation 32 and 35 we obtain the time dependence of the diameter of the corrosion expansion front (D_{eb}):

$$\begin{aligned} D_{eb} &= \sqrt[3]{\frac{6 V_{eb}}{\pi}} = \sqrt[3]{\frac{6}{\pi} \left(\frac{M_s(t)}{r_m \cdot \rho_s / \gamma} + V_b \right)} \\ &= \sqrt[3]{\frac{6}{\pi} \left[\frac{\gamma}{r_m \cdot \rho_s} \left\{ V_b \rho_s - \rho_s \left(\frac{-2.55 \times 10^{-4} \cdot \sqrt[3]{\pi} \, i_{corr} \cdot t}{\rho_s} + \sqrt[3]{V_b} \right)^3 \right\} + V_b \right]} \end{aligned} \tag{37}$$

Upon substitution of V_b with its geometric identity

$$V_b = \frac{4}{3}\pi\left(\frac{D_b}{2}\right)^3 = \frac{\pi}{6} D_b{}^3 \tag{38}$$

eq. 41 can be simplified further, yielding the desired functional relationship for the total diameter expansion due to iron corrosion over time and corrosion current density :

$$D_{eb} = D_b \sqrt[3]{\frac{\gamma}{r_m \cdot \rho_s}\left\{1 - \left(\frac{-4.63 \cdot 10^{-4} \cdot i_{corr} \cdot t}{\rho_s \cdot D_b} + 1\right)^3\right\} + 1} \tag{39}$$

We shall use this formula in order to estimate the porosity loss in the column experiments (Chapter 5.2.2.ff.).

3. Materials and Methods

3.1 Materials

3.1.1 Methylene Blue

Methylene Blue is a heterocyclic aromatic compound with the molecular formula $C_{16}H_{18}N_3SCl$. It is a well known redox indicator and cationic thiazine dye with the chemical name tetramethylthionine chloride, featuring a characteristic deep blue color in the oxidized state and is colorless in the reduced form (leukomethylene blue:LMB). Studies of crystalline MB indicate that the molecule is about 16.0 Å in length, about 8.4 Å wide and has a minimal thickness of 4.7 Å (Kipling and Wilson, 1960). Crystallized MB has a dark green color. Dissolved in water, the aqueous solutions attains a dark blue color. MB has a high adsorption affinity for solid surfaces (Imamura et al., 2002; Oguzie, 2005), especially for oppositely charged surfaces (Janoš et al., 2005), which is attributed to both electrostatic and hydrophobic interactions (Imamura et al., 2002; Pirillo et al., 2009; Saha et al., 2011; Miyajima and Noubactep, 2012a). MB is widely used as a dye and as such is often utilized for surface area determination of clay minerals (Kalor and Madsen, 1995). As a dye material, MB has ideal spectro-photometric properties, is determinable with UV-VIS spectrophotometry while being not too expensive and not as toxic as some organic pollutants, making it an excellent choice.

Tested solid materials of this study are Fe^0, sand and mangandioxide (MnO_2). Used MB concentrations were 2.0 and 10.0 mg/L corresponding to 6.3 and 31.3 µM repectively. These seemingly unusual small initial MB concentrations were selected to reflect the situation of polluted natural waters where pollutants are usually present in trace amounts (Nödler et al., 2010; Kümmerer, 2011).

3.1.2 Elemental Iron

The selection of the iron type can have great impact on the reactivity. Purity, surface area, and grain size are three important qualities that could potentially affect the treatment efficiency (Ulsamer, 2011). Discoloration agent in this work. ZVI1 has filing shape and particle sizes range from 0.2 mm to 3.0 mm. The intrinsic reactivity of ZVI1 was characterized by comparing ZVI1 to seven other commercial Fe^0 materials (ZVI2 through ZVI8) in two different tests: EDTA test and MB test (Chapter 4). Table 4 gives an overview of all ZVI materials and their respective origins and Table 5 lists the corresponding elemental compositions.

The measured removal reactivity of Fe^0 is usually normalized by the specific surface area, in order to get a universal constant, the kinetic rate constant (here $k_{SA)}$, as an indicator for the reactivity of the material under study (Johnson et al., 1996; Mcgeough et al., 2007). However recent studies by Noubactep (Noubactep, 2009a; Noubactep, 2010a) indicate that the specific surface area is not the only and might not even be the most influential contributor to the Fe^0 reactivity. Therefore in this study the kinetic rate constant of iron dissolution in Ethylenediaminetetraacetic acid (EDTA) (k_{EDTA}) and the MB discoloration efficiency of iron in the presence of MnO_2 shall be used as indicators of the reactivity of Fe^0.

Table 4: Origin, shape and size of ZVIs used in this study

Code	Run	Origin	form	Granulometry (µm) [a]
ZVI 1	7 to 9	iPutec GmbH	filings	300 to 2000 (new)
ZVI 2	10 to 12	G. Maier GmbH	filings	300 to 2000 (old)
ZVI 3	13 to 15	G. Maier GmbH	filings	1000 to 3000 (old)
ZVI 4[b]	16 to 18	MAZ, mbH	filings	80 to 4000
ZVI 5	19 to 21	Würth	spherical	1200
ZVI 6	22 to 24	G. Maier GmbH	chips	350 to 1200
ZVI 7	26 to 27	Connelly-GPM	filings	1000 to 3000
ZVI 8	28 to 30	Connelly-GPM	filings	500 to 1000

[a] Average values from material supplier; [b] Scrap iron material.

Table 5: Elemental composition of ZVIs used in this study

ZVI	Elemental (%)						
	C	Si	Mn	Cr	Mo	Ni	Fe
ZVI1	3.2	1.95	n.a.	0.023	n.a.	0.02	92.00
ZVI2	3.13	0.17	0.42	0.16	n.d.	0.23	96.7
ZVI3	1.96	0.12	0.09	0.003	n.d.	<0.001	86.3
ZVI4	3.2	1.95	n.a.	0.023	n.a.	0.02	92.00
ZVI5	3.39	0.41	1.10	0.34	n.d.	0.088	91.5
ZVI6	3.52	2.12	0.93	0.66	n.d.	n.d.	99.8
ZVI7	3.13	2.17	0.36	0.077	n.d.	0.056	96.7
ZVI8	2.85	1.85	0.60	0.10	0.15	0.13	89.82

n.a=not available, n.d=not detectable

3.1.3 Manganese Nodules (MnO_2)

In this study three MnO_2 materials were used in testing the reactivity of various ZVI samples via MB discoloration. A commercial material (X-MnO_2) purchased from Aldrich and two natural minerals (i) psilomelane (Minas Gerais- Brazil) and (ii) manganite (Ilfeld/Harz- Thueringen/Germany) were tested. While MnO_2 is a known adsorbent for MB, it is also known that MnO_2 is reductively dissolved by Fe^{2+} (Koch, 1957), which inhibits MB discoloration by Fe^0, due to accumulation of iron corrosion products on the MnO_2 surface. Therefore for this study MnO_2 was added to Fe^0 to control the availability of in situ generated corrosion products (Noubactep et al., 2005; Noubactep, 2009a; Ghauch et al., 2011; Noubactep et al., 2011). The reductive dissolution of MnO_2 has been reported to recolorize MB (Postma and Appelo, 2000). This can be understood looking at the equations in Table 6 where the electrode potential has the ability to trigger re-oxidation of reduced LMB to the oxidized state MB^+ (recoloration). Therefore MB discoloration in the presence of MnO_2 can only result from adsorption anco-precipitationd.

Table 6: Electrode potentials of redox reactions (cited from Noubactep, 2008a)

Reaction			E^0(V)	Eq.
$Fe^{2+} + 2e^-$	↔	Fe^0	-0.44	(1)
$Fe^{3+}_{(s)} + e^-$	↔	$Fe^{2+}_{(s)}$	-0.36 to -0.65	(6)
$MB^+ + 2e + H^+$	↔	LMB	0.01	(40)
$Fe^{3+}_{(aq)} + e^-$	↔	$Fe^{2+}_{(aq)}$	0.77	(6)
$O_{2(aq)} + 2H_2O + 4e^-$	↔	$4OH^-$	0.81	(2)
$MnO_2 + 4H^+ + 2e$	↔	$Mn^{2+}_{(aq)} + 2H_2O$	1.23	(41)

3.1.4 EDTA

EDTA is a well known chelating agent, sequestering metal ions. After being bound by EDTA, metal ions remain in solution and their reactivity decreases. Therefore just as with MnO_2, EDTA was used for differentiating the reactivity of various ZVIs. In this study the used EDTA is disodium salt dihydrate (CAS-No.: 6381-92-6) purchased from AppliChem (Darmstadt, Germany).

3.1.5 Sand

The sand for our study is a commercial product for aviculture ("Papageiensand" from RUT – Lehrte/Germany), with particle sizes between 2.0 and 4.0 mm. This sand was used as an operational

reference for pure adsorbent material, which has a reported adsorption capacity of 119.8 - 163.1mg/100g (Handreck, 1990; Varlikli et al., 2009) without any further pre-treatment nor characterization.

3.2 Methods

3.2.1 UV-VIS-Spectrophotometry

Spectrophotometry measures the capability of molecules to absorb electromagnetic radiation ranging from 190nm (ultraviolet) to 780nm (red). Visible spectroscopy starts above ~360nm (violet), which is detectable by human eye, while ultraviolet spectroscopy ranges from 100nm to 380nm. Depending on the electron configuration of the molecules, electrons can be excited when exposed to photons that carry the appropriate amount of energy. The photon energy is according to Plancks energy equation inversely proportional to the wavelength:

$$E = hv\ [J] = h*c/\lambda \tag{42}$$

E = energy [J], h = Plancks quantum of action = $6.626*10^{-34}$ [Js],
v = frequency [Hz] = [s^{-1}], c = vacuum speed of light, λ = wavelength [m].

Excitation of electrons in ions or molecules results in the absorption of the incident light, with the the extent of the absorption being proportional to the number of species absorbing the light. Instruments used for spectrophotometry are called spectrophotometer. It consists of a light source to emit visible and/or ultraviolet light. A quartz prism or a diffraction grating generates almost monochromatic light, which is prerequisite for the excitation of only one molecule species. Emitted photons from the light source have a certain energy. When the light passes through the sample, a number of photons get absorbed and the intensity of the light is reduced. The extent of absorption (absorbance) depends on the concentration of absorbing material in the sample. Thus the spectrophotometer measures the intensity of the light of a certain wavelength after it passes through the sample, which can be used to determine the concentration of absorbents in the solution using literature data of the molar absorptivity or by comparison with a calibration curve obtained from standards with known concentrations. The absorbance *A* is described by the Lambert-Beer Law:

$$A = \log(I_0/I) = ecl \tag{43}$$

A = absorbance [dimensionless], I_0 = intensity of light emitted by the light source, I = intensity of light after it passes through the sample, e = absorption coefficient [$dm^3mol^{-1}cm^{-1}$], c = concentration (molarity) of the analyte in the solution [mol dm^{-3}], l = path length of light in the sample [cm].

3.2.2 Shaking

Shaking is an important tool to accelerate contaminant transport (in this case MB) from the aqueous phase to the Fe^0 surface, as well as to intensify the Fe^0 dissolution and the generation of more corrosion products. The MB transportation and iron corrosion rates are the key factors of adsorption and co-precipitation, which in turn affects the MB discoloration rate. Consequently shaking the sample speeds up the reaction and shortens the reaction time needed to reach equilibrium. In several past works (Kurth, 2008; Noubactep, 2008a; 2008b; 2009a), 50 rpm was identified as the critical shaking intensity for which the formation of an oxide scale on Fe^0 is not significantly disturbed. Nevertheless a shaking intensity of 75 rpm was used in this study.

4. Experimental Part

4.1 Material Characterization

Fe^0 corrodability is an intrinsic chemical reactivity of materials. In order to quantify the corrodability, the iron corrosion rate should be measured in the absence of oxide layers (Noubactep, 2010a). Both materials, MnO_2 as well as EDTA, have the ability to inhibit/delay oxide layer formation. Therefore the reactivity of various Fe^0 materials were examined by (i) the MnO_2 method to study the MB discoloration ability and (ii) the EDTA method to study the initial iron dissolution kinetics. The results were then analyzed in order to clarify possible relationships. The experiment was carried out using 8 different types of ZVIs (see Table 4).

4.1.1 EDTA Method

As a chelating agent, EDTA has the ability to sustain iron oxidative dissolution and is used to prevent the formation of oxide-films on Fe^0 surfaces. In this study the concentration of dissolved iron of all eight ZVIs (ZVI1-ZVI8) in 50ml EDTA solution (2mM EDTA) were measured over time (10, 24, 48, 72 and 96 hours) and a linear regression was carried out that can be expressed as the formula ax+b. The place of "a" is taken by the kinetic rate constant of iron dissolution (k_{EDTA}), which characterizes the reactivity. The k_{EDTA} values were obtained for all ZVIs.

4.1.2 MnO_2 Method

As explained earlier (§ 3.1.3) MnO_2 adsorbs MB and is reductively dissolved by Fe^{2+} (Koch, 1957), which inhibits MB discoloration by Fe^0, due to accumulation of iron corrosion products on the MnO_2 surface. This accumulation hinders the iron surface from passivation and accelerates the generation of iron corrosion products (Noubactep, 2003) and the new reactive adsorbents MnOOH and FeOOH as follows.

$$Fe^{2+}_{(aq)} + MnO_2 + 2H_2O \Rightarrow FeOOH + MnOOH + 2H^+ \quad (44)$$

$$2Fe^{2+}_{(aq)} + MnO_2 + 2H_2O \Rightarrow 2FeOOH + Mn^{2+} + 2H^+ \quad (45)$$

However, it has be observed in several studies, that despite the increase in the generation of iron corrosion products, MB discoloration was not improved. This has been accounted for by an availability-delay of free corrosion products (Fe-oxides) (Noubactep et al., 2005). Usually free corrosion products are generated in the vicinity of the Fe^0 surface and contribute to MB discoloration by co-precipitation, which is the primary mechanism of contaminant removal in Fe^0/H_2O systems. However, even though as long as MnO_2 is reductively dissolved, free corrosion products are generated, they accumulate at the MnO_2 surface. Only when the oxidation capacity for Fe(II) of the present MnO_2 is exhausted and the amount of additional free corrosion products suffices to entrap MB, large scale MB discoloration can occur (Noubactep, 2008a; 2008b). Therefore if the ZVI sample is reactive, a delay of MB discoloration is to be expected (Assumption 1). In order to study the MB discoloration ability of different ZVIs, they were studied under non-shaken condition for 6 weeks and under shaken condition at 75 rpm for 3 weeks using four different system setups:

(i) ZVI alone
(ii) ZVI+sand
(iii) ZVI+ MnO_2
(iv) ZVI+MnO_2+sand.

The masses of all materials were fixed at 0.0100g ZVI, 2.0000g of sand, and 0.0500g MnO_2 (see Appendix 3). A total of 30 test tubes were prepared to study all of the 8 ZVIs and 2 blank systems, where for each configuration three samples were prepared respectively. The test tubes for 8 ZVIs were prepared with 2.0000g of sand and 0.0100g of ZVI and for reference systems (blank), (i) ZVI(0.0000g) x 6, (ii) ZVI(0.0000g)+sand(0.0000g) x 3 and ZVI(0.0000g)+sand(2.0000g) x 3 (iii) ZVI(0.0000g)+MnO_2(0.0000g) x 3 and ZVI(0.0000g)+MnO_2(0.0500g) x 3 and (iv) ZVI(0.0000g)+MnO_2(0.0000g)+sand(0.0000g) x 3 and ZVI(0.0000g)+MnO_2(0.0500g)+sand(2.000g) x 3 were used (see Appendix 3).

Impact of MnO_2 Types on MB Discoloration

In order to assess the impact different types of MnO_2 have on the MB discoloration, three types of manganese oxide (i) psilomelane, (ii) manganit and (iii) X- MnO_2 were examined under shaken condition at 75 rpm for 2 weeks using two different system setups:

(a) MnO_2(0.2500g) alone

(b) ZVI+MnO_2(0.2500g).

X- MnO_2 is synthetic MnO_2, which was used also in our study of iron reactivity (§ 4.1.2). For iron in setup (a), ZVI1 was used. Additionally, to cover influences from MnO_2 loading on the MB discoloration, the experiment was done also with ZVI1(0.1000g)+MnO_2 (0.0000, 0.0250, 0.0500, 0.0750, 0.1000, 0.1250, 0.1500, 0.2000, 0.2500g) and repeated for each of the three MnO_2 species. As reference systems (blanks) for a) Fe^0(0.0000g)+MnO_2(0.0000g) and b) Fe^0(0.0000g)+MnO_2(0.2500g) were used (see Appendix 3).

4.2 MB discoloration

4.2.1 Batch Test

In order to quantify the effect of the Fe^0/sand ratio on MB removal, the MB discoloration efficiency of systems with (I) various Fe^0 loadings and (II) various sand loadings were examined. Test tubes were prepared for (I) with varying amounts of Fe^0 (0.0000 to 1.0000 g) in Fe^0 only systems as well as Fe^0+sand mixtures where the amount of used sand was fixed at 2.0000 g, and for (II) with variable amount of sand (0.0000-2.0000 g) in Fe^0+sand mixtures where the amount of used Fe^0 was fixed at 0.1g (see Appendix 3). All test-tubes were filled up with 22.0mL (full volume) of reactive material and MB solution sealed with caps at room temperature (~20ºC) under non-shaken condition for 3 and 6 weeks, and shaken condition for 1 week. The concentration of the MB solution was 10mg/L, diluted from 1000mg/L stock solution. After the experimental duration time, up to 5mL of supernatant were carefully retrieved (no filtration) for MB measurement.

Effect of Fe^0 Loading on MB Discoloration

Three different experimental conditions were studied: (i) 6 weeks under non-shaken condition, (ii) 3 weeks under non-shaken condition and (iii) 1 week with shake intensity of 75 rpm using two different system setups:

(Ia) Fe^0_i alone

(Ib) Fe^0_i+ sand mixtures.

For both systems 10 different amounts of Fe^0 (0.0000 g x 2, 0.0100 g, 0.0250g, 0.0500 g, 0.1000 g, 0.2500 g, 0.5000 g, 0.7500 g, and 1.0000 g) were examined three times, totaling 30 test tubes per system. As reference systems (blanks) for the Fe^0 only system, two Fe^0(0.0000 g) samples and for the Fe^0+sand mixture, one Fe^0(0.0000 g)+sand(0.0000 g) sample and one Fe^0(0.0000 g)+sand(2.0000 g) sample were used.

Effect of Sand Loading on MB Discoloration

Two experimental conditions, (ii) and (iii) of chapter 4.1.1, were studied for this experiment. In order to see the difference of MB discoloration caused by the various reactive material loadings, two different system setups were used:

(Ib)Fe^0_i+ sand mixtures.

(II) Fe^0+sand $_i$ mixtures.

The results of the Fe^0+sand mixture in 4.1.1 were used as (Ib) and compared with those obtained in this experiment. 10 different amounts of sand (0.0000 g x 2, 0.2500 g, 0.5000 g, 0.7500 g, 1.0000 g, 1.2500 g, 1.5000 g, 1.7500 g, and 2.0000 g) were examined three times. As reference systems (blanks), Fe^0(0.0000 g) +sand(0.0000 g) and Fe^0(0.1000 g)+sand(0.0000 g) were used.

4.2.2 Column Experiments

The purpose of these experiments is to find out the optimal mixture ratio of Fe^0 and sand for MB discoloration. The experiment was done under saturated, continuous up-flow condition at a flow rate of 0.1mL/min regulated by a peristaltic pump. The concentration of used MB solution was 2mg/L. The equipment used in this experiment were 10 columns (length 44.0cm, diameter 2.6cm), peristaltic pump (Ismatec, ICP 24). The used pump has a total of 24 channels from which only 10 were used to generate the same flow rate for all 10 columns, pipes on the bottom side of each column connecting it to the pump and pipes leading from the top of each column to sample collecting bottles and props to fixate the columns in a vertical position. The 10 columns were carefully wet-packed to avoid bubble formation. In order to find the optimal Fe^0+sand mixture ratio, 9 different volume ratios (0, 10, 20, 30, 40, 50, 70, 80, 100%) with 100g Fe^0 and an additional sample with 200g Fe^0 (volume ratio 100%) were prepared (see Appendix 4). The column with 0% ZVI content was packed only with sand (360 g), while all other columns featured three layers: a sand layer at bottom (S1), the reactive zone with the Fe^0+sand mixture (RZ) and another sand layer on top (S2) (see Fig.5). The experiment was performed at room temperature (15-20°C) over a period of 131 days while samples were collected periodically. The initial MB concentration was 2.0 mg/L.

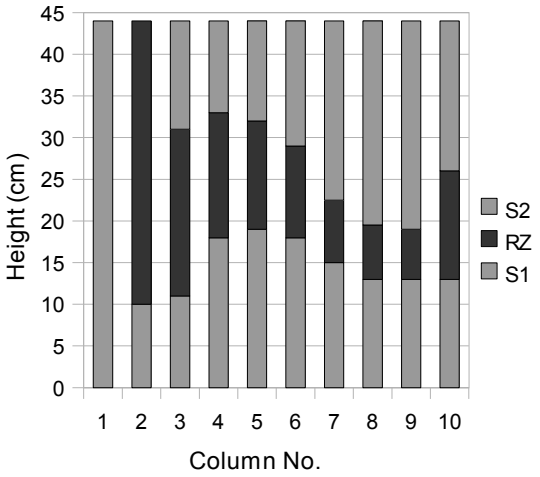

Fig.5: Position and height of each layer (S1, RZ and S2) in each column (1-10)

Tested volumetric ratios of Fe^0 in the reactive zone were built while using the volume occupied by 100 g of Fe^0 (32.0 mL – apparent volume) as unity. The resulting sand masses are documented in Tab. 7. For example, the system with 20 % (v/v) Fe^0, was made up of one volume of Fe^0 and four volumes of sand. The corresponding mass of sand was 77 g yielding a weight ratio of 43.5 %. The simple rule of proportion suggest that the commonly used 50 % (w/w) corresponds to only about 23.0 % (v/v) for the materials (iPutech Fe^0 and "Papageiensand") tested here.

Initial Porosity

The initial porosities of columns 1-10 were calculated using the relation

$$Porosity = \frac{V_{pore}}{V_{RZ}} \cdot 100 \tag{46}$$

where V_{RZ} is the volume of the reactive zone and V_{pore} is the pore (void) volume inside the reactive zone. The volume of the reactive zone is given by the cylinder volume

$$V_{RZ} = \pi r_{column}^2 \cdot L_{RZ} \tag{47}$$

where r_{column} is the column radius and L_{RZ} is the height of the reactive zone (Appendix 4). The pore volume in the reactive zone can consequently calculated as the difference between the total RZ volume and the space

needed for the ZVI and sand particles, hence

$$V_{pore} = V_{RZ} - \left(V_{Fe0} \cdot 0.64 + V_{sand} \cdot 0.64 \right) = V_{RZ} - \left(\frac{M_{Fe0}}{\rho_{Fe0}} \cdot 0.64 + V_{sand} \cdot 0.64 \right) \quad (48)$$

where we assumed the mixture to be constituent of RCP monodisperse spheres, featuring a compaction of 0.64 (§ 2.4). M_{Fe0} is the mass of iron in the reactive zone, ρ_{Fe0} is the iron bulk density and V_{sand} is the measured volume of sand in the reactive zone.
An overview of the all initial porosities obtained in this fashion is exhibited in Table 7.

Table 7: Measured mass of Fe^0 (M_{Fe0}), volume of reactive zone (V_{RZ}), volume of sand (V_{sand}), the calculated void volume (V_{void}) and porosity for each column.

Fe^0 Loading (%)	**M_{Fe0}** (g)	**V_{RZ}** (ml)	**V_{sand}** (ml)	**Sand Loading** (%)	**V_{void}** (ml)	**Porosity** (%)
0	0	233,7	460	100	84,13	36
10	100	180,59	155,9	90	67,97	37,64
20	100	106,23	69,3	80	49,06	46,18
30	100	79,67	40,4	70	40,98	51,43
40	100	69,05	26,0	60	39,59	57,34
50	100	58,43	17,3	50	34,51	59,07
70	100	39,84	7,4	30	22,26	55,88
80	100	34,52	4,3	20	18,93	54,84
100	100	31,87	0,0	0	19,05	59,77
100	200	69,04	0,00	0	43,4	62,86

4.3 Sample Preparation

For the measurement of the MB concentration, no pre-treatment of the MB solutions was needed, as they were already lucent. For the column experiment, the concentration of dissolved Fe in the outflow solutions was measured using the *1.10-phenanthroline* method, commonly used for colorimetric analysis of Fe in solution. In order to measure the total concentration of all dissolved Fe species, Fe(III) and Fe(II), the Fe(III) species was reduced to Fe(II) using ascorbic acid to enable chelate complexation with *1,10-Phenanthroline*. Since the chelate complex has a chromogenic effect at pH=4-5 the ascorbic buffer was used to keep the pH value at 4.0. The *1,10-phenanthroline* solution (1%) was produced by mixing 0.5g of the *1,10-phenanthroline* with 500mL hot deionized water and the ascorbic buffer was made by mixing 35.226g of ascorbic acid and 39.622g of Na-ascorbate in 500mL of hot deionised-water. Samples for the measurment were prepared using 10mL of the outflow solution, 1mL of the Ascorbic buffer, 8mL H_2O and 1mL of the *1,10-Phenanthroline* solution. After mixing the samples were given 15min time to react and were then measured by UV-VIS-Spectrophotometry.

4.4 Analytical Methods

The MB concentration was determined using a Cary 50 UV-Vis spectrophotometer at a wavelength of 664.5nm using cuvettes with 1cm light path. To measure the pH value of the solution combined glass electrodes (WTW Co., Germany) were employed. The Electrodes were calibrated with common tap water. To reduce statistical errors each measurement was repeated three times and the results were averaged.

4.4.1 Calibration of the Spectrophotometer

To determine the unknown concentration of the MB solution, the spectrophotometer was calibrated using standards of ten different concentrations: 0.0, 0.5, 1.0, 1.5, 2.5, 5.0, 7.5, 10.0, 12.5 and 15.0 mg/L. The standards were prepared from 1000mg/L MB stock solution and tap water with a total volume of 20mL each (Table 8). The calibration standards were measured at the beginning and at the end of the measurement in order to detect possible shifts in the MB absorption due to MB particles being adsorbed at the cuvettes' surface in the course of the repeated measurements using the same cuvette. The measured shift due to this effect was less than 3.5%, and is thus insignificant. See Fig. 6 for the measured absorbance - MB concentration calibration curve.

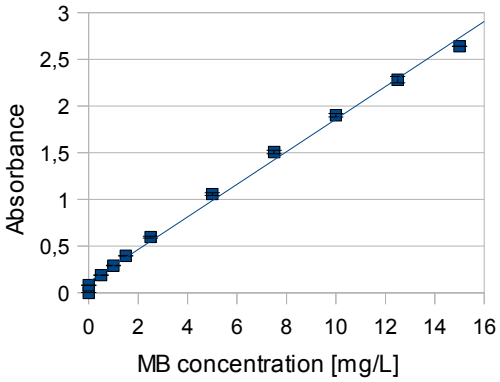

Fig.6: Calibration curve for light absorbance at different MB concentrations and its linear regression.

Table 8: MB calibration of Cary 50 UV-VIS-Spectrophotometer.

Std	**[MB]** (mg/L)	**V_{MB}** (µL)	**V_{1H2O}** (mL)	**V_{2H2O}** (µL)
1	0	0	19.5	500
2	1	20	19.5	480
3	2	40	19.5	460
4	4	80	19.5	420
5	6	120	19.5	380
6	8	160	19.5	340
7	10	200	19.5	300
8	15	300	19.5	200
9	20	400	19.5	100
10	25	500	19.5	0

For the concentration of dissolved Fe, the calibration was done using standards of ten variable concentrations: 0.0, 0.25, 0.5, 0.75, 1.0, 2.0, 4.0, 6.0, 8.0 and 10.0 mg/L. The standards were prepared from 1000mg/L stock Fe solution and tap water, with a total volume of 10mL each (see Table 9). The calibration procedure was the same as for the MB calibration, where again the measurement of the blank was repeated at the beginning and at the end of the measurement. The deviation was usually less than 3.5 %, showing that no significant shifting takes place. See Figure 7 for the measured absorbance - Fe concentration calibration curve.

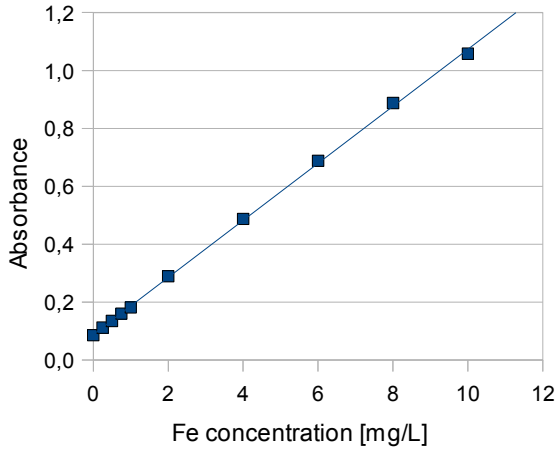

Fig.7: Calibration curve for light absorbance at different iron concentrations and its linear regression.

Table 9: Iron calibration of Cary 50 UV-VIS-Spectrophotometer.

Std	**[Fe]** (mg/L)	**V_{Fe}** (mL)	**V_{H2O}** (mL)
1	0.00	0.00	10.00
2	0.25	0.25	9.75
3	0.5	0.5	9.5
4	0.75	0.75	9.25
5	1.00	1.00	9.00
6	2.00	2.00	8.00
7	4.00	4.00	6.00
8	6.00	6.00	4.00
9	8.00	8.00	2.00
10	10.00	10.00	0.00

4.4.2. Interpretation of the UV-VIS Data

The measurements were repeated three times for each content ratio of reactive materials and the mean values and standard deviations were taken as the result used for calculation. From the difference between the measured concentration data *C*, the initial concentration *C0*, and the extent of the MB removal *P* (in %) were calculated using the following equation:

$$P = [1 - (C / C_0)] * 100 [\%] \quad (49)$$

C_0 = mean concentration of measured blank [mg/L],
C = measured concentration of sample solution [mg/L].

5. Result and Discussion

5.1 Material characterization

5.1.1 EDTA Method

The evolution of the concentration of dissolved iron by the tested ZVIs (ZVI1 through ZVI8) in 50ml EDTA solution (2mM EDTA) weas measured over time (10, 24, 48, 72 and 96 hours), and their linear regression curves, that is the function ax+b (see Fig. 8) were obtained, where "a" here is the kinetic rate constant of iron dissolution (k_{EDTA}), which characterizes the reactivity and "b" is the offset-concentration at t=0h.

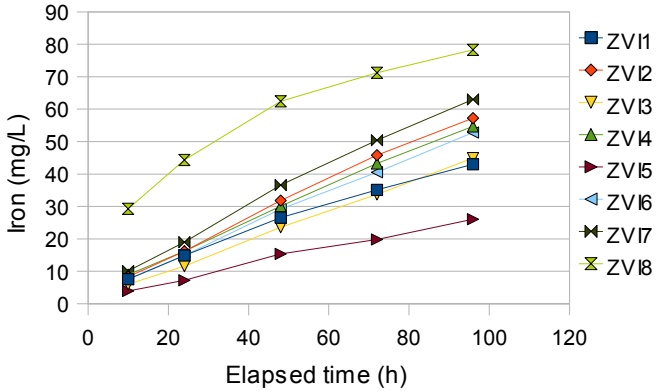

Fig.8: The reactivity of ZVI 1-8 according to the EDTA method.

The concentration of dissolved iron ranged 3mg/L for ZVI5 at 10h to 79mg/L for ZVI8 at 100h. ZVI8 shows the highest (30mg/L – 78mg/L) and ZVI5 as the least (83mg/L – 27mg/L) dissolved iron concentration during whole experimental duration.
Fig.8 summarizes the time-dependant evolution of the concentration of dissolved Fe in EDTA solution for all ZVIS. As can be seen from the graph, all materials except for ZVI5 and 8 exhibited very similar dissolution kinetics. The k_{EDTA} values and offset-concentrations are listed in Table 10.

Table 10: k_{EDTA} values and offset-concentrations for all ZVIs.

Material	k_{EDTA} (µg/h)	offset (µg)
ZVI1	24	136
ZVI2	29	117
ZVI3	24	73
ZVI4	27	173
ZVI5	13	65
ZVI6	27	108
ZVI7	32	193
ZVI8	24	1685

Figure 8 shows that ZVI8 has the highest total dissolved iron concentration, which is reflected also in its high offset value of 1685 µg (see Table 10) which is about eight times as big as the second largest value of 193 µg for ZVI7. This is consistent with the fact that only ZVI8 was physically covered by fines of rusted iron due to corrosion caused by long air exposure. Past studies indicated that the EDTA method is not suitable for the use with powdered materials and that fines should be washed off before any test is carried out (Noubactep, 2003; Noubactep et al., 2009a). Thus the iron intrinsic reactivity should not be determined taking into the offset value, which is influenced in the presence of fines but does not affect the dissolution of Fe in EDTA solution. Therefore the reactivity was evaluated again using only the value of k_{EDTA} (Table 10) leading to the ranking:

$$ZVI5 < ZVI3 < ZVI1 = ZVI8 < ZVI4 = ZVI6 < ZVI2 < ZVI7.$$

5.1.2 MnO_2 Method

To measure the iron reactivity of 8 different type of ZVIs on the MB discoloration, MB discoloration efficiency using MnO_2 ,which induce a delay of free corrosion products availability , were measured.
The MB discoloration by 8 different ZVIs in four systems (i) ZVI alone, (ii) ZVI+sand, (iii) ZVI +MnO_2 , and (iv) ZVI+MnO_2+sand, and their pH values were measured for 3 weeks to compare the reactivity of ZVIs (see Fig.9).

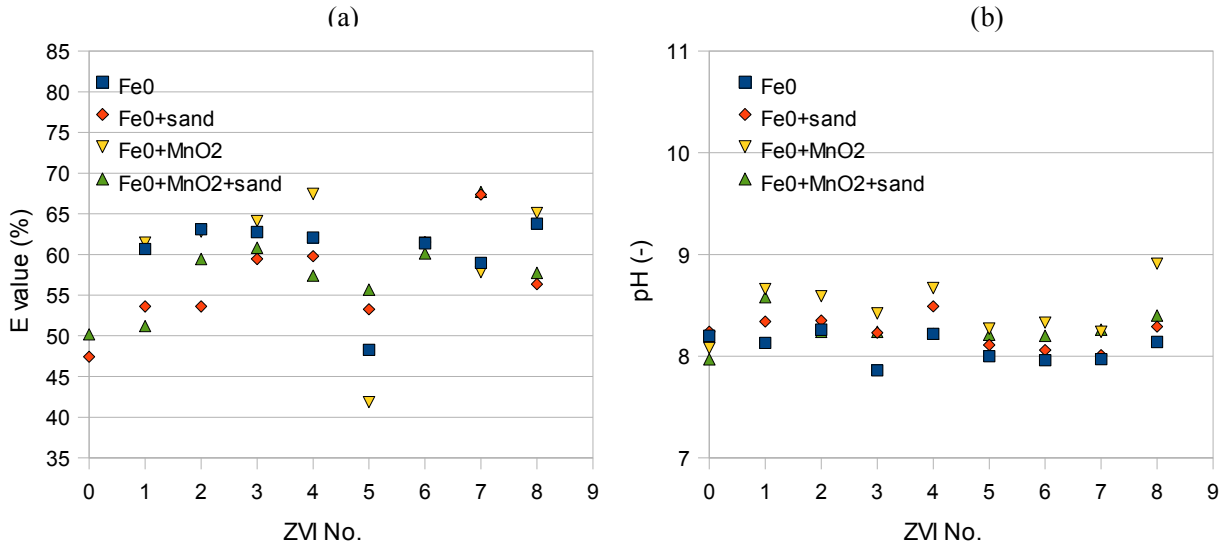

Fig.9: E value (MB discoloration efficiency) (a) and pH (b) of variable ZVIs in four different system under non-shaken condition for 3 weeks.

ZVI5 shows the least E value in three systems (ZVI alone, ZVI+sand and ZVI+MnO_2). For the ZVI+MnO_2 +sand system, ZVI1 is the least efficient.
As can be esen from Fig.9 (a) the ZVI+MnO_2 systems with ZVI5 and ZVI7 show slightly lower E value compared to Fe^0 systems, however there is no clear tendency confirming that the efficiency of Fe^0 for MB discoloration is decreased by the presence of MnO_2. On the other hand in the sand including systems, similar trend except ZVI7 that indicats the sand causes the inhibition of MB discoloration as well. Also for the pH values, there are no detectable differences among either the ZVI types and the various mixtures. Therefore these results do not support the proposal made in "Assumption 1" that if the ZVI sample is more reactive, a stronger mismatch in MB discoloration in ZVI+MnO_2 and ZVI+MnO_2 +sand systems had to be expected (§ 4.1.2). One possible explanation for this discrepancy might be that 3 weeks is already too long to observe inhibition, in the study of Noubactep (Noubactep et al., 2009b), 1 week of the experimental duration clearly demonstrated the inhibition of MB discoloration in the ZVI+MnO_2 system, which could be the ultimate proof for " Assumption 1" that MB discoloration is not quantitative, as long as free corrosion products are not available. On the other hand 3 weeks might not be enough to see the effects of free corrosion products after the exhaustion of MnO_2. To clarify this matter a long term experiment was done for 6 weeks and the results were compared. As an operational reference, the E values of pure Fe^0 systems were chosen and ordered as follows:

$$ZVI5 < ZVI7 < ZVI1 \cong ZVI6 < ZVI4 < ZVI3 \cong ZVI2 < ZVI8.$$

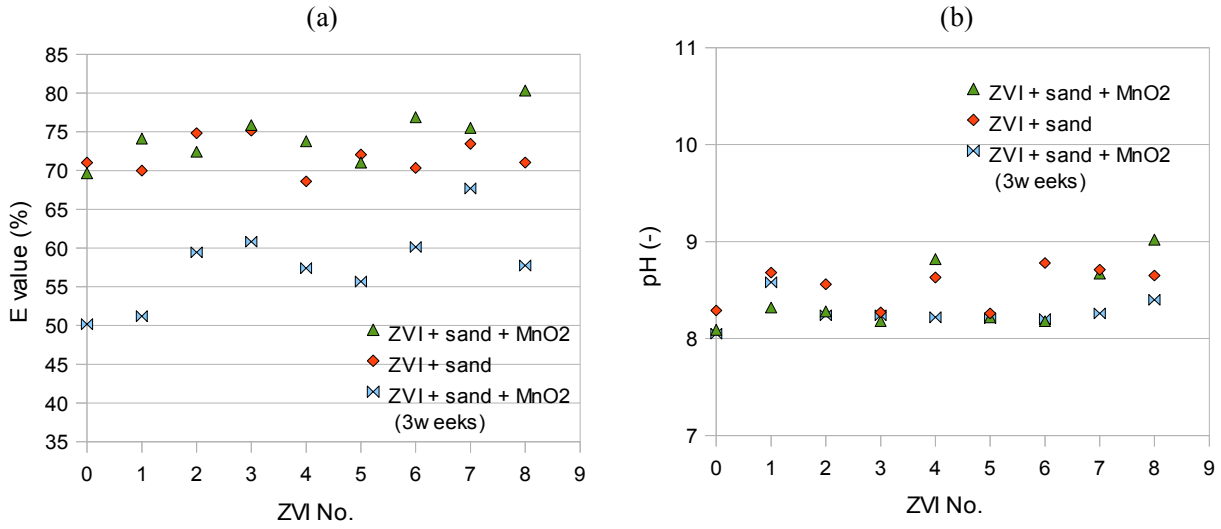

Fig.10: E value (MB discoloration efficiency) (a) and pH (b) of variable ZVIs in four different systems under non-shaken condition for 6 weeks and comparison to the corresponding values in ZVI+sand+MnO_2 systems after 3 weeks. ZVI No. 0 is blank which contains ZVI(0g)+sand(2g) and ZVI(0g)+MnO_2 (0.05g)+sand(2g).

Fig.10(a) shows that due to the extended experimental duration, the E value increased notably for all ZVIs. Furthermore after 6 weeks all ZVIs except ZVI2 and 5 show a tendency for improved MB discoloration in Fe+sand+MnO_2 systems compared to ZVI+sand systems. A possible explanation could be that due to the long experimental duration, MnO_2 was eventually exhausted and enough „free“ corrosion products were generated to increase MB discoloration by co-precipitation. The substantially older (see Table 4) ZVI2 becomes considerably less reactive after 6 weeks. Conceivably this is due to the sample being oxidized gradually by air humidity longer than the other ZVIs while being in storage and therefore could produce less new adsorbents. Therefore for both ZVIs, the discoloration was not increased in Fe^0+MnO_2 systems even for long experimental duration. Regarding the pH value, there are no detectable differences neither between the ZVIs nor the variable system constitutions.
An overview of the obtained values can be found in Fig. 11 where a comparison is made between the E-values obtained in the MnO_2 method (ZVI+MnO_2 for 3 weeks). Both curves exhibit very similar features in that they both show a very distinct minimum for ZVI5 while the other values seem to scatter rather randomly in a small range.

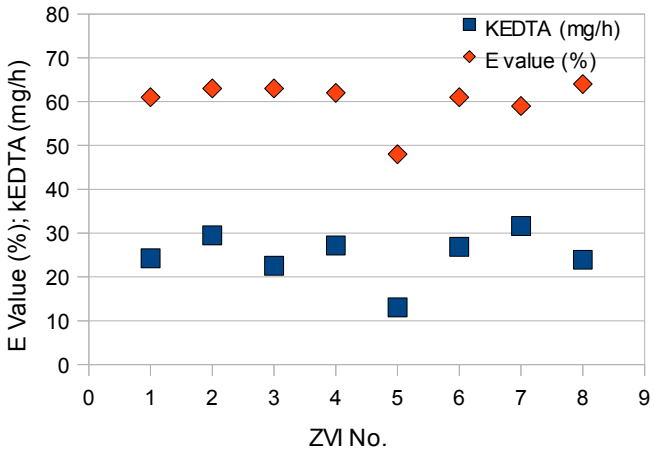

Fig.11: Comparison of the iron reactivity of ZVI1-8 obtained by MnO_2- and EDTA methods.

Impact of MnO_2 Type on MB Discoloration

The impact of different types of MnO_2 on the MB discoloration were investigated using three types of manganese oxide (i)psilomelane, (ii)manganite and (iii)X- MnO_2 for two systems of (1)MnO_2(0.2500g) and (2)ZVI+MnO_2(0.2500g) under shaken condition at 75 rpm for 2 weeks (Fig.12).

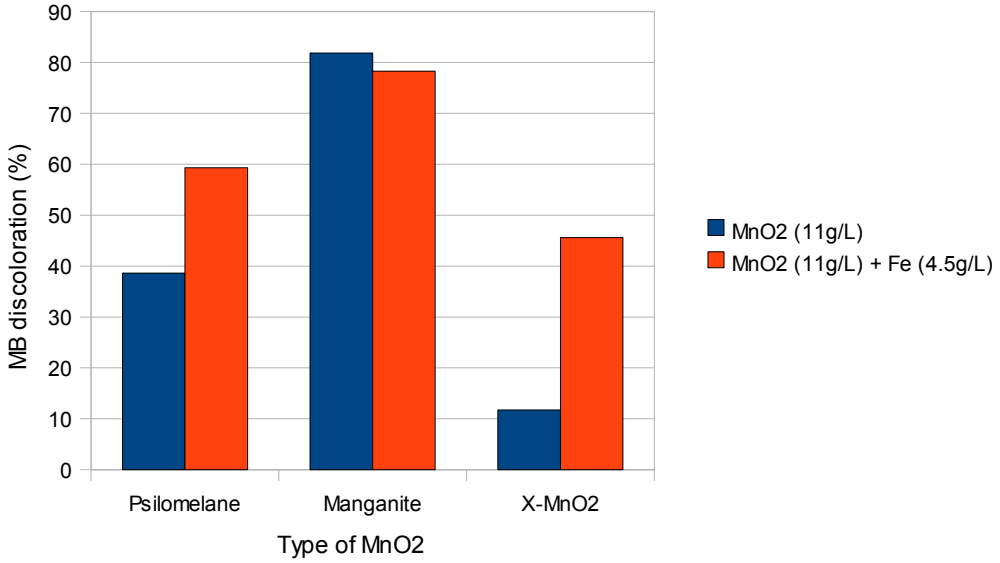

Fig.12: MB discoloration of Fe+MnO_2 for three different MnO_2 types after 2 weeks under shaken conditions at 75 rpm.

In the MnO_2 alone system, MB discoloration were observed in the rang of 82% (Manganite) > 38% (Psilomelane) > 11% (X-MnO_2), and in the mixture system, 79% (Manganite) > 60% (Psilomelane) > 45% (X-MnO_2).

Fig.12 shows that manganite has the highest MB discoloration in both systems followed by psilomelane and X-MnO_2 is the most inefficient. The observed difference is likely caused by different reaction priorities owing to the different mineral composition. The apparant reaction priorities of each MnO_2 species were summarized in Table 11.

Table11: Reaction priorities of each MnO_2 species

Reaction priority	Psilomelane	Manganite	X-MnO_2
Adsorption	+	++	-
Exhaustion	+	-	++
Generation corrosion products and new adsorbents	+	-	++

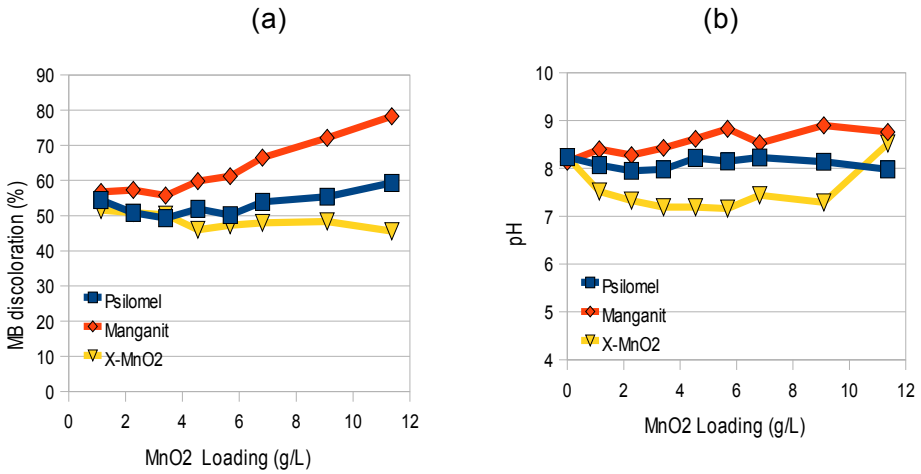

Fig.13: MB discoloration of MnO_2+Fe with variable type of MnO_2 over MnO_2 loading (a) and pH value (b)

Fig.13 (a) shows that even for increased MnO_2 loading, the MB discoloration was not improved for psilomelane and X-MnO_2. For manganite however an almost linear increase can be observed. This is probably due to the increasing available surface area for adsorption, where manganite has a good adsorption ability as indicated in Table 11. These results show clearly that while the MB discoloration of iron is improved by certain types of MnO_2 (Psilomelane and X-MnO_2), the extent of the discoloration is independent of MnO_2 loading.
Fig.13 (b) shows the pH values of the solution for all systems. Only for X--MnO_2, which as outlined in Table 11 has a higher ability for generating new adsorbent, a distinct slope can be observed, showing a clear pH decrease for higher MnO_2 loadings. The increased ability for adsorbent generation can be explained with the reaction

$$Fe^{2+} + MnO_2 + 2\ H_2O \Rightarrow FeOOH + MnOOH + 2\ H^+ \qquad (50)$$

where the proton release could be a plausible explanation for the decreasing pH value.
These results clearly demonstrate the necessity of characterizing the intrinsic reactivity of MnO_2 samples used in the MnO_2 test. The ideal situation is that of a universal reference material or at least universal protocols for testing MnO_2 (and Fe^0) reactivity. The present section has clearly demonstrated that the iPutech Fe^0 is very similar to six other available commercial materials in its chemical reactivity.

5.2 MB discoloration

5.2.1 Batch Test

Effect of Fe^0 Loading on the MB Discoloration

The effect on the MB discoloration efficiency of various amount of Fe^0 with or without sand was obtained after 6 and 3 weeks under non-shaken condition and after 1 week under shaken condition at 75 rpm. The result of these experiments was summarized in Fig.14.

Progressive MB discoloration from 20 to 80% for the Fe^0 only system and from 40 to 80% for the Fe^0+sand mixtures for 6 and 3 weeks respectively under non-disturbed conditions and 1week at shaken intensity 75rpm were observed. In the Fe^0+sand mixture systems (91g/L sand), even in the case of Fe^0 loadings of 0 g/L, MB discoloration extents of 70% for (a), 55% for (b) and 45% for (c) could be observed and MB discoloration increased only slightly for increased Fe^0 loadings.

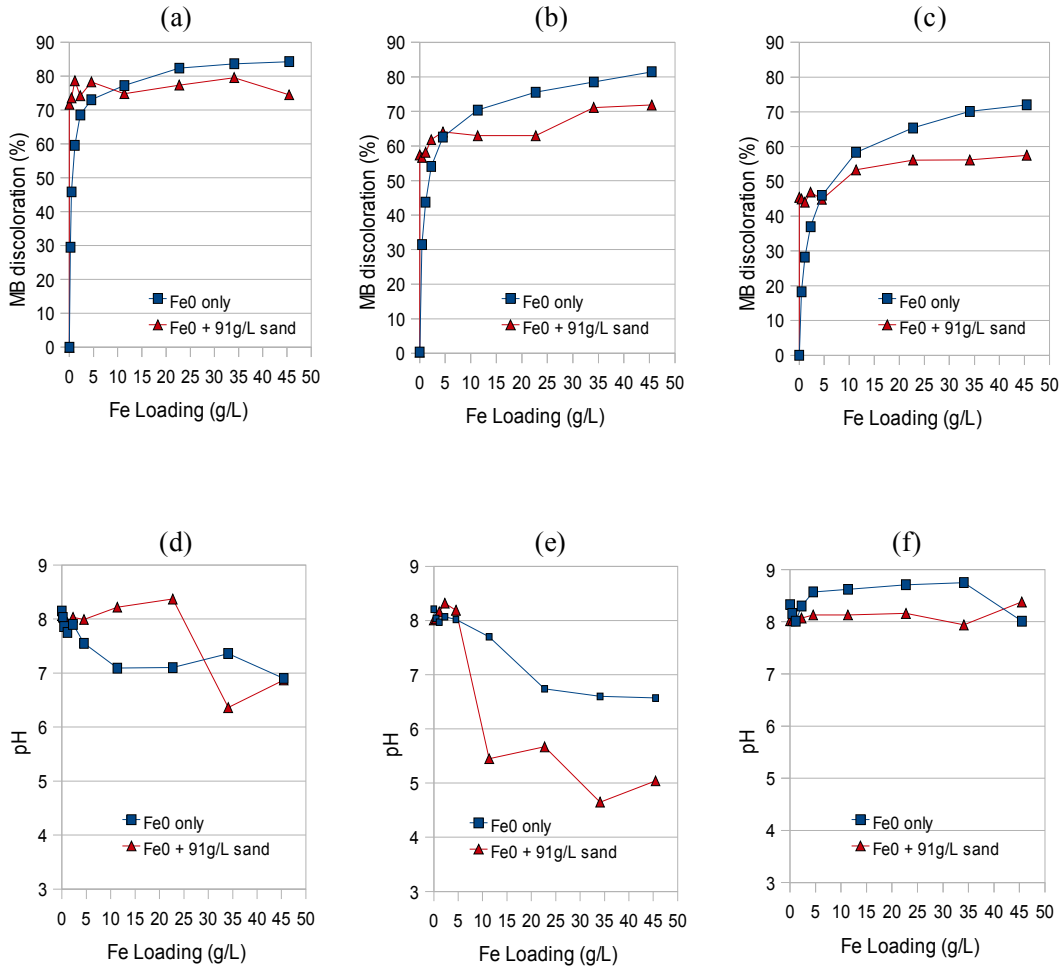

Fig.14: MB Discoloration extent of various Fe0 loadings with and without sand and under non-shaken conditions for 6 weeks (a) and (d), for 3 weeks (b) and (e) and under shaken conditions at 75 rpm for 1 week (c) and (f). The lines facilitate visualization and do not imply curve fitting.

The results show a plateau for Fe^0 loadings > 10 g/L and that the MB discoloration extent of pure Fe^0 (0 g/L sand) was higher than for the Fe^0+sand mixtures (91 g/L sand) under all three experimental conditions. In the Fe^0 only systems this plateau could correspond to either the MB diffusion limit or the existence of unused Fe^0 which was covered by other Fe^0 and had nearly no contact with MB. Under non-shaken conditions, the MB particles are transported to the reactive material by pure diffusion. As the reactive material was positioned at the bottom of the test tubes, the amount of transported and discolored MB particles was limited due to the relatively long transport distance to the reactive materials, namely the MB diffusion limit. However, although under shaken conditions the solute transport was increased, the plateau remained. A possible explanation for

this behavior would be the presence of unused Fe^0 in test tubes. Because the cross section of the test tubes is rather small so that even with a shaking intensity as high as 75 rpm, a relatively large portion of Fe^0 (>10 g/L) remained stationary, and inaccessible Fe^0 remained unused throughout the experimental duration. In the Fe^0+sand mixture systems, owing to the fact of slight increasing MB discoloration for increased Fe^0 loadings, and due to the previously explained MB diffusion limit the plateau remains at about the same value as for the pure Fe^0 systems.
Comparing the MB discoloration extents between mixed systems and Fe^0 only systems, one can see that for small Fe^0 loadings the discoloration in the mixed systems was superior to that of pure iron systems but is eventually surpassed by that of pure iron systems at Fe^0 loadings of approximately 5 g/L. It is conceivable that in the presence of sand, Fe^0 might work less effective for the MB discoloration than in pure Fe^0 systems (Assumption 2).
Obviously the sand has a certain adsorption ability with much more rapid kinetics than MB discoloration by iron corrosion, leading to the conclusion that possibly almost all MB discoloration must be accounted for by sand. It is considerable that 2.0 g of sand (91 g/L) are sufficient to screen the greater part of Fe^0 thereby inhibiting contacts between MB and Fe^0 particles where adsorption and co-precipitation would occur in the mixture systems. Another possible explanation of the observations would be given according to Mitchell (Mitchell et al., 1955), in the Fe^0+sand mixture systems, iron oxides are not free to co-precipitate, rather adsorbed onto sand to form iron oxide coated sand which has poorer adsorption ability than the parent sand. Therefore in the presence of sand, MB discoloration by Fe^0 is delayed, as long as free corrosion products are not available (Noubactep and Schöner, 2010). Fig. 14 shows the plateau at higher Fe^0 loading in the mixture system. This observation could indicate that the inhibition of MB discoloration in the mixture system was possible not caused by less adsorption ability of the iron oxide coating sand, but rather no free corrosion products were available for MB co-precipitation.
To check the validity of this assumption, the impact on the MB discoloration efficiency of Fe^0 using variable amounts of sand was investigated. We shall expand on this point in greater detail in the next section (§ 5.2.1).
The MB discoloration dependence on the experimental duration time was investigated. Comparing the results gained after 6 and 3 weeks an improvement in discoloration efficiency of 2-10 % could be observed.
While particle cementation was observed in the Fe^0 only system, such an effect could not be observed in Fe^0+sand mixtures. These observation suggest that the Fe^0 only systems reached a steady state after 6 weeks, in which no significant amount of corrosion products were produced while the Fe^0+sand mixture was still active in this sense and might indicate that the MB discoloration was still progressing by iron corrosion products in the mixture system. In long term tests it may thus be expected that the Fe^0+sand mixture will exhibit a better MB discoloration than the Fe^0 only systems. This would align well with the theory of Fe^0 mixing with sand freeing additional pore space to sustain Fe corrosion (Bi et al., 2009; Noubactep, 2011b).

pH Value
Fig. 14(d), 14(e) and 14(f) show the recorded experimental data on pH values, shown in for the experimental durations of 6, 3 and 1 week(s) respectively. The evolution of the pH values depends on the extent of iron corrosion (H^+ is consumed) and sand dissolution (H^+ is released). Iron corrosion induced a pH increase and sand dissolution the contrary. For 1 week, no pH change were observed for both systems. In the mixture system, pH decline due to sand dissolution were observed for 6 amd 3 weeks. In pure Fe^0 system, slight pH decline were observed.

Effect of Sand Loading on the MB Discoloration
As described in the previous section, the results suggest that in Fe^0+sand mixtures a substantial part of the MB discoloration may be accounted for by the sand inside the sample. To elucidate this relationship two more experiments were performed, one under non-shaken condition for 3 weeks and one using a shake intensity of 75 rpm for 1 week, with the mixtures of 4.5 g/L Fe^0+variable amounts of sand. Figure 15 shows a comparison between these results and those obtained from the previous study (§ 5.2.1) which was carried out for 91 g/L sand+various amounts of Fe^0. In the sand+various amount of Fe^0 system, MB discoloration were observed in a range of 55% - 72% for 3 weeks under non shaken conditions, and of 44% - 58% for 1week shaking intensity at 75 rpm. In the Fe^0 +various amount of sand system, MB discoloration were ranged between 48% -62% for 3 weeks, and 29%-50% for 1 week.

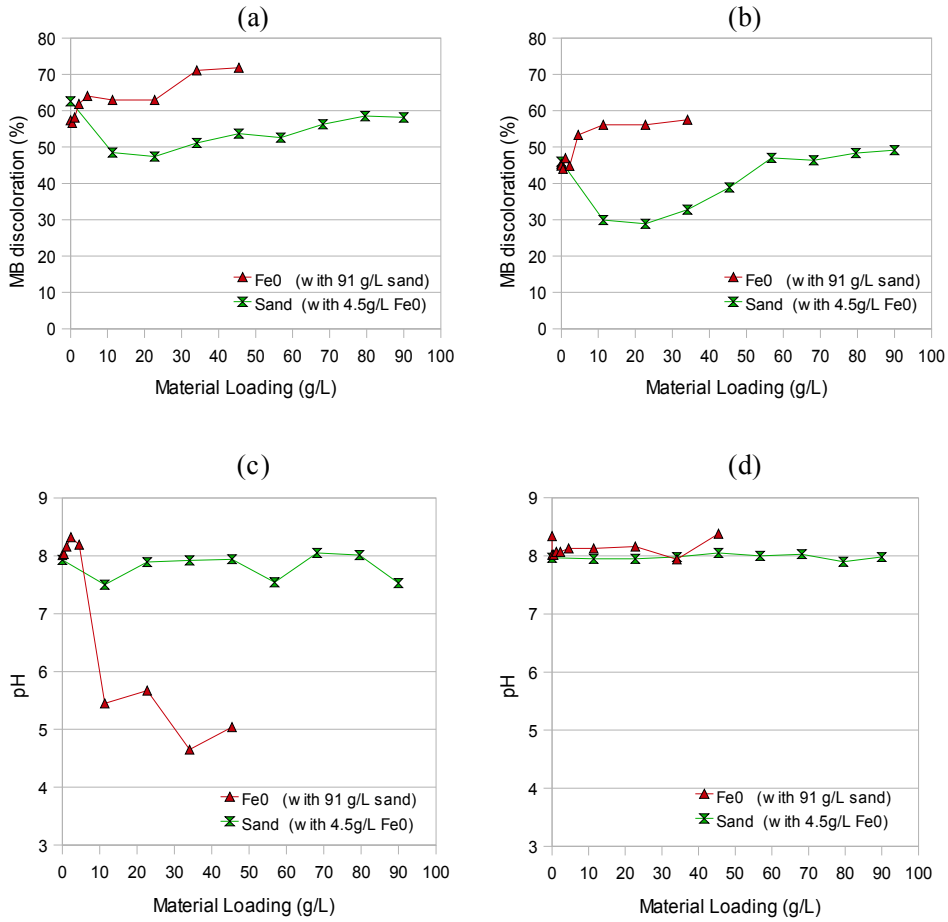

Fig.15: MB discoloration of various loading of different materials (Fe^0 and sand) after 3 weeks (a,c) and after 1 week at a shake intensity of 75 rpm (b,d).

Notably for variable sand loadings, the first points of the curves (sand loading at 0 g/L) showing MB discoloration are pretty high compared to all other points on the curve. For (a) this point even marks the maximum efficiency and for (b) it is about the same efficiency as the maximum reached at a loading of 60 g/L. For slightly increased sand loadings of 10 and 20 g/L, that is 0.25 and 0.50 g of sand, a drop in MB discoloration is observed, causing the curve to reach its minimum value at 20 g/L, whereafter an almost monotonous raise in discoloration with increasing sand loadings takes place under both experimental conditions. These observations support our „Assumption 2“ from the previous chapter (§ 5.2.1) where we propose that sand inhibits contacts between MB solution and Fe^0, causing the Fe^0 to work less for the MB discoloration in the presence of sand. Furthermore, looking at curve (b) we can even see the approximate range of sand loadings in which sand works as an inhibitor for MB discoloration, is 0.25-1.00 g (10 to 40 g/L). So according to our proposal that means that 0.25 g of sand is already enough to screen most part of 0.10 g (4.5 g/L) of Fe. The almost monotonous increase in discoloration for sand loadings >20 g/L, is attributed to the increase in available adsorption surface area upon sand addition and therefore expect all non-monotonic behavior to be random statistical deviations.
The results strongly suggest that in mixed systems and within the ranges of used amounts of materials for this experiment, which was 0 – 15 % expressed as the volume fraction of Fe^0, the Fe^0 is screened by sand, causing the MB discoloration activity to be decreased. However, since both materials have the ability to adsorb MB, the screening effect becomes more and more obfuscated as the amount of sand and with it the available adsorption surface area is increased.

pH Value
Iron corrosion induced a pH increase and sand dissolution contrary. For 1 week and 3weeks in the mixture system, no change on pH value was observed, however in Fe^0 pure system for 3 weeks, pH decrease was observed.

5.2.2 Column Experiment

This experiment was done aiming at the investigation of the impact on contaminant removal of various proportion of Fe^0/sand mixture.

A long term column experiment was carried out using ten columns, which were packed with 9 different Fe^0 volumetric ratio (0, 10, 20, 30, 40, 50, 70, 80, 100%). One column contained only sand, one contained 200g Fe^0, and the remaining 8 columns contained 100 g Fe^0. A 2 mg/L MB solution was pumped into the 10 columns at 0.1mL/min for 131 days. This experimental duration corresponds to about 73 % of the duration of the master thesis. Lengthening the experimental duration would have eased result's interpretation, but this was already a relatively too long time. The whole outlet solution was collected in pre-acidified sample bottles (Fig. 16). MB and dissolved Fe concentrations in the outlet solution were measured and the extent of MB discoloration per column were obtained (see Fig.17). MB breakthrough could be observed after 27-42 days for column 2-10, and after 72 days for column1 (Table 13).

Fig.16: Photograph of the ten test columns after 130 days.

Evidence for flow disturbance in Fe^0-containing columns

Fig.16 shows the experimental setup after 90 days in a state where the MB breakthrough has already occurred in all columns, as can be see from the blue colored outlet solution. Inside the columns MB adsorption onto sand can be seen as the blue color in the lower sand layers S1 in all columns. The brown color at the entrance of the reactive zones (RZ) indicates the presence of Fe(III) oxides. Iron oxides with mixed oxidation states (Fe(II)/Fe(III)) within the RZ and upward exhibits a dark green/black coloring which indicates prevailing anoxic conditions, meaning that most of the oxygen might have been used up at the entrance of the reactive zone. Finally at the top of each column there is the upper sand layer S2, which still remained most of its white color. This photographic documentation evidenced a flow disturbance within the reactive zone and upward because the homogeneous blue coloration of sand was limited to Column 1 and S1 in all other columns.

In order to investigate further the oxygen exhaustion at the entrance of the reactive zone, while disassembling the columns after completion of the experiment, the interior was taken out and inspected. Doing so it was found that indeed, only the lower brownish region of the RZ (1 to 3 cm) was subject to particle cementation, as had to be expected for areas in which oxidization occurred due to oxygen (Mackenzie et al., 1999). The particle cementation was harder at positions close to the entrance of the RZ. In the upper region no cementation could be found, meaning that indeed little amounts of dissolved oxygen reached the upper region of the reactive zone. These observations confirmed that oxygen is quantitatively consumed in a Fe^0 layer. However, the impact of compaction on the flow regime merit closer attention. It seems that after the O_2 scavenging layer/column a 'flow redistribution' room is necessary to obtain useful anoxic conditions for a second 'remediation Fe^0 layer'. This is particularly necessary for systems working under atmospheric conditions (O_2 levels 6.0 to 8.0 mg/L).

MB Breakthrough Curve

Fig.17 shows an overview of the measured MB breakthrough curves (a), the cumulative discolored MB (mg) (b), and the flow rate over time for each column (c). $[MB]_0$ in Fig.17 (a) means the initial concentration of MB solution (2.0 mg/L). Fig,17 (a) shows the different time of MB breakthrough of each columns, the earliest MB breakthrough were the column 7,8 and 9 and the latest was the column 1. The extent of unfiltered MB in outlet solution ($[MB]/[MB]_0$) were observed increasing steeply after the breakthrough from 0% to almost 100% of the column 1 after 120th day. Fig. 17(b) shows gradual increment of removed MB(mg) over time and total amount of removed MB at the end of experimental duration ranged from 29mg as the least amount of the column 8 to 50mg the most of the column1. Fig.17(c) shows the constant flow rate all over the experimental duration. For an unknown reason the inflow velocity for the column with 80 % Fe^0 loading was unexpectedly low at the onset of the experiment, however all subsequent measurements showed normal behavior.

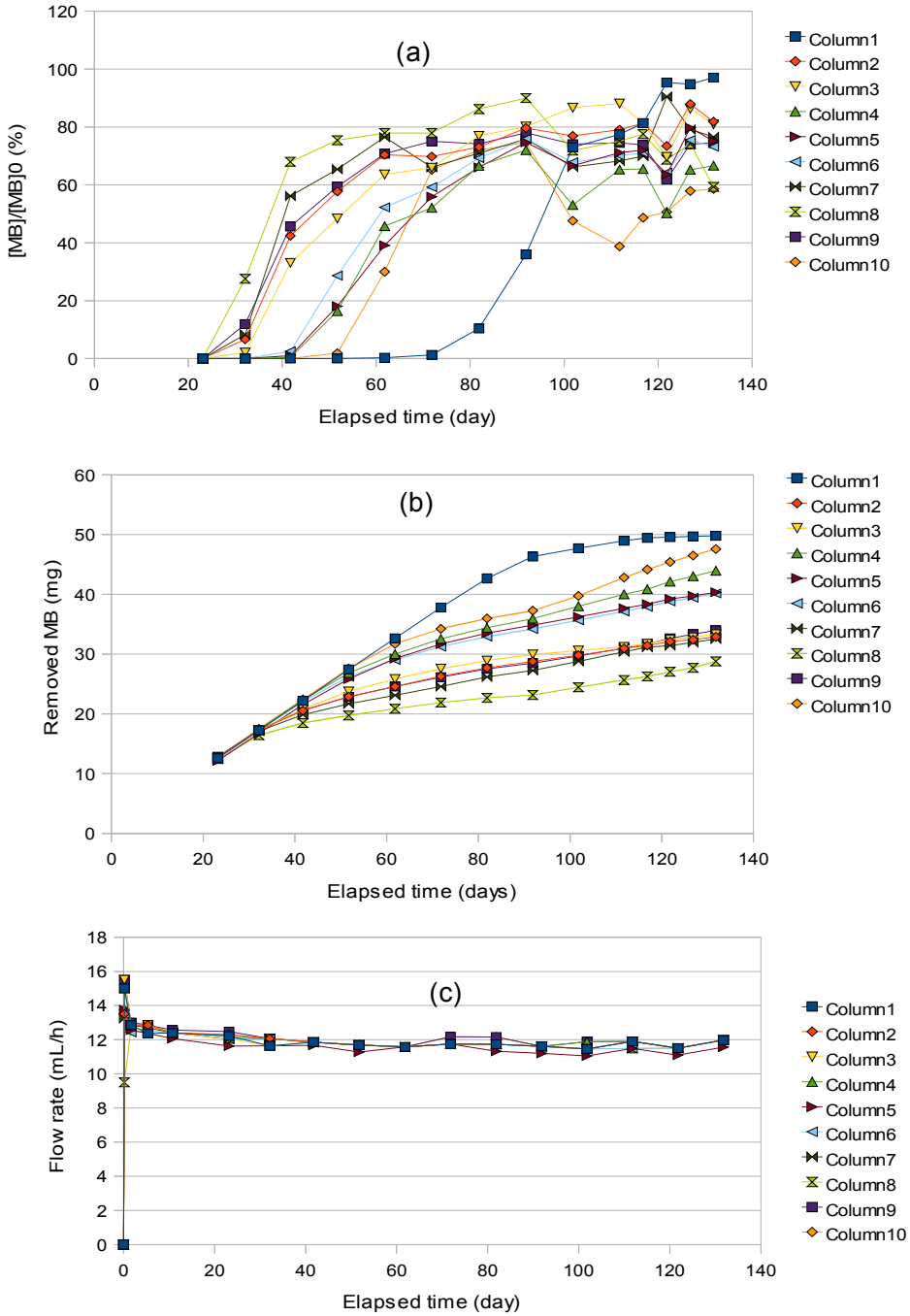

Fig.17: (a) Extent of unfilterd MB outflow[MB]/[MB]0 (%), (b) amount of discolored MB (mg) over time, (c) the evolution of flow velocity(mL/h).

Early Breakthrough of Fe^0 Amended Columns

The main objective of this study was to find the optimal proportion of Fe^0+sand mixtures that facilitates the most efficient MB discoloration, based on the assumption that Fe^0+sand mixtures (columns 2 to 8) have a higher discoloration efficiency than sand. In particular, in pure material systems (columns 1, 9 and 10 - Fig.17(a)) MB breakthrough should first occur in column 1 (0 g Fe^0), then in column 9 (100 g Fe^0) and lastly in column 10 (200 g Fe^0). On first sight however, experimental result disproves this trend. In fact, the order of efficiency was I >> X > IX, where each column is symbolized by his roman number. Considering the cumulative amount of discolored MB for the whole experimental duration (Fig. 17(b)) it is seen that system IX is one of the least efficient one. Only system VIII (80 % Fe^0) was less efficient. Systems II (10 % Fe^0), III (20 % Fe^0), VII (70 % Fe^0) were very closed to VII in their discoloration efficiency.

At first glance, the results of pure material systems (I, IX and X) are quite unexpected. However, they could be rationalized by the differential kinetics of MB adsorption on sand and MB co-precipitation with iron corrosion products. While the extent of adsorption onto sand solely depends on the available sand surface and the solution flow (contact time), MB co-precipitation additionally depends on the kinetics of Fe^0 oxidative dissolution. Accordingly, MB breakthrough in Fe^0-containing systems may be due to too rapid flow and too slow Fe^0 oxidation. This assumption is validated by system X (200 g Fe^0) being more efficient that system IX (100 g Fe^0). This result also clearly demonstrates that Fe^0 filtration is a deep-bed filtration process. In such systems, contaminants are removed in the whole system and not only at a reaction front (Noubactep 2010a). Remember that MB is not discolor by the redox couple Fe^{II}/Fe^0 and that contrarily to batch systems, not time is left for quantitative MB co-precipitation. In other words, there are little reasons for MB removal in a Fe^0 filter. This makes MB a tracer-like compound to characterize processes occurring within the system, in particular the porosity loss and the evolution of the hydraulic conductivity.

Considering the 10 systems, it is clear from Fig. 17 (a, b) it is evident that system I (0 % Fe^0) is the most efficient. The first explanation concerns the experimental time. From Fig. 17(a) we can see that after the breakthrough system I shows the steepest increase in MB concentrations of the effluent and on day 130 the $[[MB]/[MB]_0$ ratio already reaches 96%, meaning only 4 % of the inflowing MB is filtered, while almost all other columns have not yet surpassed $[MB]/[MB]_0 < 80$ %. Fig.17(b) also shows that system I reaches a plateau after 110 days while in the other columns the removal is still rising. Therefore we assume that for longer experimental durations the removal efficiency would have been proven inferior to that of mixed systems. This explanation is in tune with the relative kinetics of MB adsorption on sand and MB co-precipitation with iron oxides.

Another possible explanation for the observed superior discoloration efficiency of system I regards the constant inflow velocity. Generally in the Fe^0+sand mixtures, iron is corroded and expanded continuously. This iron corrosion expansion and transport of colloidal corrosion products causes a porosity reduction which would naturally lead to a decreasing inflow rate. However, as can be seen from Fig.17(c), the flow rates of all columns are almost constant. Hence, even though the porous pathway became smaller over time due to iron corrosion expansion and the transport of colloidal corrosion products, the inlet flow rate from the pump was almost constant, effectively causing the pore flow velocity to increase. We assume that an increased pore flow velocity will lead to less MB solution to be brought into contact with the reactive materials in these columns and so called preferential flow will be the result.

The increased pore velocity induces a heterogeneous pressure distribution, causing non-uniformity in the reformation of reactive materials inside the columns. Only column 1 kept uniformity inside, as can be seen from the photograph in Fig. 16 where the MB color is distributed equally over all the sand in the column. The non-uniformity shows looking at the other columns, where system II to VI and system VII to X do not show blue color in the S2 layers, while on the left hand side of the S2 layer in system VII blue color can be seen. Also in system VIII, Fe(III) oxide (brown color) is observed on top of the RZ, where actually the dissolved oxygen should have been captured and reduced at the bottom of RZ as explained above (§ 5.3). This might proof that the solution had less contact with iron due to the increased pore flow velocity. For these reasons we assume that the early breakthrough in the Fe^0+sand mixture systems was not caused by the exhaustion of reactive materials like it was the case for the sand column, but caused by the inhibition of MB discoloration of Fe by sand as explained in batch test, and the higher pore velocity as a possible reason.

Under the experimental conditions of this work (constant flow and 131 days experimental duration), the sand column showed the best MB discoloration efficiency. This result could be surprising if one considers that sand is an inert material, a pure adsorbent, while Fe^0 is a reactive material. Even though it is observed for the first time that Fe^0 can impair the efficiency of a sand filter, this result does not mean that sand is more

efficient that Fe^0 for MB discoloration in the long term. Sand is a pure adsorbent and its adsorption capacity is limited. In Fe^0-amended systems, the removal capacity is comparatively huge but the removing agent are only slowly generated in situ. This observation delineates the paramount importance of characterizing the reactivity of used Fe materials. The ideal material is the one producing enough corrosion product for contaminant removal at a given water flow rate. Accordingly, early MB breakthrough can be first attributed to the relative high pumping rate. This hypothesis is supported by the fact that the column with 200 g Fe^0 was the second more efficient system.

Modeling MB Discoloration of Pure Material Systems (I, IX and X)

As the discoloration dynamics as well as time scales of system I and the sand layer (S1) of all other systems can be assumed to be identical, we can calculate the masses of removed MB in the reactive zones (ΣMB_{RZ}) for system IX and X using the following equation:

$$\Sigma MB_{\mathrm{RZ}} = \Sigma MB_{\mathrm{dis}} - \Sigma MB_{\mathrm{S1}} = \Sigma MB_{\mathrm{dis}} - \frac{\Sigma MB_{\mathrm{column1,\ 0\text{-}BT}}}{H_{\mathrm{column1}}} \cdot H_{\mathrm{S1}} \tag{51}$$

Here ΣMB_{dis} is the sum of the total MB mass removed in the column, $\Sigma MB_{Column1,0\text{-}BT}$ is the sum of removed MB mass in system I from the beginning of the experiment to the onset of breakthrough ($\Sigma MB_{column1,0\text{-}BT}$ = 37.78mg), $H_{column1}$ is the height of system I ($H_{column1}$ = 44cm), and H_{S1} is the height of the S1 layer. For simplicity, the removed MB after the breakthrough in system I was not considered.

In order to calculate the MB removal by pure Fe^0 in the reactive zone, that is the extent of MB discoloration (*Discoloration*), the formula

$$Discoloration = \frac{\Sigma MB_{\mathrm{dis}}}{\Sigma MB_{\mathrm{in}}} \cdot 100 \quad (\%) \tag{52}$$

was used, where ΣMB_{dis} is the sum of discolored *MB* in the column, ΣMB_{in} is the sum of incoming *MB*, and M_{RM} is the mass of the reactive material (sand or Fe^0) in the RZ. For the material efficiency, the mass of discolored MB in the RZ per unit reactive material (*Efficiency*) was obtained using

$$Efficiency = \frac{\Sigma MB_{RZ}}{M_{RM}} \quad (mg/g) \ . \tag{53}$$

The calculated results are exhibited in Table 12. For system I, considering the whole column as the reactive zone, an efficiency of 0.041mg/g was obtained. The pure Fe^0 columns contain sand in S1 and S2 layer, but that this sand is not considered as the reactive materials.

Table 12: Calculated input/discolored mass of MB in S1, RZ and total, the extent of MB discoloration and the discolored MB per unit mass of reactive material.

	M_{RM}		Input			Discolored			in RZ	
Column	**Sand** (g)	**Fe^0** (g)	**ΣMB_{S1}** (mg)	**ΣMB_{RZ}** (mg)	**ΣMB_{dis}** (mg)	**ΣMB_{S1}** (mg)	**ΣMB_{RZ}** (mg)	**ΣMB_{dis}** (mg)	**Discoloration** (%)	**Efficiency** (mg/g)
1	**1205.3**	**0**	-	-	58.53	-	-	48.96	79.83	0.04
9	**0**	**100**	11.18	48.23	59.41	11.16	19.83	30.99	41.11	0.20
10	**0**	**200**	11.18	48.01	59.19	11.16	31.66	42.82	65.94	0.16

The resulting ranking of the MB discoloration extent is: IX < X < I. Even though Fe^0 is the more effective discoloration material, system I shows the highest discoloration efficiency. As explained above, this is conceivably caused by the preferential flow resulting from the non-uniformity due to the iron corrosion expansion. The higher discoloration in system X compared to system IX can easily explained with the different masses of Fe^0 in these two systems.
Table 12 shows that although the extent of MB discoloration in system IX is the lowest, its *efficiency* is the highest, rendering it most efficient. For column 1 the *efficiency* can be interpreted as the adsorption capacity of unit sand, while for system X this value means the existence of more unused Fe^0 than in system IX, where the Fe^0 depletion will never happen due to the porosity loss in systems with 100 % Fe^0 loading. Therefore we conclude that system X is the most unproductive system. To reduce the unused Fe^0 and improve the reactivity of Fe^0, as explained in § 2.4 'Column Design' the Fe^0 should be mixed with sand to gain more void space for the iron corrosion expansion. To this end, in order to find the optimal proportion in sand+Fe^0 mixtures for MB discoloration in this constant flow system, Fe^0+sand mixtures with Fe^0 loadings ranging from 10 to 100% were investigated in next chapter.

Modeling MB Discoloration of Fe^0 +Sand Mixtures (Systems II to VIII)
In Fig.17 (a) and 17 (b), the systems IV, V and VI (Fe^0 loading 30, 40 and 50 %) show higher removal efficiency than all other systems (II, III, VII and IX) and also the MB breakthrough which started after approximately 40 days was roughly 10 days later than for the other systems (VII, IIIX). As explained before, this delay of MB breakthrough could correspond to the different heights of the lower sand layer (S1 layer) . An illustration of the multi-layered columns of the Fe^0+sand mixtures, with their S1, RZ and S2 layers can be found in the bar chart in Fig.5. As depicted, the columns of Fe^0 loadings 30 (IV), 40 (V) and 50 % (VI) have considerably larger S1 layers than all other columns. These enlarged sand layers contribute to raise the discoloration amount of MB, as the MB adsorption front evolves first in the S1 layer and only after exhaustion of this layer reaches the RZ. When the MB adsorption front arrives at the reactive zone, MB is transported with higher pore flow velocity and less contact to adsorbent (sand, Fe^0 and iron oxides). To gain a better understanding of the processes in each layer, the MB removal rates in S1 and RZ are discussed in the next chapter.

MB Discoloration in S1 and RZ Layer (Systems II through IX)
The onset of MB breakthrough is different for each column. Table 13 summarizes the durations from the beginning of the experiment to the first observation of MB breakthrough, and from the breakthrough to the end of the experiment. The discolored MB per unit Fe^0 (*Efficiency*) was calculated using Eq.53 and listed in Table 13. In these terms, 30 % Fe^0 loading is the most efficient system with a value of 0.25 (mg/g). An efficiency ranking based on these values from the most to the least efficient system can be established:

IV > II = III = VI > V >IX > VII > VIII

For systems VI (70 %) and VII (80 % Fe^0 loading), the *Efficiency* is lower than in the system with 100% Fe^0 loading (system IX).

Table 13: The duration from the start of the experiment to the first observation of MB breakthrough (0-BT), and from the breakthrough to the end of the experiment (BT-end) and the mass of discolored MB per unit Fe^0 (*Efficiency*).

Column	**Fe^0** (%)	**0 - BT** (days)	**BT-end** (days)	**Efficiency** (mg/g)
2	**10**	27.29	104.52	0.22
3	**20**	32.13	99.68	0.22
4	**30**	41.74	90.07	0.25
5	**40**	41.74	90.07	0.21
6	**50**	41.74	90.07	0.22
7	**70**	32.13	99.68	0.18
8	**80**	27.29	104.52	0.15
9	**100**	32.13	99.68	0.2

We therefore conclude that for over 70% Fe^0 loading in the Fe^0+sand mixture systems, the effectiveness of Fe^0 becomes less than in the pure Fe^0 system. As the iron masses were identical (100g) for all systems, the ranking just presented should also reflect in the extent of the MB discoloration.in the RZ, as will be discussed below.

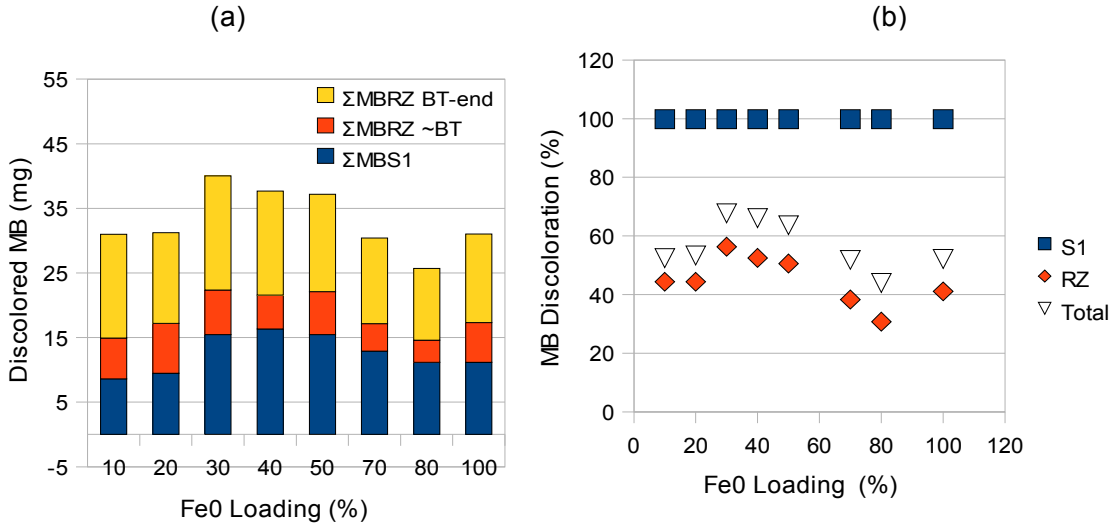

Fig18: (a) Cumulative mass of discolored MB before and after BT, (b) Total MB removal rate (Σdiscolored MB / Σ inlet MB) for each layer.

Fig. 18 (a) shows the cumulative mass of discolored MB in the S1 layer (blue colored bar) and in the RZ before (red bar) and after (yellow bar) the BT. Here ΣMB represents the total mass of the discolored MB in the given timespan/region: ΣMBS1 is the mass of discolored MB in the S1 layer, ΣMBRZ~BT is the mass of discolored MB in the RZ until the onset of BT, ΣMBRZ BT-end is the mass of discolored MB in the RZ from the onset of BT until the end of the experiment. Fig. 18 (b) shows the same data giving the discolored amount as the percentage of the total MB that passed through the filter (Σdiscolored MB / Σ inlet MB) for each layer.

The red parts of the bar-chart in Fig. 18 (a) show the discolored MB in the RZ until the onset of the BT, that is the breakthrough did not happen immediately after the MB solution reached the reactive zone, but a certain amount was discolored inside the reactive zone. The blue parts of the bars indicate the amounts of discolored MB inside the S1 layer (ΣMB_{S1}), showing clearly that due to their larger S1 layers the Fe^0 loadings 30, 40 and 50 % removed more MB in this layer than all other systems. Furthermore, as can be seen more clearly in Fig. 18 (b), even in the reactive zone (RZ) they show a significantly higher removal efficiency. Using this data of the total MB discoloration extent in Fig. 18(b) another efficiency ranking from the most to the least efficient setup can be created, reading:

$$IV > V > VI > II = III > IX > VII > VIII.$$

Both rankings share similar features in that the Fe^0 loading of 30 % ranks best and 70 and 80 % rank lower than the system with 100 % Fe^0 loading. We therefore conclude that the column with Fe^0 loadings 30 % has the optimal Fe^0 /sand mixture for MB discoloration and accordingly, that the Fe^0 loadings 70 and 80 % have the worst mixture. However there is some disagreement in between the two rankings concerning the ranks of Fe^0 loadings 10, 20, 40 and 50 %. From Fig. 18 (a), one can see, that there is little difference in the masses of the discolored MB in the RZ (ΣMBRZ ~BT+ΣMBRZ BT-end) for these four columns. The difference in the MB discolorations in these four columns however can be explained from the differences of the MB volumes entering the RZ (Σ inlet MBRZ). The length of the S1 layers for Fe^0 loadings 10 and 20 % were approximately only half as long as for the systems with Fe^0 loadings 40 and 50 %, and consequently the filtering capabilities of this layer were exhausted much earlier in the former systems, starting the MB discoloration in the RZ. This results in higher Σ inlet MBRZ for Fe^0 loadings 10 and 20 % compared to the 40 and 50 % cases, leading to the observed inconsistency in the ranking of these four systems.

As has been discussed in § 5.2.2, the MB solution in the reactive zone is transported with higher pore flow velocity due to the porosity reduction. It is conceivable that this change in pore flow velocity is related to the differences in the MB removal efficiency (Assumption 3). To elucidate this matter, the iron corrosion expansion rates, the porosity reduction and flow velocity changes were calculated as described in the next section.

Iron Release

Fig. 19 shows the concentrations of dissolved iron - Fe(II) and Fe(III) species - in the outlet solution, where every curve shows a peak after approximately 30 days. It may be assumed that the dissolved iron was somehow captured or accumulated in the RZ and S2 layers until it was eventually released. For the column with 10 % Fe^0 loading (System II), the dissolved iron concentration is clearly measurable right from the beginning of the experiment and also the peak value is much higher than in all other cases. This is due to the fact that this column is the only one that does not have a S2 layer, which apparently retains most of the iron in all other cases. The transport of dissolved iron above the RZ and the retention in both layers can be visually observed as the black color in the S2 layer in the photograph shown in Fig. 16. We attribute mechanism of retention to (i) the adsorption of iron oxides onto sand, and (ii) the precipitation as iron (hydr)oxides.

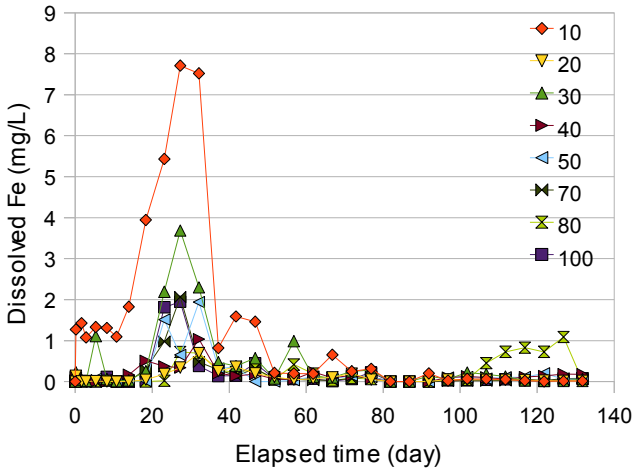

Fig.19: Concentration of dissolved iron in the effluent of columns with Fe^0 loadings 10-100%.

Application of Iron Corrosion Induced Rust Expansion Model

Using Eq. 39, the diameter change in time and the volume expansion fraction due to the corrosion expansion were modeled considering spherical particles with an average the initial diameter of 1.2mm (see Fig. 20).
In this study a constant corrosion current density of i_{corr} = 1 μA/cm^2 was assumed, which corresponds to a moderate corrosion risk (Chen and Mahadevan, 2006), i_{corr} = 6.3 μA/cm^2 for a stagnant aerated solution with pH 5 at room temperature and i_{corr} = 63 (μA/cm^2) for an agitated aerated solution with pH 5 at room temperature (Roberge, 2008). For our experimental setup the condition i_{corr} = 63 μA/cm^2 seems to be most appropriate to be used. However in using this value, the calculated porosities of the Fe^0 loadings 70,80 and 100 % become zero after 80 days, which contradicts the experimental observation. This inability of the i_{corr} value taken from the literature to match the experimental condition may well be associated with the non-uniform corrosion state depending on the position. As can be seen from Fig.16 the color of corrosion products shows that the dissolved oxygen was exhausted at the entrance of the reactive zone while the upper reactive zone was corroded under anoxic condition. Thus the corrosion current density at the upper part of the RZ is likely to be much smaller than at its entrance.

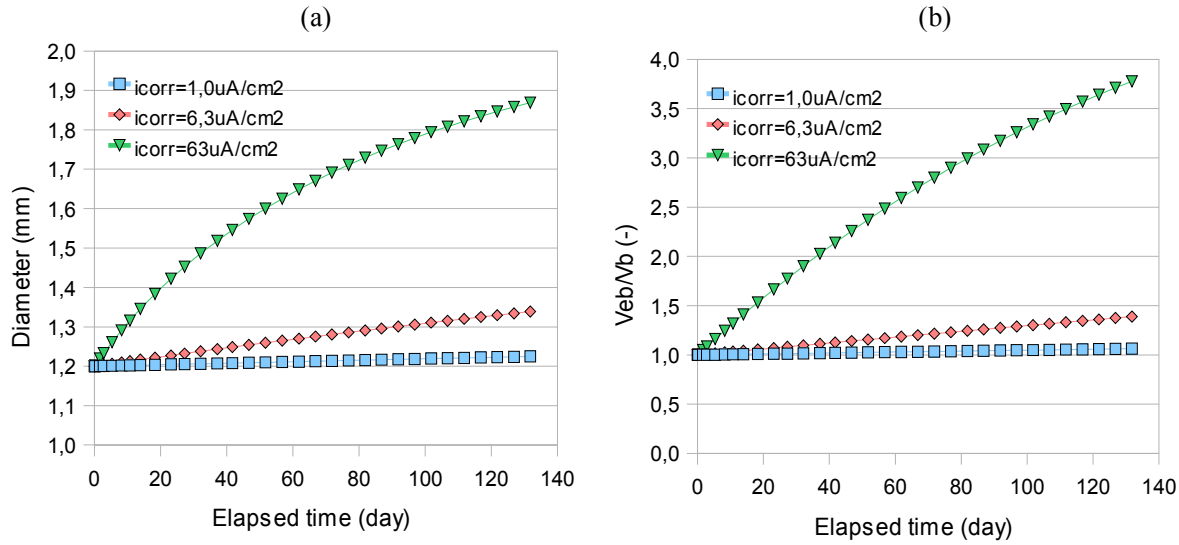

Fig.20: Diameter expansion (a) and fraction of volume expansion (b) over time calculated for three different corrosion current densities.

Modeling Porosity Reduction

The porosity change due to iron corrosion expansion at i_{corr} = 63 ($\mu A/cm^2$) were modeled using Eq. 36 and Eq. 48 and plotted as functions in time, as can be seen in Fig. 21. The graph shows that higher Fe^0 loadings are accompanied by a more rapid porosity reduction (steeper declinations). Accordingly, Fe^0 loadings of 70, 80 and 100 % have the steepest declinations and the Fe^0 loading of 10% has the most gradual declination of all cases. Furthermore, in the former case the porosities of the columns become zero earlier before day 80 of the experiment, whereas for Fe^0 loadings of 50 % this is the case only after 130 days. Due to the inverse proportionality Fe loading as well as porosity decrease over time, even though at the beginning of the experiment the system with Fe^0 loading of 100 % had the highest porosity, at the end of the experimental duration, the Fe^0 loading of 10 % shows the highest porosity.

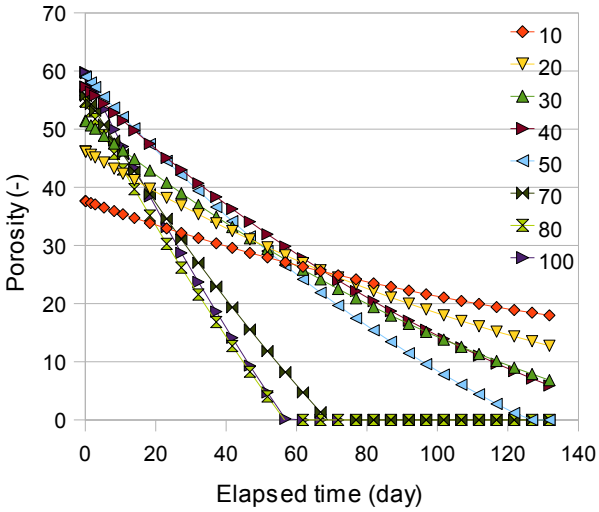

Fig.21: Porosity evolution over time of Fe^0 loadings 10 to 100 %.

Pore flow velocity Change due to Porosity Reduction and MB Discoloration

The pore flow velocity change was derived from the porosity reduction for i_{corr} = 63µA/cm² using the formula:

$$Poreflowvelocity(cm/h) = \frac{Flowrate(ml/h)}{Columncrosssection(cm^2) \times porosity} \quad (56)$$

Since the flow rate was almost constant in time (compare Fig. 17 (c)), its mean value (12 ml/h) was used for calculation. At the time the porosity becomes zero, also the pore flow velocity is considered to be zero. The pore flow velocities of each Fe^0 loading at several time steps calculated for i_{corr} = 63µA/cm² are exhibited together with the MB discoloration extent ([MB]/[MB]$_0$) in Fig.22. As can be seen from the graph those Fe^0 loadings where the pore flow velocity is high, usually have a high extent of [MB]/[MB]$_0$, that is the output of unfiltered MB is high. The overall shape of both curves (S-shape) the pore flow velocity and [MB]/[MB]$_0$ remains more or less the same throughout day 27 to day 46. Because in our model the pore flow velocities of systems with high Fe loading tend to zero, their flow velocities can not be compared for later times and are set to zero, hence the change in the shape of the curves for high Fe loadings after day 46. The apparent correlation between the evolution of the pore flow velocity and the ratio [MB]/[MB]$_0$ at each point in time clearly suggests that MB leaking is caused by the increased pore flow velocity due to the porosity loss. Thus "Assumption 3", i.e. that the change in pore flow velocity change might be related to the differences in MB removal efficiency (see section 5.2.2), was verified leading to the conclusion that under continuous flow condition the MB discoloration efficiency is affected by the pore flow velocity change due to porosity reduction. Before the pore flow velocities of systems with Fe loadings 80 and 100 % go to zero, that is before day 56, the flow velocities in descending order read:

V < IV < VI < III < II < VII < IX < VIII

This ranking has a striking similarity to the order of the MB discoloration extent obtained in § 5.2.2. In fact it almost resembles its reverse order, meaning that those systems with high pore flow velocities were found to have low MB discoloration extent and those with low pore flow velocities have a high MB discoloration extent. This conclusion is consistent with the fact that Fe^0 filtration is a size-exclusion process that is optimized by in-situ generated iron corrosion products reducing the pore space or increasing size-exclusion. In other words, the view is confirmed that properly designing a Fe^0 bed is finding a balance between increased reactivity (larger Fe^0 amounts) and larger porosity (lower Fe^0 amounts). In all the cases it is clear that a 100 % Fe^0 bed is not sustainable as a rule, even the currently used rule of thumb (1:1 weight ration Fe^0:sand corresponding to about 25 % v/v) seem not to be optimal.

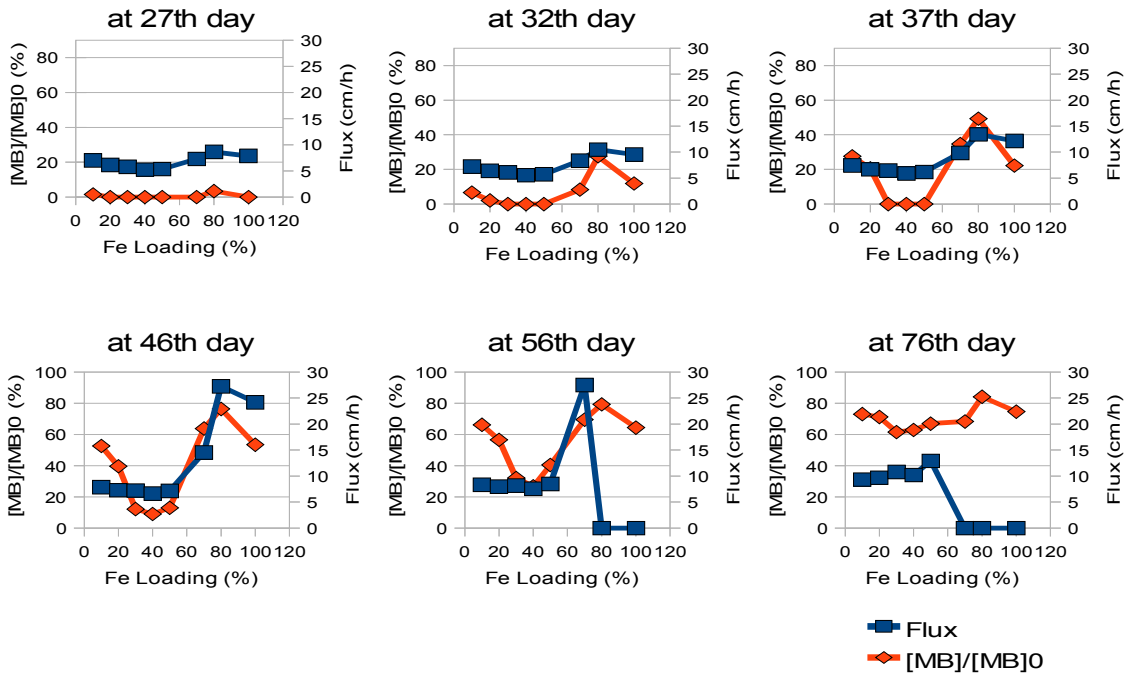

Fig.22:Evolution of pore flow velocities (expressed as flux) and the extent of the unfiltered MB outflow [MB]/[MB]$_0$ at several time steps (27th-76th day).

5.2.3 Summary of Results

The present study has clearly shown that: (i) sand is a good MB adsorbent (adsorptive discoloration), (ii) Fe^0 is a good discoloration agent (MB co-precipitation). However, upon admixture (Fe^0+sand), the discoloration kinetics of both materials is lessened. From the open literature, it is known that adsorption of MB onto metal oxide is very low (e.g. Saha et al., 2011).

In the presence of sand, Fe(II)/Fe(III) species from Fe^0 oxidative dissolution are adsorbed onto the surface of sand, progressively forming an oxide coating. Iron oxide coated sand has been demonstrated a worse MB adsorbent than pure sand (Mitchell et al., 1955). However, not the coating is responsible for decrease MB adsorption on sand in batch studies, but rather the non availability for free corrosion products for MB co-precipitation. Similar results have been reported for the Fe^0/MnO_2 systems were the absence of free corrosion products is due to Fe(II) consumption of the reductive dissolution of MnO_2 (Noubactep, 2009a; Ghauch et al., 2011). In the long term, when the adsorption capacity of available sand for Fe oxide is exhausted, excess free corrosion products will co-precipitate MB. This stage was only partly achieved in this study.

Inversely, in the presence of Fe^0, the surface of sand competes for the adsorption of three cationic species: MB, Fe(II) and Fe(III). Because MB is present at maximal level at the start of the experiment, there is no real competition since Fe(II) and Fe(III) species are only slowly and progressively generated from Fe^0. Accordingly, the inhibition of MB removal in Fe^0/sand occurs with the same mechanism regardless which material is abundant.

In column experiments, MB adsorptive discoloration is impaired by the presence of Fe^0 in two different ways: (i) in situ sand coating with iron oxides accelerates MB breakthrough by decreasing MB adsorption onto sand, (ii) pore filling with in situ generated iron oxides increased the flow resistance at the entrance zone of the reactive layer. The system reacts to increased resistance at the entrance zone of the reactive layer by locally creating privileged flow paths (so-called preferential flow) which results in less particle/solution interaction in the whole column and not only in the Fe^0-containing zone. Thus more than a simple model contaminant, MB is an indicator (or a 'pseudo-tracer') for the identification of process occurring in Fe^0systems. It is essential in this regards to recall that MB can not be significantly discolored by a reductive reaction coupled to Fe^0 oxidation. On the other hand the experimental conditions, in particular the trace amounts of MB (micro-pollutants) can not favor any significant oxidative degradation of MB (Li et al., 2012). Accordingly, repeating the experiment herein with slower flow rate will enable the experimental determination of the optimal Fe^0/sand ratio that conciliate minimal porosity loss (maximal amount of sand) and maximal contaminant removal efficiency (maximal amount of Fe^0). The results herein clearly indicate that the optimal ratio is lower than 50 %. In other words, future investigations should concentrate on Fe^0/sand ratios < 50 %, while eventually using 100 and 50 % as negative references. Beside these 'negative references', the use of a pure adsorbent systems (e.g. anthracite, gravel, pumice, sand), longer experimental duration, and the same S1 layer will accelerate knowledge acquisition for the optimal design of Fe^0 filtration systems.

6. Conclusion

In this work, we studied the influence that different volumetric ratio of Fe^0 have on the contaminant removal efficiency of Fe^0+sand filtration systems using Methylene Blue (MB) as a model contaminant. A number of experimental configurations have been studied utilizing batch (Batch Test 1) as well column studies. In Batch Test 1 an inhibiting property on the sand on the efficiency of Fe^0 for MB discoloration was observed as pure Fe^0 systems were more efficient than Fe^0/sand mixtures. We account for this behavior by the sand covering large parts of the iron surface, thereby reducing the contact area between solution and iron and hence adversely affecting the contaminant transport to the iron surface (§ 5.1.1. and 5.1.2). However studying the interior of the columns that have been using in the long time column study, we found in accordance with expectation that sand also successfully avoids particle cementation of iron corrosion products. In doing so it sustains the reactivity of Fe^0 as well as the contaminant removal process due to iron corrosion in the long term much better than would be the case with pure Fe^0 systems (§ 5.1.1. and 5.3.5). In conclusion this means, that despite the reactivity decrease the overall filtration system becomes more efficient and also cheaper, by making better use of the reactive material.

The intrinsic reactivity of different Fe^0 materials have been characterized using two different methods: In EDTA solution and by addition of MnO_2 (§ 5.2.1 and 5.2.2). With either method, we find that ZVI5, which has a spherical shape, shows the least reactivity (§ 5.2.2). While further investigation might be necessary to ensure this finding, both methods were found reliable for material screening (Noubactep, 2010a; 2011c; 2012c).

In a column study, we determine the volumetric proportion of iron and sand in Fe^0+sand filtration systems necessary for optimal MB discoloration efficiency under continuous upflow conditions. The experiment lasted for 131 days, comparing 10 different setups in the range of 0 to 100 % Fe^0 loading, where three of the systems were pure systems: 0 g Fe^0 (pure sand system) for comparison, a 100 g Fe^0 system as a representative for pure iron system and a 200g Fe^0 system as double amount of pure iron system. The other eight systems featured various iron loadings in order to determine the optimal proportionality. It was found that the most efficient Fe^0+sand systems were the ones containing 30 to 50 % Fe^0 loading, which is in good agreement with the theoretical prediction by Noubactep (Noubactep and Schöner, 2010) who showed that for iron loadings over 50 % (v/v) early filter clogging will occur. The least efficient combination were those setups with 70 and 80 % Fe^0 loading, the efficiency of which was even lower than in the pure Fe^0 system. All Fe^0+sand mixtures were found seemingly to feature early MB breakthrough when compared to the pure sand system. All Fe^0+sand mixtures were found seemingly to feature early MB breakthrough when compared to the pure sand system. The fact that sand is a good adsorbent for MB is well documented (Mitchell et al., 1955; Varlikli et al., 2009). Intuitively, however, using Fe^0 aims at increasing the removal capacity for any contaminant. On the other hand, it is well-known that MB adsorption onto iron oxides is comparatively low (Pirillo et al., 2009; Saha et al., 2011). Moreover, Mitchell et al (1955) have demonstrated that iron oxide coated sand is a poorer MB adsorbent than pure sand. Accordingly, the results presented here are by no means unexpected. Rather, they demonstrated that rather than a 'simple' model contaminant, MB may be regarded as an indicator (a tracer-like compound) for processes in Fe^0/H_2O systems. In fact, in-situ generated iron oxides occupy the pore volume and lessen the adsorption capacity of sand for MB. These experimental observations open new avenues for the research on ' remediation with Fe^0". The experiments herein could be repeated with other dyes having better adsorptive affinity to iron oxides and/or with other admixing materials having a lower affinity to MB than sand.A possible relationship between the pore flow velocity and the unfiltered MB outflow ($[MB]/[MB]_0$) was investigated. For that sake, a mathematical model originally developed by Chen and Mahadevan (2006) for the study of iron rod corrosion expansion has been adopted to calculate the porosity decrease in Fe^0+sand mixtures over time. Indeed do the results of this comparison indicate that there could be seemingly a positive correlation showing that an increase in the flux is accompanied by an increase in unfiltered MB outflow, i.e. MB discoloration decrease (§ 5.2.2).

As demonstrated in this study, the model at hand can elegantly be applied to study the porosity decrease in active porous media due to iron corrosion or generally particle growth in order to target the contaminant transport dynamics and finally the breakthrough of dissolved contaminants, giving prospect to applications in permeable reactive barriers. However in order to confirm the correctness of the mathematical relationship between the flux change and contaminant breakthrough, further experiments with variable flow conditions and filter sizes need to be performed.

7. Epilogue

The presented work corresponds to the original manuscript submitted and available in the Geoscience library of the University of Göttingen. Minor revisions were performed, mostly limited at actualising bibliographic references and slightly ameliorate the readability.

This work determines a 17 years-lasting discussion (from 1995 on) discussion on the role of sand admixing on the performance of Fe^0 in Fe^0-based filtration systems. While some previous works have correctly regarded inert material admixture as a powerful tool to sustain permeability (e.g. Gottinger et al., 2010; Moraci and Calabrò, 2010; Calabrò et al., 2012), the relationship between observed increased reactivity and inert material admixture was not (and is still not) clear (Song et al., 2005; Bi et al., 2009; Ulsamer, 2011; Ruhl et al., 2012a; 2012b). The research group of Dr. Noubactep has clearly demonstrated theoretically that sustainable Fe^0-based filtration systems are only those containing less than 51 % Fe^0 (vol/vol) (Noubactep et al., 2010; Noubactep and Caré, 2011; Noubactep et al., 2012a; 2012b).

It is essential to point out that the volumetric proportions are given here. The ratio of 51 % Fe^0 is valid for a compact material like quartz, for porous materials (e.g. pumice) the internal porosity, its accessibility and its interconnectivity have to be properly considered (Noubactep and Caré, 2010; Biliardi et al., 2013). Furthermore, the size, the shape and the smoothness of used particles (Fe^0 and admixing materials) should be considered (Kubare and Haarhof, 2010; Btatkeu et al., 2013). In particular, the smoothness of the surface is coupled to the ability to adsorb both contaminants and Fe species to form in situ Fe-oxide-coated material. If all these parameters are not properly considered, seemingly controversial results will continue to be published. A typical example is a recent paper by Ruhl et al. (2012b) entitled "Evaluation of two-component Fe(0) fixed bed filters with porous materials for reductive dechlorination."

Disregarding any reaction mechanism (e.g. extent of dechlorination), Ruhl et al. (2012b) primarily tested anthracite (porous), gravel (compact), pumice (porous) and sand (compact) as admixing agents to Fe^0 in long term column experiments for trichloroethylene (TCE) decontamination. The aim of their experiments was to test the ability of used materials to sustain the long term efficiency (reactivity and permeability) of the filtration system. Results confirmed sustained permeability in columns containing porous additive but no significant difference could be documented in terms of reactivity (H_2 evolution). The results of Ruhl et al. (2012b) seemingly challenge the common use of pumice as better material than sand for water treatment (e.g. Ghebremichael et al., 2012) and the concept that admixture of non expansive materials is a prerequisite for filter sustainability. However, a close look on the used experimental design reveals that Ruhl et al. (2012b) have solely characterized the reactivity of the same mass of Fe^0 (100 g) in all four systems. To properly discuss their results with respect to the named objectives, Ruhl et al. (2012b) should have performed at least a parallel experiment in a column containing a pure layer of 100 g Fe^0 (100 % Fe^0). Four additional parallel columns containing each only one of the tested additives (0 % Fe^0) would have eased results´ discussion. One merit of the present thesis has been to implement a 0 % Fe^0 system which was crucial for the discussion of the obtained results.

Finally, in finding out that a species with little affinity to Fe corrosion products exceeds a Fe^0-based filtration system sooner than a pure adsorbent filtration system, the present thesis has opened new avenues for the research on designing Fe^0 filters. Methylene blue (MB) could be used to investigate processes in Fe^0/H_2O systems within a short time. Parallel experiments with species having more affinity to Fe oxides will necessarily last for longer times and give complementary information. More research with MB is needed before some rule of thumb or design criteria for Fe^0-based filtration systems may be formulated.

8. References

BARTZAS G., KOMNITSAS K. (2010): Solid phase studies and geochemical modelling of low-cost permeable reactive barriers. Journal of Hazardous Materials 183, 301–308.

BTATKEU K. B.D., MIYAJIMA K., CARÉ S., NOUBACTEP C. (2013): Testing the suitability of metallic iron for environmental remediation: Discoloration of methylene blue in column studies. Chemical Engineering Journal, doi:10.1016/j.cej.2012.11.072.

BENJAMIN M.M., SLETTEN R.S., BAILEY R.P., BENNETT T. (1996): Sorption and filtration of metals using iron-oxide coated sand. Water Research 30, 2609–2620.

BI E., DEVLIN J.F., HUANG B. (2009): Effects of mixing granular iron with sand on the kinetics of trichloroethylene reduction. Ground Water Monitoring and Remediation 29, 56–62.

BILIARDI S., CALABRÒ P.S., CARÉ S., MORACI N., NOUBACTEP C. (2013): Effect of pumice and sand on the sustainability of granular iron beds for the removal of CuII, NiII, and ZnII. Clean - Soil, Air, Water. Doi: 10.1002/clen.201100472.

BURRIS D.R., CAMPBELL T.J., MANORANJAN V.S. (1995): Sorption of trichloroethylene and tetrachloroethylene in a batch reactive metallic iron–water system. Environmental Science & Technology 29, 2850–2855.

CALABRÒ P.S., MORACI N., SURACI P. (2012): Estimate of the optimum weight ratio in zero-valent iron/pumice granular mixtures used in permeable reactive barriers for the remediation of nickel contaminated groundwater. J. Hazard. Mater. 207-208, 111-116.

CARÉ S., CRANE R., CALABRO P.S., GHAUCH A., TEMGOUA E., NOUBACTEP C. (2012): Modelling the permeability loss of metallic iron water filtration systems. Clean - Soil, Air, Water, doi: 10.1002/clen.201200167.

CHEN D., MAHADEVAN S. (2006): Chloride-induced reinforcement corrosion and concrete cracking simulation. Cement & Concrete Composites 30, 227–238.

COMBA S., MOLFETT D.A., SETHIR R. (2011): A Comparison between field applications of nano-, micro-, and millimetric zerovalent iron for the remediation of contaminated aquifers. Water, Air, and Soil Pollution 215, 595–607.

CORNELL R.M., SCHWERTMANN U. (2003): The iron oxides: Structure, properties, reactions, occurrences and uses. VCH Verlag, Weinheim.

CRANE R., NOUBACTEP C. (2012): Elemental metals for environmental remediation: learning from hydrometallurgy. Fresenius Environmental Bulletin 21, 1192–1196.

CRAWFORD R.J., HARDING I.H., MAINWARING D.E. (1993) Adsorption and co-precipitation of single heavy metal ions onto the hydrated oxides of iron and chromium. Langmuir 9, 3050–3056.

CRITTENDEN J.C., TRUSSELL R.R., HAND D.W., HOWE K.J., TCHOBANOGLOUS G. (2005): Water treatment: Principles and design, 2nd ed., John Wiley & Sons, Inc., New Jersey.

DEVLIN J.F., PATCHEN J. (2004): The effect of diluting granular iron with a non-reactive porous medium on contaminant transformation rates. Presented at the 5th Joint Conference of the IAH-CNC and the Canadian Geotechnical Society (CGS), Quebec City, October 24-27.

DIAO M., YAO M. (2009): Use of zero-valent iron nanoparticles in inactivating microbes. Water Research 43, 5243–5251.

DOE (1993): FUNDAMENTALS HANDBOOK CHEMISTRY Volume 1 of 2.

FARADAY R.S. (1961): Consults the scholars: The origins of the terms of electrochemistry. Notes and Records of the Royal Society of London 16, 87–220.

FENDORF S.E., LI G. (1996): Kinetics of chromate reduction by ferrous iron. Environmental Science & Technology 30, 1614–1617.

GHAUCH A., ABOU ASSI H., TUQAN A. (2010) : Investigating the mechanism of clofibric acid removal in Fe^0/H_2O systems. Journal of Hazardous Materials 176, 48–55.

GHAUCH A., ABOU ASSI H., BAYDOUN H., TUQAN A., BEJJANI A. (2011): Fe^0-based trimetallic systems for the removal of aqueous diclofenac, Mechanism and kinetics. Chemical Engineering Journal 172, 1033–1044.

GHEBREMICHAEL K., WASALA L.D., KENNEDY M., GRAHAM N.J.D. (2012): Comparative treatment performance and hydraulic characteristics of pumice and sand biofilters for point-of-use water treatment. J. Water Supply Res. Technol. AQUA 61 (4), 201-209.

GHEJU M. (2011): Hexavalent chromium reduction with zero-valent iron (ZVI) in aquatic systems. Water, Air, and Soil Pollution 222, 103–148

GHOSEMI J., ASADPOUR S. (2007): Thermodynamics studies of the adsorption process of methylene blue on activated carbon at different ionic strengths. Journal of Chemical Thermodynamics 39, 967–971.

GOTTINGER A.M., WILD D.J., MCMARTIN D., MOLDOVAN B., WANG D. (2010): Development of an iron-amended biofilter for removal of arsenic from rural Canadian prairie potable water. In: Water Pollution X. A.M. Marinov and C.A. Brebbia, Eds.; WIT Press: Ashurst, Southampton, 2010, 333–344.

GUNAWARDANA B., SINGHAL N., SWEDLUND P. (2011): Degradation of chlorinated phenols by zero valent iron and bimetals of iron: A review. Environmental Engineering Research 16, 187–203.

HANNA K. (2007a): Adsorption of aromatic carboxylate compounds on the surface of synthesized iron oxide-coated sands. Applied Geochemistry 22, 2045–2053.

HANNA K. (2007b): Sorption of two aromatic acids onto iron oxides: Experimental study and modeling. Journal of Colloid and Interface Science 309, 419–428.

HANDRECK K.A. (1990): Extractants for assessing the availability of copper to Chrysanthemum morifolium cultivar 'Yellow Mandalay' growing in soil-less media. Scientia Horticulturae, 44, 323–334.

HENDERSON A.D., DEMOND A.H. (2011): Impact of solids formation and gas production on the permeability of ZVI PRBs. Journal of Environmental Engineering 137, 689-696.

HOLDICH R.G. (2002): Fundamentals of particle technology. Shepshed: Midland Information Technology and Publishing, 173 pp.

HONRATH R.E. (1995): Environmental Engineering Fundamentals: Part I. Physical Processes,

Michigan Technological University January, 1995.

HUANG G.J., CHEN H.J., CHANG Y.S., SHEU M.J., LIN Y.H. (2007): Recombinant sporamin and its synthesized peptides with antioxidant activities in vitro. Botanical Studies 48, 133–140.

HUSSAM A., MUNIR A.K.M. (2007): A simple and effective arsenic filter based on composite iron matrix: Development and deployment studies for groundwater of Bangladesh. Journal of Environmental Science and Health Part A 42, 1869–1878.

HUSSAM A. (2009): Contending with a development disaster: SONO filters remove arsenic from well water in Bangladesh. Innovations 4, 89–102.

IMAMURA K., IKEDA E., NAGAYASU T., SAKIYAMA T., NAKANISHI K. (2002): Adsorption behaviour of methylene blue and its congeners on a stainless steel surface. Journal of Colloidal and Interface Science 245, 50–57.

JANOŠ P., ŠEDIVÝ P., RÝZNAROVÁ M., GRÖTSCHELOVÁ S. (2005): Sorption of basic and acid dyes from aqueous solutions onto oxihumolite. Chemosphere 59, 881–886.

JOHNSON T.L., SCHERER M.M., TRATNYEK P.G. (1996): Kinetics of Halogenated Organic Compound Degradation by Iron. Metal Environmental Science & Technology 30, 2634–2640.

KALOR G., MADSEN F.T. (1995): Determination of the cation exchange capacity and the surface area of bentonite, illite and kaolinite by methylene blue adsorption. Applied Clay Science 9, 327–336.

KARTHIKEYAN K.G., ELLIOTT H.A., CANNON F.S. (1997): Adsorption and coprecipitation of copper with the hydrous oxides of iron and aluminum. Environmental Science & Technology 31, 2721–2725.

KIPLING J.J., WILSON R.B. (1960): Adsorption of methylene blue in the determination of surface areas. Journal of Applied Chemistry 10, 109–113.

KOCH D.F.A. (1957): Kinetics of the reaction between manganese dioxide and ferrous iron. Australian Journal of Chemistry 10, 150–159.

KOELLE W., ROSCH H. (1980): Untersuchungen an RohrnetzInkrustierungen unter mineralogischen Gesichtspunkten. Vom Wasser 55, 159–178.

KUBARE M., HAARHOFF J. (2010): Rational design of domestic biosand filters. J. Water Supply: Res. Technol. - AQUA 59 (1), 1-15.

KURTH A.M. (2008): Discoloration of methylene blue by elemental iron: Influence of the shaking intensity. Bachelor Dissertation, Georg-August-University of Goettingen.

kÜMMERER k. (2011): Emerging contaminants versus micro-pollutants. Clean Soil, Air, Water 39, 889–890.

LEA M. (2008): Biological sand filters: Low-cost bioremediation technique for production of clean drinking water. Curr. Prot. Microbiol. 11, 1G.1.1–1G.1.28.

LEUPIN O. X., HUG S.J. (2005): Oxidation and removal of arsenic (III) from aerated groundwater by filtration through sand and zero-valent iron. Water Research 39, 1729–1740.

LI P., ZHAO G., ZHAO K., GAO J., WU T. (2012): An efficient and energy saving approach to photocatalytic degradation of opaque high-chroma methylene blue wastewater by electrocatalytic

pre-oxidation. Dyes and Pigments 92, 923–928.

LIGER E., CHARLET L., VAN CAPPELLEN P. (1999): Surface catalysis of uranium(VI) reduction by iron(II). Geochimica et Cosmochimica Acta 63, 2939–2955 .

MACKENZIE P.D., HORNEY D.P., SIVAVEC T.M. (1999): Mineral precipitation and porosity losses in granular iron columns, Journal of Hazardous Materials 68, 1–17.

MACLEOD I.D. (1989): The application of corrosion science to the management of maritime archaeological sites. The bulletin of the Australian Institute for Maritime Archaeology 13, 7–16.

MCGEOUGH K.L., KALIN R.M., MYLES P. (2007): Carbon disulfide removal by zero valent iron. Environmental Science & Technology 41, 4607–4612.

MITCHELL G., POOLE P., SEGROVE H.D. (1955): Adsorption of methylene blue by high-silica sands. Nature 176, 1025–1026.

MIYAJIMA K., NOUBACTEP C. (2012a): Effects of mixing granular iron with sand on the efficiency of methylene blue discoloration. Chemical Engineering Journal 200-202, 433–438.

MIYAJIMA K., NOUBACTEP C. (2012b): Impact of Fe0 amendment on methylene blue discoloration by sand columns. Chemical Engineering Journal (Accepted -30.11.2012).

MORACI N., CALABRÒ P.S. (2010): Heavy metals removal and hydraulic performance in zero-valent iron/pumice permeable reactive barriers. Journal of Environmental Management 91, 2336–2341.

NASSAR N.N., RINGSRED A. (2012): Rapid adsorption of methylene blue from aqueous solutions by goethite nanoadsorbents. Environmental Engineering Science 29, 790–797.

NEKU A., TANDULKER N. (2003): An overview of arsenic contamination in groundwater of Nepal and its removal at household level. Journal de Physique IV 107, 941–941.

NESIC S. (2007): Key issues related to modelling of internal corrosion of oil and gas pipelines - A review. Corrosion Science 49, 4308-4338.

NORDSVEEN N., NESIC S., NYBORG R., STANGELAND A. (2003): A mechanistic model for carbon dioxide corrosion of mild steel in the presence of protective iron carbonate films. Part 1: Theory and verification. Corrosion 59, 443–456.

NOUBACTEP C. (2003) Investigations for the passive in-situ immobilization of uranium (VI) from water (in German). Dissertation, TU Bergakademie Freiberg, Wiss. Mitt. Institut für Geologie der TU Bergakademie Freiberg, Band 21.ISSN1433-1284. 140 pp

NOUBACTEP C., MEINRATH G., DIETRICH P., SAUTER M., MERKEL B. (2005): Testing the suitability of zerovalent iron materials for reactive walls. Environmental Chemistry 2, 71–76.

NOUBACTEP C. (2007): Processes of contaminant removal in "Fe^0–H_2O" systems revisited: The importance of co-precipitation. Open Environmental Journal 1, 9–13.

NOUBACTEP C. (2008a): A critical review on the mechanism of contaminant removal in Fe^0–H_2O systems. Environmental Technology 29, 909–920.

NOUBACTEP C. (2008b): Comments on "Sorption of triazoles to soil and iron minerals" by Y. Jia et al. [Chemosphere 67 (2007) 250-258]. Chemosphere 71 (4), 802-806.

NOUBACTEP C. (2009a): Characterizing the discoloration of methylene blue in Fe^0/H_2O systems. Journal of Hazardous Materials 166, 79–87.

NOUBACTEP C. (2009b): Characterizing the reactivity of metallic iron upon methylene blue discoloration in $Fe^0/MnO_2/H_2O$ systems. Journal of Hazardous Materials 168, 1613–1616.

NOUBACTEP C., SCHÖNER A. (2009): Fe0-based alloys for environmental remediation: Thinking outside the box. Journal of Hazardous Materials 165, 1210–1214.

NOUBACTEP C., SCHÖNER A., WOAFO P. (2009a): Metalic iron filters for universal access to safe drinking water. Clean – Soil, Air, Water 37, 930–937.

NOUBACTEP C., LICHA T., SCOTT T.B., FALL M., SAUTER M. (2009b): Exploring the influence of operational parameters on the reactivity of elemental iron materials. Journal of Hazardous Materials 172, 943–951.

NOUBACTEP C. (2010a): Metalic iron for safe drinking water worldwide, Chemical Engineering Journal 165, 740–749.

NOUBACTEP C. (2010b): Characterizing the reactivity of metallic iron in Fe^0 /EDTA/H_2O systems with column experiments. Chemical Engineering Journal 162, 656–661.

NOUBACTEP C. (2010c): The suitability of metallic iron for environmental remediation. Environmental Progress & Sustainable Energy 29, 286–291.

NOUBACTEP C. (2010d): Review The fundamental mechanism of aqueous contaminant removal by metallic iron, Water SA 36, 663–670.

NOUBACTEP C., CARÉ S. (2010): Dimensioning metallic iron beds for efficient contaminant removal. Chemical Engineering Journal 163, 454–460.

NOUBACTEP C., SCHÖNER A. (2010): Metallic iron: dawn of a new era of drinking water treatment research? Fresenius Environmental Bulletin 19, 1661–1668.

NOUBACTEP C., CARÉ S., TOGUE-KAMGA F., SCHÖNER A., WOAFO P. (2010): Extending service life of household water filters by mixing metallic iron with sand. Clean – Soil, Air, Water 38, 951–959.

NOUBACTEP C. (2011a): Aqueous contaminant removal by metallic iron: Is the paradigm shifting? Water SA 37, 419–426.

NOUBACTEP C. (2011b): Metallic iron for water treatment: A knowledge system challenges mainstream science. Fresenius Environmental Bulletin 20, 2632–2637.

NOUBACTEP C. (2011c): Characterizing the reactivity of metallic iron in $Fe^0/U^{VI}/H_2O$ systems by long-term column experiments. Chemical Engineering Journal 171, 393–399.

NOUBACTEP C., CARÉ S. (2011) Designing laboratory metallic iron columns for better result comparability. Journal of Hazardous Materials 189, 809–813.

NOUBACTEP C., BTATKEU K.B.D., TCHATCHUENG J.B. (2011): Impact of MnO_2 on the efficiency of metallic iron for the removal of dissolved metal. Chemical Engineering Journal 178, 78–84.

NOUBACTEP C. (2012a): Relevant reducing agents in remediation Fe^0 /H_2O systems. Clean: Soil, Air, Water, doi:10.1002/clen.201200406.

NOUBACTEP C. (2012b): Investigating the processes of contaminant removal in Fe^0/H_2O systems. Korean Journal of Chemical Engineering 29, 1050–1056.

NOUBACTEP C. (2012c): Characterizing the reactivity of metallic iron in Fe^0/As-rock/H_2O systems by long-term column experiments. Water SA 38, 511–517.

NOUBACTEP C., TEMGOUA E., RAHMAN M.A. (2012a): Designing iron-amended biosand filters for decentralized safe drinking water provision. Clean: Soil, Air, Water 40 (8), 798-807.

NOUBACTEP C., CARÉ S., BTATKEU K.B.D., NANSEU-NJIKI C.P. (2012b): Enhancing the sustainability of household Fe^0/sand filters by using bimetallics and MnO_2. Clean - Soil, Air, Water 40, 100–109.

NOUBACTEP C. (2013): Metallic iron for water treatment: A critical review. Clean - Soil, Air, Water, doi: 10.1002/clen.201200502.

NÖDLER K., LICHA T., BESTER B.K., SAUTER M. (2010): Development of a multi-residue analytical method, based on liquid chromatography–tandem mass spectrometry, for the simultaneous determination of 46 micro-contaminants in aqueous samples. Journal of Chromatography A, 1217, 6511–6521.

OGUZIE E.E. (2005): Corrosion inhibition of mild steel in hydrochloric acid solution by methylene blue dye. MATERIALS LETTERS 59 (8-9), 1076-1079

O'HANNESIN S.F., PRZEPIORA A., GILLHAM R.W. (2004): Effect of temperature and iron content on iron PRB Design. Presented at The Fourth International Conference on Remediation of Chlorinated and Recalcitrant Compounds, Monterey, California, May 24-27.

PACHOCKA M. (2010): Intermittent slow sand filters: Improving their design for developing world applications. Master Dissertation, University of Delaware.

PIRILLO S., PEDRONI V., RUEDA E., FERREIRA M.L. (2009): Elimination of dyes from aqueous solutions using iron oxides and chitosan as adsorbents: a comparative study. Química Nova 32, 1239–1244.

POKHREL D., BHANDARI B.S., VIRARAGHAVAN T. (2009): Arsenic contamination of groundwater in the Terai Region of Nepal: An overview of health concerns and treatment options. Environment International 35, 157–161.

POSTMA D. (1985): Concentration of Mn and separation from Fe in sediments – I. Kinetics and stoichiometry of the reaction between birnessite and dissolved Fe(II) at 10°C. Geochimica et Cosmochimica Acta 49, 1023–1033.

POSTMA D., APPELO C.A.J. (2000): Reduction of Mn-oxides by ferrous iron in a flow system: column experiment and reactive transport modelling. Geochimica et Cosmochimica Acta 64, 1237–1247.

RADIN C. (2008): Random close packing of granular matter. Journal of Statistical Physics 131, 567–573.

ROBERGE P. (2008): Handbook of Corrosion engineering. McGraw-Hill.

RUHL A.S., WEBER A., JEKEL M. (2012a): Influence of dissolved inorganic carbon and calcium on gas formation and accumulation in iron permeable reactive barriers. Journal of Contaminant Hydrology 142–143, 22–32.

RUHL A.S., ÜNAL N., JEKEL M. (2012b): Evaluation of two-component Fe(0) fixed bed filters with porous materials for reductive dechlorination. Chemical Engineering Journal 209, 401–406.

SAHA B., DAS S., SAIKIA J., DAS G. (2011): Preferential and enhanced adsorption of different dyes on iron oxide nanoparticles: A comparative study. Journal of Physical Chemistry C 115, 8024–8033.

SARIN P., SNOEYINK V.L., LYTLE D.A., KRIVEN W.M. (2004a): Iron corrosion scales: Model for scale growth, iron release, and colored water formation. Journal of Environmental Engineering 130, 364–373.

SARIN P., SNOEYINK V.L., BEBEE J., JIM K.K., BECKETT M.A., KRIVEN W.M., Clement J.A. (2004b): Iron release from corroded iron pipes in drinking water distribution systems: effect of dissolved oxygen. Water Research 38, 1259–1269.

SCHERER M.M., RICHTER S., VALENTINE R.L., ALVAREZ P.J. (2000): Chemistry and microbiology of permeable reactive barriers for in situ groundwater clean up. Critical Reviews in Environmental Science and Technology 30, 363–411.

SCOTT T.B., POPESCU I.C., CRANE R.A., NOUBACTEP C. (2011): Nano-scale metallic iron for the treatment of solutions containing multiple inorganic contaminants. Journal of Hazardous Materials 186, 280–287.

SONG.D.-I., KIM Y.H., SHIN W.S. (2005): A simple mathematical analysis on the effect of sand in Cr(VI) reduction using zero valent iron. Korean Journal of Chemical Engineering 22, 67-69.

SONTHEIMER H., KOLLE W. and SNOEYINK V. L. (1981): The siderite model of the formation of corrosion-resistant scales J. Am. Water Works Assoc. 73(11), 572–579

STIPP S., HANSEN M., KRISTENSEN R., HOCHELLA JR. M., BENNEDSEN L., DIDERIKSEN K., BALICZUNIC T., LEONARD D., MATHIEU H.J. (2002):Behaviour of Fe-oxides relevant to contaminant uptake in the environment. Chemical Geology 190 321–337.

STRATMANN M., MÜLLER J. (1994): The mechanism of the oxygen reduction on rustcovered metal substrates.Corrosion Science 36, 327–359.

TOGUE-KAMGA F., BTATKEU K.B.D., NOUBACTEP C., WOAFO P. (2012a): Metallic iron for environmental remediation: Back to textbooks. Fresenius Environmental Bulletin 21, 1992–1997.

TOGUE-KAMGA F., NOUBACTEP C., WOAFO P. (2012b): Modeling and simulation of iron/sand filters. Revue des Sciences de l'Eau 25, 95–101.

ULSAMER S. (2011): A model to characterize the kinetics of dechlorination of tetrachloroethylene and trichloroethylene by a zero valent iron permeable reactive barrier, Master dissertation. Wrcester Polytechnic Institute.

UNICEF and World Health Organisation (2012): Progress on Drinking Water and Sanitation.

USAPHC (2011): Filtration in the use of individual water purification devices, Technical Information. Paper # 31-004-0211.

VAN DER KAMP G., VAN STEMPVOORT D.R. WASSENAAR L.I. (1996): The radial diffusion method 1. Using intact cores to determine isotopic composition, chemistry and effective porosities for groundwater in aquitards. Water Resources Research 32, 1815–1822.

VARLIKLI C., BEKIARI V., KUS M., BODUROGLU N., ONER I., LIANOS P., LYBERATOS G., ICLI S. (2009): Adsorption of dyes on Sahara desert sand. Journal of Hazardous Materials 170, 27–34.

VASIREDDY D. (2005): Arsenic adsorption onto iron-chitosan composite from drinking water. Master Thesis of University of Missouri-Columbia.

WESTERHOFF P., JAMES J. (2003): Nitrate removal in zero-valent iron packed columns, Water Research 37, 1818–1830.

WILSON E.R. (1923): The Mechanism of the corrosion of iron and steel in natural waters and the calculation of specific rates of corrosion. Industrial and Engineering Chemistry 15, 127–133.

YOU Y., HAN J., CHIU P.C., JIN. Y. (2005): Removal and inactivation of waterborne viruses using zerovalent iron. Environmental Science & Technology 39, 9263–9269.

9. Appendix

This section includes all experimental data, including:
(i) the weighed amount of material for individual test tubes,
(ii) measured methylene blue concentrations in the individual test tubes, statistical data included,
(iii) mean MB concentrations with statistical data.
The calibration data of the used spectrophotometer is presented for the 26 calibration measurements performed.

Appendix 1: Used Chemicals and Experimental Devices

Chemicals
Methylene blue (MB)
Ascorbic acid to remove adsorbed MB and to dissolve Fe(III) species from the used test tubes (in experiments containing Fe0)
HCl to acidificate the washing solution and to favor Fe(III)/Fe(III) removal

Experimental devices
Balance Fisherbrand PF 323 (0.001 g)
Dispenser Walu Labortechnik, Germany
Racks for 80 test tubes
Test tubes with 22 mL graduated capacity
Precision pipettes with volumes of either 10 μ L- 100 μ L or 100 μ L – 1000 μ L, Fischer Scientific
Shaker HS 501 D by “Janke & Kunkel”, DCM Laborservice, with shaking intensity 75 rpm
UV-VIS spectrophotometer Cary 50 by Varian.
10 columns (length 44cm, diameter 2.6cm)
Peristaltic pump (Ismatec, ICP 24)
Pipes connecting pump, columns and sample bottles
Sample bottles with 1.5L capacity

Appendix 2: Calibration of the UV-VIS Spectrophotometer

Table A2.1: Procedure for the calibration of the UV-VIS spectrophotometer (Cary 50 by Varian). Total volume of each essay tube: 22 mL.

Std.No.	[MB] (mg/L)	V_{MB} (µL)	V_{1H2O} (mL)	V_{2H2O} (µL)
1	0.00	0	19.5	500
2	1.00	20	19.5	480
3	2.00	40	19.5	460
4	4.00	80	19.5	420
5	6.00	120	19.5	380
6	8.00	160	19.5	340
7	10,00	200	19.5	300
8	15,00	300	19.5	200
9	20,00	400	19.5	100
10	25,00	500	19.5	0

Table A2.2: Results of the calibration of the UV-VIS spectrophotometer. The presented results are the mean values of 8 calibrations.

Std.No.	[MB]	Absorbance	
	(mg/L)	Mean values	Standard deviation
1	0.00	0.08	0.00
2	0.50	0.19	0.00
3	1.00	0.29	0.00
4	1.50	0.40	0.00
5	2.50	0.60	0.00
6	5.00	1.06	0.01
7	7.50	1.51	0.01
8	10.00	1.90	0.02
9	12.50	2.28	0.02
10	15.00	2.64	0.03

Appendix 3: Material Characterization and Batch Test

Table A3: Summary of the performed experiments. Elemental iron (Fe^0) is the main material. Sand, Manganese nodules (MnO2) and (EDTA) are added to aid the investigation in Fe^0-H2O systems.

	Experiment No.	Chapter No.	Intensity [rpm]	Duration [week]	Volume [mL]	Used materials	Description
Batch Test	1	4.1.1	0	6	22	Fe^0	Impact on MB discoloration by various mass of materials.
	2	4.1.1	0	6	22	Fe^0+Sand	
	3	4.1.1	0	3	22	Fe^0	
	4	4.1.1	0	3	22	Fe^0+Sand	
	5	4.1.2	0	3	22	Fe^0+Sand	
	6	4.1.1	75	1	22	Fe^0	
	7	4.1.1	75	1	22	Fe^0+Sand	
	8	4.1.2	75	1	22	Fe^0+Sand	
Material Chara.	9	4.2.1	0	3	22	Fe^0	Impact on MB discoloration by 8 different ZVI (Fe^0) species.
	10	4.2.1	0	3	22	Fe^0+Sand	
	11	4.2.1	0	3	22	Fe^0+MnO_2	
	12	4.2.1	0	3	22	Fe^0+MnO_{2+}Sand	
	13	4.2.1	0	6	22	Fe0+Sand	
	14	4.2.1	0	6	22	Fe^0+MnO_{2+}Sand	
	15	4.2.2	0	10h	22	Fe^0+EDTA	Intrinsic iron reactivity of 8 different ZVI (Fe^0) species.
	15	4.2.2	0	24h	22	Fe^0+EDTA	
	15	4.2.2	0	48h	22	Fe^0+EDTA	
	15	4.2.2	0	72h	22	Fe^0+EDTA	
	15	4.2.2	0	96h	22	Fe^0+EDTA	
	16	4.2.3	75	2	22	Fe^0+MnO_2 (Psilomel)	Impact on MB discoloration by 3 different MnO2 species and thier various masses.
	17	4.2.3	75	2	22	Fe^0+MnO_2 (Manganit)	
	18	4.2.3	75	2	22	Fe^0+MnO_2 (d4)	

Batch Test

Experiment 1: Non-disturbed experiment performed for Fe^0 for 6 weeks.

Table A3.1.1: Experimental conditions and result

Exp.1 22mL 0rpm 6 weeks								
	ZVI				**Result**			
Run	**set point ZVI [g]**	**weighted ZVI [g]**	**mean [g]**	**standard dev. [g]**	**[MB] [mg/L]**	**mean [mg/L]**	**stand.dev. [mg/L]**	**result [mg/L]**
1	0	0	0	0	10.4	10.4	0	10.4±0.0
2	0	0			10.4			
3	0	0			10.4			
4	0.01	0.01	0.01	0	7.5	7.33	0.38	7.3±0.4
5	0.01	0.01			6.9			
6	0.01	0.01			7.6			
7	0.01	0.01	0.01	0	5.2	5.63	0.45	5.6±05
8	0.01	0.02			5.6			
9	0.01	0.01			6.1			
10	0.03	0.03	0.03	0	4.3	4.2	0.1	4.2±0.1
11	0.03	0.03			4.1			
12	0.03	0.03			4.2			
13	0.05	0.06	0.06	0.01	3.1	3.27	0.15	3.3±0.2
14	0.05	0.06			3.3			
15	0.05	0.05			3.4			
16	0.1	0.11	0.1	0	2.8	2.8	0	2.8±0.0
17	0.1	0.11			2.8			
18	0.1	0.1			2.8			
19	0.25	0.25	0.25	0.01	2.3	2.37	0.06	2.4±0.1
20	0.25	0.26			2.4			
21	0.25	0.25			2.4			
22	0.5	0.5	0.5	0	1.8	1.83	0.06	1.8±0.1
23	0.5	0.5			1.8			
24	0.5	0.51			1.9			
25	0.75	0.76	0.75	0	1.7	1.7	0	1.7±0.0
26	0.75	0.75			1.7			
27	0.75	0.75			1.7			
28	1	1.01	1.01	0	1.6	1.63	0.06	1.6±0.1
29	1	1.01			1.7			
30	1	1.01			1.6			

Experiment 2: Non-disturbed experiment performed for the mixture Fe^0+Sand for 6 weeks.

Table A3.1.2a: Experimental conditions

Exp.2 22mL 0rpm 6 weeks								
	ZVI				Sand			
Run	set point ZVI [g]	weighted ZVI [g]	mean [g]	standard dev. [g]	set point Sand [g]	weighted Sand [g]	mean [g]	standard dev. [g]
1	0	0	0	0	0	0	0	0
2	0	0			0	0		
3	0	0			0	0		
4	0	0	0	0	2	2.01	2.01	0
5	0	0			2	2.01		
6	0	0			2	2.01		
7	0.01	0.01	0.02	0	2	2.01	2.01	0
8	0.01	0.01			2	2.01		
9	0.01	0.02			2	2.01		
10	0.03	0.03	0.03	0	2	2.01	2	0
11	0.03	0.03			2	2		
12	0.03	0.03			2	2.01		
13	0.05	0.05	0.05	0.01	2	2.01	2.01	0
14	0.05	0.05			2	2		
15	0.05	0.06			2	2.01		
16	0.1	0.1	0.1	0.01	2	2	2.01	0
17	0.1	0.1			2	2.01		
18	0.1	0.1			2	2.01		
19	0.25	0.25	0.25	0	2	2.01	2	0
20	0.25	0.25			2	2.01		
21	0.25	0.26			2	2		
22	0.5	0.51	0.5	0	2	2	2	0
23	0.5	0.5			2	2.01		
24	0.5	0.5			2	2		
25	0.75	0.75	0.75	0.01	2	2	2	0
26	0.75	0.76			2	2.01		
27	0.75	0.75			2	2.01		
28	1	1.01	1	0	2	2.01	2.01	0
29	1	1.01			2	2.01		
30	1	1			2	2.01		

Experiment 2: Non-disturbed experiment performed for the mixture Fe^0+sand for 6 weeks.

Table A3.1.2b: Result

Exp.2	22mL	0rpm	6 weeks	
		Result		
Run	[MB] [mg/L]	mean [mg/L]	stand.dev. [mg/L]	result [mg/L]
1	10.6	10.6	0	10.6±0.0
2	10.6			
3	10.6			
4	3.3	3	0.44	3.0±0.4
5	3.2			
6	2.5			
7	2.4	2.8	0.46	2.8±05
8	2.7			
9	3.3			
10	2.6	2.27	0.49	2.3±0.5
11	1.7			
12	2.5			
13	2.3	2.73	0.45	2.7±0.5
14	2.7			
15	3.2			
16	1.2	2.3	1.05	2.3±1.1
17	2.4			
18	3.3			
19	2.2	2.67	0.42	2.7±0.4
20		3		
21	2.8			
22	2.6	2.4	0.72	2.4±0.7
23	1.6			
24		3		
25	1.9	2.17	0.31	2.2±0.3
26	2.5			
27	2.1			
28	2.8	2.7	0.17	2.7±0.2
29	2.8			
30	2.5			

Experiment 3: Non-disturbed experiment performed for Fe^0 for 3 weeks.

Table A3.1.3: Experimental conditions and result

Exp.3 22mL		0rpm		3 weeks				
	ZVI				Result			
Run	set point ZVI [g]	weighted ZVI [g]	mean [g]	standard dev. [g]	[MB] [mg/L]	mean [mg/L]	stand.dev. [mg/L]	result [mg/L]
1	0	0	0	0	9	8.93	0.06	8.9±0.1
2	0	0			8.9			
3	0	0			8.9			
4	0	0	0	0	8.9	8.97	0.06	9.0±0.1
5	0	0			9			
6	0	0			9			
7	0.01	0.01	0.01	0	6.3	6.17	0.12	6.2±0.1
8	0.01	0.01			6.1			
9	0.01	0.01			6.1			
10	0.03	0.02	0.03	0	5.3	5.07	0.21	5.1±0.2
11	0.03	0.03			4.9			
12	0.03	0.03			5			
13	0.05	0.05	0.05	0	4.1	4.13	0.06	4.1±0.1
14	0.05	0.05			4.2			
15	0.05	0.05			4.1			
16	0.1	0.1	0.1	0	3.4	3.37	0.06	3.4±0.1
17	0.1	0.1			3.3			
18	0.1	0.1			3.4			
19	0.25	0.25	0.25	0	2.7	2.67	0.06	2.7±0.1
20	0.25	0.25			2.6			
21	0.25	0.25			2.7			
22	0.5	0.51	0.5	0	2.2	2.2	0	2.2±0.0
23	0.5	0.5			2.2			
24	0.5	0.5			2.2			
25	0.75	0.76	0.76	0	1.9	1.93	0.06	1.9±0.1
26	0.75	0.76			2			
27	0.75	0.76			1.9			
28	1	1	1	0	1.7	1.67	0.06	1.7±0.1
29	1	1			1.6			
30	1	1			1.7			

Experiment 4: Non-disturbed experiment performed for the mixture Fe^0+sand for 3 weeks.

Table A3.1.4a: Experimental conditions

Exp.4 22mL 0rpm 3 weeks								
	ZVI				**Sand**			
Run	**set point ZVI [g]**	**weighted ZVI [g]**	**mean [g]**	**standard dev. [g]**	**set point Sand [g]**	**weighted Sand [g]**	**mean [g]**	**standard dev. [g]**
1	0	0	0	0	0	0	0	0
2	0	0			0	0		
3	0	0			0	0		
4	0	0	0	0	2	2.01	2.01	0
5	0	0			2	2.01		
6	0	0			2	2.01		
7	0.01	0.01	0.02	0	2	2.01	2.01	0
8	0.01	0.01			2	2.01		
9	0.01	0.02			2	2.01		
10	0.03	0.03	0.03	0	2	2.01	2	0
11	0.03	0.03			2	2		
12	0.03	0.03			2	2.01		
13	0.05	0.05	0.05	0.01	2	2.01	2.01	0
14	0.05	0.05			2	2		
15	0.05	0.06			2	2.01		
16	0.1	0.1	0.1	0.01	2	2	2.01	0
17	0.1	0.1			2	2.01		
18	0.1	0.1			2	2.01		
19	0.25	0.25	0.25	0	2	2.01	2	0
20	0.25	0.25			2	2.01		
21	0.25	0.26			2	2		
22	0.5	0.51	0.5	0	2	2	2	0
23	0.5	0.5			2	2.01		
24	0.5	0.5			2	2		
25	0.75	0.75	0.75	0.01	2	2	2	0
26	0.75	0.76			2	2.01		
27	0.75	0.75			2	2.01		
28	1	1.01	1	0	2	2.01	2.01	0
29	1	1.01			2	2.01		
30	1	1			2	2.01		

Experiment 4: Non-disturbed experiment performed for the mixture Fe^0+sand for 3 weeks.

Table A3.1.4b: Result

Exp.4	22mL	0rpm	3 weeks	
		Result		
Run	[MB] [mg/L]	mean [mg/L]	stand.dev. [mg/L]	result [mg/L]
1	8.9	8.97	0.06	9.0±0.1
2	9.0			
3	9.0			
4	3.7	3.83	0.61	3.8±0.6
5	4.5			
6	3.3			
7	4.0	3.9	0.17	3.9±0.2
8	4.0			
9	3.7			
10	4.1	3.77	0.42	3.8±0.4
11	3.3			
12	3.9			
13	3.2	3.43	0.32	3.4±0.3
14	3.3			
15	3.8			
16	3.1	3.23	0.15	3.2±0.2
17	3.4			
18	3.2			
19	3.5	3.33	0.21	3.3±0.2
20	3.1			
21	3.4			
22	3.3	3.33	0.35	3.3±0.4
23	3.0			
24	3.7			
25	2.7	2.6	0.17	2.6±0.2
26	2.4			
27	2.7			
28	2.5	2.53	0.15	2.5±0.2
29	2.4			
30	2.7			

Experiment 5: Non-disturbed experiment performed for the mixture Fe^0+sand for 3 weeks.

Table A3.1.5a: Experimental conditions

Exp.5 22mL 0rpm 3 weeks								
	ZVI				**Sand**			
Run	**set point ZVI [g]**	**weighted ZVI [g]**	**mean [g]**	**standard dev. [g]**	**set point Sand [g]**	**weighted Sand [g]**	**mean [g]**	**standard dev. [g]**
1	0	0	0	0	0	0	0	0
2	0	0			0	0		
3	0	0			0	0		
4	0	0	0	0	2	2	2	0
5	0	0			2	2		
6	0	0			2	2.01		
7	0.1	0.1	0.1	0	0.25	0.25	0.25	0
8	0.1	0.1			0.25	0.25		
9	0.1	0.1			0.25	0.25		
10	0.1	0.11	0.1	0	0.5	0.5	0.5	0
11	0.1	0.11			0.5	0.5		
12	0.1	0.1			0.5	0.5		
13	0.1	0.1	0.1	0	0.75	0.75	0.75	0
14	0.1	0.1			0.75	0.75		
15	0.1	0.1			0.75	0.75		
16	0.1	0.1	0.1	0.01	1	1	1	0.01
17	0.1	0.1			1	1		
18	0.1	0.1			1	1.01		
19	0.1	0.1	0.1	0	1.25	1.26	1.26	0
20	0.1	0.11			1.25	1.26		
21	0.1	0.1			1.25	1.26		
22	0.1	0.1	0.1	0.01	1.5	1.5	1.5	0
23	0.1	0.11			1.5	1.5		
24	0.1	0.1			1.5	1.51		
25	0.1	0.11	0.1	0.01	1.75	1.75	1.75	0
26	0.1	0.1			1.75	1.75		
27	0.1	0.1			1.75	1.75		
28	0.1	0.1	0.1	0	2	2.01	2.01	0
29	0.1	0.1			2	2		
30	0.1	0.1			2	2.01		

Experiment 5: Non-disturbed experiment performed for the mixture Fe^0+sand for 3 weeks.

Table A3.1.5b: Result

Exp.5	22mL	0rpm	6 weeks	
		Result		
Run	[MB] [mg/L]	mean [mg/L]	stand.dev. [mg/L]	result [mg/L]
1	8.9	9.00	0.1	9.0±0.1
2	9.0			
3	9.1			
4	3.6	4.00	0.3	4.0±0.3
5	4.2			
6	4.2			
7	3.8	3.60	0.9	3.6±0.9
8	4.6			
9	5.5			
10	4.8	4.20	0.2	4.2±0.2
11	4.5			
12	4.9			
13	4.2	4.83	0.2	4.8±0.2
14	4.4			
15	4.6			
16	4.6	4.93	0.5	4.9±0.5
17	4.3			
18	3.6			
19	4.5	5.17	0.3	5.2±0.3
20	4.3			
21	4.0			
22	4.0	5.63	0.1	5.6±0.1
23	3.8			
24	4.0			
25	3.7	5.73	0.1	5.7±0.1
26	3.7			
27	3.8			
28	4.1	6.13	0.4	6.1±0.4
29	3.4			
30	3.8			

Experiment 6: Experiment performed for Fe^0 at shaken intensity 75 rpm for 1 week.

Table A3.1.6: Experimental conditions and result

Exp.6 22mL 75rpm 1 week								
	ZVI				**Result**			
Run	**set point ZVI [g]**	**weighted ZVI [g]**	**mean [g]**	**standard dev. [g]**	**[MB] [mg/L]**	**mean [mg/L]**	**stand.dev. [mg/L]**	**result [mg/L]**
1	0	0	0	0	8.24	8.33	0.08	8.3±0.1
2	0	0			8.37			
3	0	0			8.39			
4	0	0	0	0	8.39	8.35	0.05	8.4±0.1
5	0	0			8.3			
6	0	0			8.38			
7	0.01	0.01	0.01	0	6.76	6.81	0.16	6.8±0.2
8	0.01	0.01			6.67			
9	0.01	0.01			6.99			
10	0.03	0.03	0.03	0	6.09	5.98	0.12	6.0±0.1
11	0.03	0.03			5.86			
12	0.03	0.03			5.99			
13	0.05	0.06	0.06	0	5.37	5.25	0.15	5.2±0.2
14	0.05	0.06			5.3			
15	0.05	0.06			5.08			
16	0.1	0.1	0.1	0	4.59	4.5	0.1	4.5±0.1
17	0.1	0.1			4.52			
18	0.1	0.1			4.39			
19	0.25	0.25	0.25	0	3.62	3.47	0.19	3.5±0.2
20	0.25	0.25			3.26			
21	0.25	0.25			3.52			
22	0.5	0.51	0.5	0	2.81	2.88	0.07	2.9±0.1
23	0.5	0.5			2.94			
24	0.5	0.5			2.9			
25	0.75	0.75	0.75	0	2.57	2.49	0.07	2.5±0.1
26	0.75	0.75			2.43			
27	0.75	0.75			2.46			
28	1	1.01	1.01	0	2.34	2.33	0.02	2.3±0.0
29	1	1.01			2.31			
30	1	1.01			2.34			

Experiment 7: Experiment performed for the mixture Fe^0+Sand at shaken intensity 75 rpm for 1 week.

Table A3.1.7a: Experimental conditions

Exp.7 22mL 75rpm 1 week								
	ZVI				**Sand**			
Run	**set point ZVI [g]**	**weighted ZVI [g]**	**mean [g]**	**standard dev. [g]**	**set point Sand [g]**	**weighted Sand [g]**	**mean [g]**	**standard dev. [g]**
1	0	0	0	0	0	0	0	0
2	0	0			0	0		
3	0	0			0	0		
4	0	0	0	0	2	2	2	0
5	0	0			2	2		
6	0	0			2	2.01		
7	0.01	0.01	0.01	0	2	2.01	2.02	0.01
8	0.01	0.01			2	2.02		
9	0.01	0.01			2	2.02		
10	0.03	0.03	0.03	0	2	2.01	2.02	0.01
11	0.03	0.03			2	2.03		
12	0.03	0.03			2	2.02		
13	0.05	0.05	0.05	0	2	2.01	2.01	0.01
14	0.05	0.05			2	2.02		
15	0.05	0.05			2	2.01		
16	0.1	0.1	0.1	0	2	2.01	2.02	0.01
17	0.1	0.1			2	2.01		
18	0.1	0.1			2	2.03		
19	0.25	0.25	0.25	0	2	2.01	2	0
20	0.25	0.25			2	2		
21	0.25	0.25			2	2.01		
22	0.5	0.5	0.5	0	2	2.01	2.01	0.01
23	0.5	0.5			2	2.02		
24	0.5	0.51			2	2.01		
25	0.75	0.76	0.75	0	2	2.02	2.01	0.01
26	0.75	0.75			2	2.01		
27	0.75	0.75			2	2		
28	1	1	1	0	2	2	2.01	0
29	1	1			2	2.01		
30	1	1.01			2	2		

Experiment 7: Experiment performed for the mixture Fe^0+Sand at shaken intensity 75 rpm for 1 week.

Table A3.1.7b: Result

Exp.7	22mL	75rpm	1 week	
		Result		
Run	[MB] [mg/L]	mean [mg/L]	stand.dev. [mg/L]	result [mg/L]
1	8.42	8.49	0.07	8.5±0.1
2	8.51			
3	8.55			
4	4.75	4.63	0.36	4.6±0.4
5	4.23			
6	4.92			
7	4.71	4.67	0.18	4.7±0.2
8	4.48			
9	4.83			
10	4.65	4.75	0.09	4.8±0.1
11	4.82			
12	4.79			
13	4.44	4.51	0.08	4.5±0.1
14	4.49			
15	4.59			
16	5.03	4.68	0.33	4.7±0.3
17	4.38			
18	4.65			
19	3.97	3.96	0.07	4.0±0.1
20	4.02			
21	3.89			
22	3.97	3.73	0.52	3.7±0.5
23	4.08			
24	3.13			
25	2.89	3.72	0.72	3.7±0.7
26	4.17			
27	4.11			
28	3.67	3.61	0.17	3.6±0.2
29	3.74			
30	3.41			

Experiment 8: Experiment performed for the mixture Fe^0+sand at shaken intensity 75 rpm for 1 week.

Table A3.1.8a: Experimental conditions

Exp.8 22mL 75rpm 1 week								
	ZVI				Sand			
Run	set point ZVI [g]	weighted ZVI [g]	mean [g]	standard dev. [g]	set point Sand [g]	weighted Sand [g]	mean [g]	standard dev. [g]
1	0	0	0	0	0	0	0	0
2	0	0			0	0		
3	0	0			0	0		
4	0	0	0	0	2	2.02	2.03	0.03
5	0	0			2	2.06		
6	0	0			2	2.01		
7	0.1	0.1	0.1	0	0.25	0.24	0.25	0.01
8	0.1	0.1			0.25	0.25		
9	0.1	0.11			0.25	0.26		
10	0.1	0.11	0.11	0	0.5	0.5	0.51	0.01
11	0.1	0.1			0.5	0.51		
12	0.1	0.11			0.5	0.51		
13	0.1	0.1	0.1	0	0.75	0.76	0.75	0
14	0.1	0.1			0.75	0.75		
15	0.1	0.1			0.75	0.75		
16	0.1	0.1	0.1	0	1	1.02	1.06	0.03
17	0.1	0.11			1	1.07		
18	0.1	0.1			1	1.08		
19	0.1	0.1	0.1	0	1.25	1.25	1.25	0
20	0.1	0.1			1.25	1.26		
21	0.1	0.1			1.25	1.26		
22	0.1	0.11	0.11	0	1.5	1.5	1.51	0
23	0.1	0.1			1.5	1.51		
24	0.1	0.11			1.5	1.51		
25	0.1	0.11	0.1	0	1.75	1.76	1.75	0
26	0.1	0.1			1.75	1.76		
27	0.1	0.1			1.75	1.75		
28	0.1	0.11	0.1	0	2	2.01	2.01	0
29	0.1	0.1			2	2		
30	0.1	0.1			2	2.01		

Experiment 8: Experiment performed for the mixture Fe^0+sand at shaken intensity 75 rpm for 1 week.

Table A3.1.8b: Result

Exp.8	22mL	75rpm	1 week	
		Result		
Run	[MB] [mg/L]	mean [mg/L]	stand.dev. [mg/L]	result [mg/L]
1	8.53	8.53	0	8.5±0
2	8.53			
3	8.53			
4	3.88	4.22	0.55	4.2±0.6
5	3.92			
6	4.85			
7	5.71	5.98	0.32	6.0±0.3
8	5.9			
9	6.33			
10	6.59	6.07	0.6	6.1±0.6
11	6.2			
12	5.41			
13	5.99	5.73	0.22	5.7±0.2
14	5.57			
15	5.64			
16	5.39	5.22	0.16	5.2±0.2
17	5.08			
18	5.18			
19	4.93	4.52	0.77	4.5±0.8
20	5.01			
21	3.63			
22	4.71	4.57	0.19	4.6±0.2
23	4.65			
24	4.36			
25	4.49	4.41	0.15	4.4±0.1
26	4.24			
27	4.49			
28	4.27	4.34	0.2	4.3±0.2
29	4.18			
30	4.56			

Material Characterization

Experiment 9: Non-disturbed experiments performed for 8 different ZVIs for 3 weeks.

Table A3.2.9: Experimental conditions and result

Exp.19 22mL 0rpm 3 weeks										
		ZVI					Result			
Run	ZVI	set point ZVI [g]	weighted ZVI [g]	mean [g]	standard dev. [g]	ZVI	[MB] [mg/L]	mean [mg/L]	stand.dev. [mg/L]	result [mg/L]
1	none	0	0	0	0	none	9.6	9.7	0.06	9.7±0.1
2	none	0	0			none	9.7			
3	none	0	0			none	9.7			
4	ZVI1	0.1	0.1	0.1	0	ZVI1	3.7	3.7	0.06	3.7±0.1
5	ZVI1	0.1	0.1			ZVI1	3.7			
6	ZVI1	0.1	0.1			ZVI1	3.8			
7	ZVI1	0.1	0.1	0.1	0	ZVI1	3.9	3.8	0.1	3.8±0.1
8	ZVI1	0.1	0.1			ZVI1	3.8			
9	ZVI1	0.1	0.1			ZVI1	3.7			
10	ZVI2	0.1	0.11	0.1	0	ZVI2	3.9	3.6	0.42	3.6±0.4
11	ZVI2	0.1	0.1			ZVI2	3.7			
12	ZVI2	0.1	0.11			ZVI2	3.1			
13	ZVI3	0.1	0.1	0.1	0	ZVI3	3.5	3.6	0.1	3.5±0.1
14	ZVI3	0.1	0.1			ZVI3	3.6			
15	ZVI3	0.1	0.1			ZVI3	3.7			
16	ZVI4	0.1	0.1	0.1	0.01	ZVI4	3.1	3.7	0.9	3.7±0.9
17	ZVI4	0.1	0.1			ZVI4	3.2			
18	ZVI4	0.1	0.1			ZVI4	4.7			
19	ZVI5	0.1	0.1	0.1	0	ZVI5	4.9	5	0.26	5.0±0.3
20	ZVI5	0.1	0.1			ZVI5	5.3			
21	ZVI5	0.1	0.1			ZVI5	4.8			
22	ZVI6	0.1	0.1	0.1	0	ZVI6	3.7	3.7	0.06	3.7±0.1
23	ZVI6	0.1	0.11			ZVI6	3.7			
24	ZVI6	0.1	0.1			ZVI6	3.8			
25	ZVI7	0.1	0.1	0.1	0	ZVI7	4.1	4	0.32	4.0±0.3
26	ZVI7	0.1	0.1			ZVI7	3.6			
27	ZVI7	0.1	0.1			ZVI7	4.2			
28	ZVI8	0.1	0.1	0.1	0	ZVI8	3.4	3.5	0.1	3.5±0.1
29	ZVI8	0.1	0.1			ZVI8	3.6			
30	ZVI8	0.1	0.1			ZVI8	3.5			

Experiment 10: Non-disturbed experiments with the mixture of 8 different ZVI+sand performed for 3 weeks.

Table A3.2.10a: Experimental conditions

Exp.10 22mL 0rpm 3 weeks									
		ZVI				**Sand**			
Run	**ZVI**	**set point ZVI [g]**	**weighted ZVI [g]**	**mean [g]**	**standard dev. [g]**	**set point Sand [g]**	**weighted Sand [g]**	**mean [g]**	**standard dev. [g]**
1	none	0	0	0	0	2	2	2	0
2	none	0	0			2	2		
3	none	0	0			2	2.01		
4	ZVI1	0.1	0.1	0.1	0	0	0	0	0
5	ZVI1	0.1	0.1			0	0		
6	ZVI1	0.1	0.1			0	0		
7	ZVI1	0.1	0.1	0.1	0	2	2.01	2.02	0.01
8	ZVI1	0.1	0.1			2	2.02		
9	ZVI1	0.1	0.1			2	2.02		
10	ZVI2	0.1	0.1	0.1	0	2	2.01	2.02	0.01
11	ZVI2	0.1	0.1			2	2.03		
12	ZVI2	0.1	0.1			2	2.02		
13	ZVI3	0.1	0.1	0.1	0	2	2.01	2.01	0.01
14	ZVI3	0.1	0.11			2	2.02		
15	ZVI3	0.1	0.11			2	2.01		
16	ZVI4	0.1	0.1	0.1	0.01	2	2.01	2.02	0.01
17	ZVI4	0.1	0.1			2	2.01		
18	ZVI4	0.1	0.1			2	2.03		
19	ZVI5	0.1	0.1	0.1	0	2	2.01	2	0
20	ZVI5	0.1	0.1			2	2		
21	ZVI5	0.1	0.1			2	2.01		
22	ZVI6	0.1	0.1	0.1	0	2	2.01	2.01	0.01
23	ZVI6	0.1	0.1			2	2.02		
24	ZVI6	0.1	0.1			2	2.01		
25	ZVI7	0.1	0.1	0.1	0	2	2.02	2.01	0.01
26	ZVI7	0.1	0.11			2	2.01		
27	ZVI7	0.1	0.11			2	2		
28	ZVI8	0.1	0.1	0.1	0	2	2	2.01	0
29	ZVI8	0.1	0.1			2	2.01		
30	ZVI8	0.1	0.1			2	2		

Experiment 10: Non-disturbed experiments performed for 8 different ZVI+sand mixtures for 3 weeks.

Table A3.2.10b: Result

Exp.10	**22mL**	**0rpm**	**3 weeks**		
			Result		
Run	**ZVI**	**[MB] [mg/L]**	**mean [mg/L]**	**stand.dev. [mg/L]**	**result [mg/L]**
1	none	5.1	5.1	0.1	5.1±0.1
2	none	5.2			
3	none	5			
4	ZVI1	3.9	3.9	0.3	3.9±0.3
5	ZVI1	4.2			
6	ZVI1	3.6			
7	ZVI1	4.8	4.5	0.36	4.5±0.4
8	ZVI1	4.1			
9	ZVI1	4.6			
10	ZVI2	4.8	4.5	0.26	4.5±0.3
11	ZVI2	4.3			
12	ZVI2	4.4			
13	ZVI3	3.8	3.93	0.23	3.9±0.2
14	ZVI3	3.8			
15	ZVI3	4.2			
16	ZVI4	3.8	3.9	0.1	3.9±0.1
17	ZVI4	3.9			
18	ZVI4	4			
19	ZVI5	4.9	4.53	0.4	4.5±0.4
20	ZVI5	4.1			
21	ZVI5	4.6			
22	ZVI6	3.7	3.73	0.25	3.7±0.3
23	ZVI6	3.5			
24	ZVI6	4			
25	ZVI7	2.2	3.17	1.19	3.2±1.2
26	ZVI7	2.8			
27	ZVI7	4.5			
28	ZVI8	4.3	4.23	0.4	4.2±0.4
29	ZVI8	4.6			
30	ZVI8	3.8			

Experiment 11: Non-disturbed experiments performed for 8 different ZVI+MnO_2 mixtures for 3 weeks.

Table A3.2.11a: Experimental conditions

Exp.11 22mL 0rpm 3 weeks									
		ZVI				**MnO_2**			
Run	**ZVI**	**set point ZVI [g]**	**weighted ZVI [g]**	**mean [g]**	**standard dev. [g]**	**set point Sand [g]**	**weighted Sand [g]**	**mean [g]**	**standard dev. [g]**
1	none	0	0	0	0	0	0	0	0
2	none	0	0			0	0		
3	none	0	0			0	0		
4	none	0	0	0	0	0.05	0.05	0.05	0
5	none	0	0			0.05	0.05		
6	none	0	0			0.05	0.06		
7	ZVI1	0.1	0.1	0.1	0	0.05	0.06	0.05	0
8	ZVI1	0.1	0.11			0.05	0.05		
9	ZVI1	0.1	0.1			0.05	0.06		
10	ZVI2	0.1	0.1	0.1	0	0.05	0.05	0.05	0
11	ZVI2	0.1	0.1			0.05	0.05		
12	ZVI2	0.1	0.1			0.05	0.05		
13	ZVI3	0.1	0.1	0.1	0	0.05	0.06	0.05	0
14	ZVI3	0.1	0.1			0.05	0.05		
15	ZVI3	0.1	0.1			0.05	0.05		
16	ZVI4	0.1	0.1	0.1	0.01	0.05	0.06	0.05	0
17	ZVI4	0.1	0.1			0.05	0.05		
18	ZVI4	0.1	0.1			0.05	0.05		
19	ZVI5	0.1	0.1	0.1	0	0.05	0.05	0.05	0
20	ZVI5	0.1	0.1			0.05	0.05		
21	ZVI5	0.1	0.11			0.05	0.05		
22	ZVI6	0.1	0.09	0.1	0	0.05	0.06	0.05	0.01
23	ZVI6	0.1	0.1			0.05	0.05		
24	ZVI6	0.1	0.1			0.05	0.06		
25	ZVI7	0.1	0.1	0.1	0	0.05	0.05	0.05	0
26	ZVI7	0.1	0.1			0.05	0.05		
27	ZVI7	0.1	0.1			0.05	0.05		
28	ZVI8	0.1	0.1	0.1	0	0.05	0.05	0.05	0
29	ZVI8	0.1	0.1			0.05	0.05		
30	ZVI8	0.1	0.1			0.05	0.05		

Experiment 11: Non-disturbed experiments performed for 8 different ZVI+MnO_2 mixtures for 3 weeks.

Table A3.2.11b: Result

Exp.11	22mL	0rpm	3 weeks		
		Result			
Run	ZVI	[MB] [mg/L]	mean [mg/L]	stand.dev. [mg/L]	result [mg/L]
1	none	9.9	10.1	0.12	10.1±0.1
2	none	10.1			
3	none	10.1			
4	none	10.1	10	0.1	10.0±0.1
5	none	10.2			
6	none	10			
7	ZVI1	3.8	3.87	0.06	3.9±0.1
8	ZVI1	3.9			
9	ZVI1	3.9			
10	ZVI2	3.5	3.73	0.25	3.7±0.3
11	ZVI2	4			
12	ZVI2	3.7			
13	ZVI3	3.6	3.6	0.1	3.6±0.1
14	ZVI3	3.7			
15	ZVI3	3.5			
16	ZVI4	3.2	3.27	0.06	3.3±0.1
17	ZVI4	3.3			
18	ZVI4	3.3			
19	ZVI5	5.8	5.83	0.06	5.8±0.1
20	ZVI5	5.9			
21	ZVI5	5.8			
22	ZVI6	3.9	3.87	0.15	3.9±0.2
23	ZVI6	3.7			
24	ZVI6	4			
25	ZVI7	4.1	4.23	0.42	4.2±0.4
26	ZVI7	4.7			
27	ZVI7	3.9			
28	ZVI8	3.7	3.5	0.26	3.5±0.3
29	ZVI8	3.2			
30	ZVI8	3.6			

Experiment 12: Non-disturbed experiments performed for 8 different ZVI+MnO_2+sand mixtures for 3 weeks.

Table A3.2.12a: Experimental conditions

Exp.12 22mL 0rpm 3 weeks													
		ZVI				Sand				MnO_2			
Run	ZVI	set point ZVI [g]	weighted ZVI [g]	mean [g]	standard dev. [g]	set point Sand [g]	weighted Sand [g]	mean [g]	standard dev. [g]	set point Sand [g]	weighted Sand [g]	mean [g]	standard dev. [g]
1	none	0	0	0	0	0	0	0	0	0	0	0	0
2	none	0	0			0	0			0	0		
3	none	0	0			0	0			0	0		
4	none	0	0	0	0	2	2.01	2.01	0	0.05	0.05	0.05	0
5	none	0	0			2	2.01			0.05	0.05		
6	none	0	0			2	2.01			0.05	0.05		
7	ZVI1	0.1	0.1	0.1	0	2	2.01	2.01	0	0.05	0.05	0.05	0
8	ZVI1	0.1	0.1			2	2.01			0.05	0.05		
9	ZVI1	0.1	0.1			2	2.01			0.05	0.05		
10	ZVI2	0.1	0.1	0.1	0.01	2	2.01	2	0	0.05	0.05	0.05	0
11	ZVI2	0.1	0.1			2	2			0.05	0.05		
12	ZVI2	0.1	0.11			2	2.01			0.05	0.05		
13	ZVI3	0.1	0.1	0.1	0	2	2.01	2.01	0	0.05	0.05	0.05	0
14	ZVI3	0.1	0.11			2	2			0.05	0.05		
15	ZVI3	0.1	0.1			2	2.01			0.05	0.05		
16	ZVI4	0.1	0.11	0.1	0	2	2	2.01	0	0.05	0.05	0.05	0
17	ZVI4	0.1	0.11			2	2.01			0.05	0.05		
18	ZVI4	0.1	0.1			2	2.01			0.05	0.05		
19	ZVI5	0.1	0.1	0.1	0	2	2.01	2	0	0.05	0.05	0.05	0
20	ZVI5	0.1	0.11			2	2.01			0.05	0.05		
21	ZVI5	0.1	0.1			2	2			0.05	0.05		
22	ZVI6	0.1	0.11	0.1	0	2	2	2	0	0.05	0.05	0.05	0
23	ZVI6	0.1	0.1			2	2.01			0.05	0.05		
24	ZVI6	0.1	0.1			2	2			0.05	0.05		
25	ZVI7	0.1	0.1	0.1	0	2	2	2	0	0.05	0.05	0.05	0
26	ZVI7	0.1	0.1			2	2.01			0.05	0.05		
27	ZVI7	0.1	0.1			2	2.01			0.05	0.05		
28	ZVI8	0.1	0.1	0.1	0	2	2.01	2.01	0	0.05	0.05	0.05	0
29	ZVI8	0.1	0.1			2	2.01			0.05	0.05		
30	ZVI8	0.1	0.1			2	2.01			0.05	0.05		

Experiment 12: Non-disturbed experiments performed for 8 different ZVI+MnO_2+sand mixtures for 3 weeks.

Table A3.2.12b: Result

Exp.12	22mL	0rpm	3 weeks		
			Result		
Run	ZVI	[MB] [mg/L]	mean [mg/L]	stand.dev. [mg/L]	result [mg/L]
1	none	5.1	4.83	0.25	4.8±0.3
2	none	4.6			
3	none	4.8			
4	none	5.1	4.83	0.23	4.8±0.2
5	none	4.7			
6	none	4.7			
7	ZVI1	4.5	4.73	0.25	4.7±0.3
8	ZVI1	4.7			
9	ZVI1	5			
10	ZVI2	4.4	3.93	0.42	3.9±0.4
11	ZVI2	3.8			
12	ZVI2	3.6			
13	ZVI3	3.7	3.8	0.17	3.8±0.2
14	ZVI3	4			
15	ZVI3	3.7			
16	ZVI4	4.4	4.13	0.46	4.1±0.5
17	ZVI4	4.4			
18	ZVI4	3.6			
19	ZVI5	4.2	4.3	0.56	4.3±0.6
20	ZVI5	3.8			
21	ZVI5	4.9			
22	ZVI6	3.5	3.87	0.35	3.9±0.4
23	ZVI6	4.2			
24	ZVI6	3.9			
25	ZVI7	2.7	3.13	0.45	3.1±0.5
26	ZVI7	3.6			
27	ZVI7	3.1			
28	ZVI8	3.7	4.1	0.36	4.1±0.4
29	ZVI8	4.2			
30	ZVI8	4.4			

Experiment 13: Non-disturbed experiment performed for a single ZVI+sand mixture for 6 weeks.

Table A3.2.13a: Experimental conditions

Exp.13 22mL 0rpm 6 weeks									
		ZVI				**Sand**			
Run	**ZVI**	**set point ZVI [g]**	**weighted ZVI [g]**	**mean [g]**	**standard dev. [g]**	**set point Sand [g]**	**weighted Sand [g]**	**mean [g]**	**standard dev. [g]**
1	none	0	0	0	0	2	2	2	0
2	none	0	0			2	2		
3	none	0	0			2	2.01		
4	ZVI1	0.1	0.1	0.1	0	0	0	0	0
5	ZVI1	0.1	0.11			0	0		
6	ZVI1	0.1	0.1			0	0		
7	ZVI1	0.1	0.11	0.1	0	2	2.01	2.02	0.01
8	ZVI1	0.1	0.11			2	2.02		
9	ZVI1	0.1	0.1			2	2.02		
10	ZVI2	0.1	0.1	0.1	0	2	2.01	2.02	0.01
11	ZVI2	0.1	0.1			2	2.03		
12	ZVI2	0.1	0.1			2	2.02		
13	ZVI3	0.1	0.1	0.1	0,01	2	2.01	2.01	0.01
14	ZVI3	0.1	0.11			2	2.02		
15	ZVI3	0.1	0.1			2	2.01		
16	ZVI4	0.1	0.1	0.1	0	2	2.01	2.02	0.01
17	ZVI4	0.1	0.1			2	2.01		
18	ZVI4	0.1	0.1			2	2.03		
19	ZVI5	0.1	0.1	0.1	0	2	2.01	2	0
20	ZVI5	0.1	0.1			2	2		
21	ZVI5	0.1	0.1			2	2.01		
22	ZVI6	0.1	0.1	0.1	0	2	2.01	2.01	0.01
23	ZVI6	0.1	0.1			2	2.02		
24	ZVI6	0.1	0.1			2	2.01		
25	ZVI7	0.1	0.1	0.1	0.01	2	2.02	2.01	0.01
26	ZVI7	0.1	0.1			2	2.01		
27	ZVI7	0.1	0.11			2	2		
28	ZVI8	0.1	0.1	0.1	0	2	2	2.01	0
29	ZVI8	0.1	0.11			2	2.01		
30	ZVI8	0.1	0.1			2	2		

Experiment 13: Non-disturbed experiments performed for a single ZVI+Sand mixture for 6 weeks.

Table A3.2.13b: Result

Exp.13	22mL	0rpm	6 weeks		
		Result			
Run	ZVI	[MB] [mg/L]	mean [mg/L]	stand.dev. [mg/L]	result [mg/L]
1	none	2.9	2.8	0.1	2.8±0.1
2	none	2.7			
3	none	2.8			
4	ZVI1	2.9	2.9	0.3	2.9±0.3
5	ZVI1	3.2			
6	ZVI1	2.6			
7	ZVI1	3.3	2.83	0.4	2.8±0.4
8	ZVI1	2.6			
9	ZVI1	2.6			
10	ZVI2	2.8	2.43	0.32	2.4±0.3
11	ZVI2	2.3			
12	ZVI2	2.2			
13	ZVI3	2.8	2.4	0.35	2.4±0.3
14	ZVI3	2.2			
15	ZVI3	2.2			
16	ZVI4	3.4	3.03	0.35	3.0±0.4
17	ZVI4	3			
18	ZVI4	2.7			
19	ZVI5	2.9	2.7	0.2	2.7±0.2
20	ZVI5	2.5			
21	ZVI5	2.7			
22	ZVI6	3	2.87	0.23	2.9±0.2
23	ZVI6	3			
24	ZVI6	2.6			
25	ZVI7	2.5	2.57	0.31	2.6±0.3
26	ZVI7	2.3			
27	ZVI7	2.9			
28	ZVI8	2.7	2.8	0.1	2.8±0.1
29	ZVI8	2.9			
30	ZVI8	2.8			

Experiment 14: Non-disturbed experiments performed for a single ZVI+Sand+MnO_2 mixture for 6 weeks.

Table A3.2.14a: Experimental conditions

Exp.14 22mL 0rpm 6 weeks													
		ZVI				Sand				MnO_2			
Run	ZVI	set point ZVI [g]	weighted ZVI [g]	mean [g]	standard dev. [g]	set point Sand [g]	weighted Sand [g]	mean [g]	standard dev. [g]	set point Sand [g]	weighted Sand [g]	mean [g]	standard dev. [g]
1	none	0	0	0	0	0	0	0	0	0	0	0	0
2	none	0	0			0	0			0	0		
3	none	0	0			0	0			0	0		
4	none	0	0	0	0	2	2.01	2.01	0	0.05	0.05	0.05	0.01
5	none	0	0			2	2.01			0.05	0.05		
6	none	0	0			2	2.01			0.05	0.06		
7	ZVI1	0.1	0.1	0.1	0	2	2.01	2.01	0	0.05	0.06	0.05	0
8	ZVI1	0.1	0.1			2	2.01			0.05	0.05		
9	ZVI1	0.1	0.11			2	2.01			0.05	0.05		
10	ZVI2	0.1	0.1	0.1	0	2	2.01	2	0	0.05	0.05	0.05	0
11	ZVI2	0.1	0.1			2	2			0.05	0.05		
12	ZVI2	0.1	0.1			2	2.01			0.05	0.06		
13	ZVI3	0.1	0.1	0.1	0	2	2.01	2.01	0	0.05	0.05	0.05	0.01
14	ZVI3	0.1	0.11			2	2			0.05	0.06		
15	ZVI3	0.1	0.1			2	2.01			0.05	0.05		
16	ZVI4	0.1	0.1	0.1	0.01	2	2	2.01	0	0.05	0.05	0.05	0
17	ZVI4	0.1	0.1			2	2.01			0.05	0.05		
18	ZVI4	0.1	0.1			2	2.01			0.05	0.05		
19	ZVI5	0.1	0.1	0.1	0	2	2.01	2	0	0.05	0.05	0.05	0
20	ZVI5	0.1	0.1			2	2.01			0.05	0.05		
21	ZVI5	0.1	0.1			2	2			0.05	0.05		
22	ZVI6	0.1	0.09	0.1	0	2	2	2	0	0.05	0.05	0.05	0
23	ZVI6	0.1	0.1			2	2.01			0.05	0.06		
24	ZVI6	0.1	0.1			2	2			0.05	0.05		
25	ZVI7	0.1	0.11	0.1	0.01	2	2	2	0	0.05	0.05	0.05	0
26	ZVI7	0.1	0.1			2	2.01			0.05	0.05		
27	ZVI7	0.1	0.1			2	2.01			0.05	0.05		
28	ZVI8	0.1	0.11	0.1	0	2	2.01	2.01	0	0.05	0.05	0.05	0
29	ZVI8	0.1	0.1			2	2.01			0.05	0.05		
30	ZVI8	0.1	0.1			2	2.01			0.05	0.05		

Experiment 14: Non-disturbed experiments performed for a single ZVI+Sand+MnO_2 mixture for 6 weeks.

Table A3.2.14b: Result

Exp.14	**22mL**	**0rpm**	**6 weeks**		
			Result		
Run	**ZVI**	**[MB] [mg/L]**	**mean [mg/L]**	**stand.dev. [mg/L]**	**result [mg/L]**
1	none	3	2.93	0.31	2.9±0.3
2	none	2.6			
3	none	3.2			
4	none	3	2.5	0.5	2.5±0.5
5	none	2			
6	none	2.5			
7	ZVI1	2.6	2.27	0.31	2.3±0.3
8	ZVI1	2.2			
9	ZVI1	2			
10	ZVI2	2.2	2.67	0.57	2.7±0.6
11	ZVI2	3.3			
12	ZVI2	2.5			
13	ZVI3	2.2	2.33	0.23	2.3±0.2
14	ZVI3	2.2			
15	ZVI3	2.6			
16	ZVI4	2.7	2.53	0.29	2.5±0.3
17	ZVI4	2.7			
18	ZVI4	2.2			
19	ZVI5	3	2.8	0.44	2.8±0.4
20	ZVI5	3.1			
21	ZVI5	2.3			
22	ZVI6	2.6	2.23	0.32	2.2±0.3
23	ZVI6	2			
24	ZVI6	2.1			
25	ZVI7	2.5	2.37	0.12	2.4±0.1
26	ZVI7	2.3			
27	ZVI7	2.3			
28	ZVI8	2.4	1.9	0.5	1.9±0.5
29	ZVI8	1.4			
30	ZVI8	1.9			

Experiment 15: Intrinsic iron reactivity in EDTA solution for 10h, 24h, 48h, 72h and 96h.

Table A3.2.15: Result

Exp.15 22mL 0rpm EDTA													
	ZVI					Result (10h)				Result (24h)			
Run	ZVI	set point ZVI [g]	weighted ZVI [g]	mean [g]	standard dev. [g]	[Fe] [mg/L]	mean [mg/L]	stand.dev. [mg/L]	result [mg/L]	[Fe] [mg/L]	mean [mg/L]	stand.dev. [mg/L]	result [mg/L]
1	ZVI1	0.1	0.11	0	0.14	8.05	7.54	0.55	7.5±0.6	15.51	14.87	2.3	14.9±2.3
2	ZVI1	0.1	0.11			6.95				12.32			
3	ZVI1	0.1	0.11			7.6				16.79			
4	ZVI2	0.1	0.11	0.12	0.01	7.04	8.28	1.24	8.3±1.2	14.05	16.23	1.89	16.2±1.9
5	ZVI2	0.1	0.13			8.26				17.27			
6	ZVI2	0.1	0.11			9.52				17.36			
7	ZVI3	0.1	0.11	0.11	0	6.27	6.01	0.58	6.0±0.6	11.47	11.62	1.89	11.6±1.9
8	ZVI3	0.1	0.12			5.35				9.81			
9	ZVI3	0.1	0.11			6.41				13.58			
10	ZVI4	0.1	0.12	0.12	0.01	8.45	8.92	2.26	8.9±2.3	15.48	16.19	4.21	16.2±4.2
11	ZVI4	0.1	0.11			6.94				12.39			
12	ZVI4	0.1	0.13			11.38				20.71			
13	ZVI5	0.1	0.12	0.12	0.01	3.05	3.96	1.02	4.0±1.0	5.64	7.2	1.36	7.2±1.4
14	ZVI5	0.1	0.13			3.77				8.07			
15	ZVI5	0.1	0.11			5.06				7.9			
16	ZVI6	0.1	0.11	0.1	0.02	7.73	7.54	0.53	7.5±0.5	14.15	14.86	2.01	14.9±2.0
17	ZVI6	0.1	0.13			7.96				17.13			
18	ZVI6	0.1	0.12			6.95				13.31			
19	ZVI7	0.1	0.12	0.12	0	9.65	10.08	1.37	10.1±1.4	16.56	19	3.04	19.0±3.0
20	ZVI7	0.1	0.12			11.62				22.41			
21	ZVI7	0.1	0.12			8.98				18.05			
22	ZVI8	0.1	0.11	0.11	0	31.75	29.3	2.64	29.3±2.6	46.79	44.32	2.44	44.3±2.4
23	ZVI8	0.1	0.11			29.65				44.25			
24	ZVI8	0.1	0.11			26.5				41.92			
	Result (48h)					Result (72h)				Result (96h)			
Run	ZVI	[Fe] [mg/L]	mean [mg/L]	stand.dev. [mg/L]	result [mg/L]	[Fe] [mg/L]	mean [mg/L]	stand.dev. [mg/L]	result [mg/L]	[Fe] [mg/L]	mean [mg/L]	stand.dev. [mg/L]	result [mg/L]
1	ZVI1	30.02	26.55	3.04	26.5±3.0	44.9	35.15	11.21	35.2±11.2	55.9	43.01	14.71	43.0±14.7
2	ZVI1	25.2				37.66				46.13			
3	ZVI1	24.41				22.9				26.99			
4	ZVI2	26	31.79	5.64	31.8±5.6	36.23	45.82	9.42	45.8±9.4	45.41	57.2	11.28	57.2±11.3
5	ZVI2	37.26				55.07				67.9			
6	ZVI2	32.11				46.17				58.28			
7	ZVI3	21.95	23.58	2.56	23.6±2.6	30.9	33.72	4.55	33.7±4.5	40.41	44.92	7	44.9±7.0
8	ZVI3	22.25				31.29				41.37			
9	ZVI3	26.53				38.97				52.99			
10	ZVI4	28.83	30.11	6.1	30.1±6.1	39.98	43.28	8.04	43.3±8	51.28	54.71	9.36	54.7±9.4
11	ZVI4	24.75				37.42				47.55			
12	ZVI4	36.75				52.45				65.3			
13	ZVI5	12.12	15.38	2.83	15.4±2.8	17.17	19.8	2.28	19.8±2.3	22.19	26.07	3.36	26.1±3.4
14	ZVI5	16.95				21.28				27.84			
15	ZVI5	17.08				20.94				28.18			
16	ZVI6	26.59	29.22	3.18	29.2±3.2	37.46	40.55	4.37	40.5±4.4	48.39	52.81	5.44	52.8±5.4
17	ZVI6	32.76				45.55				58.88			
18	ZVI6	28.3				38.63				51.16			
19	ZVI7	32.05	36.56	5.14	36.6±5.1	46.42	50.4	5.83	50.4±5.8	59	63.01	5.02	63.0±5.0
20	ZVI7	42.16				57.09				68.63			
21	ZVI7	35.48				47.69				61.4			
22	ZVI8	63.72	62.41	1.74	62.4±1.7	70.2	71.19	1.49	71.2±1.5	77.58	78.34	0.85	78.3±0.9
23	ZVI8	63.08				72.9				79.26			
24	ZVI8	60.44				70.46				78.17			

Experiment 16: Experiment performed for the mixture Fe^0+MnO_2 (Psilomel) at shaken intensity 75 rpm for 2 weeks.

Table A3.2.16a: Experimental conditions

Exp.16 22mL 75rpm 2 weeks Psilomel								
	ZVI				MnO_2			
Run	set point ZVI [g]	weighted ZVI [g]	mean [g]	standard dev. [g]	set point Sand [g]	weighted Sand [g]	mean [g]	standard dev. [g]
1	0	0	0	0	0	0	0	0
2	0	0			0	0		
3	0	0			0	0		
4	0	0	0	0	0.25	0.26	0.25	0
5	0	0			0.21	0.25		
6	0	0			0.25	0.25		
7	0.1	0.1	0.1	0	0.03	0.02	0.03	0
8	0.1	0.1			0.03	0.03		
9	0.1	0.1			0.03	0.03		
10	0.1	0.1	0.1	0	0.05	0.05	0.05	0
11	0.1	0.1			0.05	0.05		
12	0.1	0.1			0.05	0.05		
13	0.1	0.1	0.1	0	0.08	0.08	0.07	0
14	0.1	0.1			0.08	0.07		
15	0.1	0.1			0.08	0.08		
16	0.1	0.1	0.1	0	0.1	0.1	0.1	0
17	0.1	0.1			0.1	0.1		
18	0.1	0.1			0.1	0.1		
19	0.1	0.1	0.1	0	0.13	0.13	0.13	0
20	0.1	0.1			0.13	0.13		
21	0.1	0.1			0.13	0.12		
22	0.1	0.1	0.1	0	0.15	0.16	0.15	0
23	0.1	0.1			0.15	0.15		
24	0.1	0.1			0.15	0.15		
25	0.1	0.1	0.1	0	0.2	0.2	0.2	0
26	0.1	0.1			0.2	0.2		
27	0.1	0.1			0.2	0.2		
28	0.1	0.1	0.1	0	0.25	0.25	0.25	0
29	0.1	0.1			0.25	0.25		
30	0.1	0.1			0.25	0.25		

Experiment 16: Experiment performed for the mixture Fe^0+ MnO_2 (Psilomel) at shaken intensity 75 rpm for 2 weeks.

Table A3.2.16b: Result

Exp.16	22mL	75rpm	2 weeks	Psilomel
		Result		
Run	[MB] [mg/L]	mean [mg/L]	stand.dev. [mg/L]	result [mg/L]
1	8.31	8.59	0.25	8.6±0.2
2	8.69			
3	8.77			
4	5.35	5.27	0.18	5.3±0.2
5	5.4			
6	5.06			
7	4.02	3.91	0.09	3.9±0.1
8	3.84			
9	3.87			
10	4.09	4.22	0.12	4.2±0.1
11	4.27			
12	4.31			
13	4.31	4.36	0.07	4.4±0.1
14	4.33			
15	4.43			
16	4.31	4.13	0.16	4.1±0.2
17	4.03			
18	4.04			
19	4.11	4.28	0.27	4.3±0.3
20	4.59			
21	4.14			
22	4.02	3.96	0.13	4.0±0.1
23	3.81			
24	4.04			
25	3.56	3.83	0.25	3.8±0.3
26	3.88			
27	4.05			
28	3.31	3.49	0.25	3.5±0.3
29	3.39			
30	3.8			

Experiment 17: Experiment performed for the mixture Fe^0+MnO_2 (Manganit) at shaken intensity75 rpm for 2 weeks.

Table A3.2.17a: Experimental conditions

Exp.17 22mL 75rpm 2 weeks Manganit								
	ZVI				MnO_2			
Run	set point ZVI [g]	weighted ZVI [g]	mean [g]	standard dev. [g]	set point Sand [g]	weighted Sand [g]	mean [g]	standard dev. [g]
1	0	0	0	0	0	0	0	0
2	0	0			0	0		
3	0	0			0	0		
4	0	0	0	0	0.25	0.25	0.25	0
5	0	0			0.21	0.25		
6	0	0			0.25	0.26		
7	0.1	0.1	0.1	0	0.03	0.03	0.03	0
8	0.1	0.1			0.03	0.03		
9	0.1	0.11			0.03	0.03		
10	0.1	0.1	0.1	0	0.05	0.05	0.05	0
11	0.1	0.1			0.05	0.05		
12	0.1	0.1			0.05	0.05		
13	0.1	0.11	0.4	0.52	0.08	0.07	0.08	0
14	0.1	1			0.08	0.08		
15	0.1	0.1			0.08	0.07		
16	0.1	0.1	0.1	0	0.1	0.1	0.1	0
17	0.1	0.1			0.1	0.1		
18	0.1	0.1			0.1	0.11		
19	0.1	0.1	0.1	0	0.13	0.12	0.12	0
20	0.1	0.1			0.13	0.12		
21	0.1	0.11			0.13	0.12		
22	0.1	0.1	0.1	0	0.15	0.15	0.15	0
23	0.1	0.1			0.15	0.15		
24	0.1	0.1			0.15	0.15		
25	0.1	0.11	0.1	0	0.2	0.2	0.2	0
26	0.1	0.1			0.2	0.2		
27	0.1	0.1			0.2	0.2		
28	0.1	0.1	0.1	0	0.25	0.25	0.25	0
29	0.1	0.1			0.25	0.25		
30	0.1	0.1			0.25	0.25		

Experiment 17: Experiment performed for the mixture Fe^0+ MnO_2 (Manganit) at shaken intensity 75 rpm for 2 weeks.

Table A3.2.17b: Result

Exp.17	22mL	75rpm	2 weeks	Manganit
		Result		
Run	[MB] [mg/L]	mean [mg/L]	stand.dev. [mg/L]	result [mg/L]
1	8.75	8.75	0.08	8.7±0.1
2	8.67			
3	8.83			
4	1.66	1.59	0.11	1.6±0.1
5	1.64			
6	1.46			
7	4	3.78	0.27	3.8±0.3
8	3.48			
9	3.87			
10	3.74	3.73	0.12	3.7±0.1
11	3.61			
12	3.86			
13	3.61	3.87	0.26	3.9±0.3
14	4.13			
15	3.88			
16	3.27	3.51	0.25	3.5±0.2
17	3.76			
18	3.51			
19	3.55	3.39	0.29	3.4±0.3
20	3.56			
21	3.06			
22	2.94	2.93	0.06	2.9±0.1
23	2.86			
24	2.98			
25	2.31	2.44	0.14	2.4±0.1
26	2.59			
27	2.42			
28	1.8	1.9	0.24	1.9±0.2
29	1.72			
30	2.18			

Experiment 18: Experiment performed for the mixture Fe^0+MnO_2 (X- MnO_2) at shaken intensity 75 rpm for 2 weeks.

Table A3.2.18a: Experimental conditions

Exp.18 22mL 75rpm 2 weeks d4								
	ZVI				MnO_2			
Run	set point ZVI [g]	weighted ZVI [g]	mean [g]	standard dev. [g]	set point Sand [g]	weighted Sand [g]	mean [g]	standard dev. [g]
1	0	0	0	0	0	0	0	0
2	0	0			0	0		
3	0	0			0	0		
4	0	0	0	0	0.25	0.26	0.25	0
5	0	0			0.21	0.25		
6	0	0			0.25	0.25		
7	0.1	0.1	0.1	0	0.03	0.03	0.03	0
8	0.1	0.1			0.03	0.03		
9	0.1	0.1			0.03	0.03		
10	0.1	0.1	0.1	0	0.05	0.05	0.05	0
11	0.1	0.11			0.05	0.05		
12	0.1	0.1			0.05	0.05		
13	0.1	0.1	0.1	0	0.08	0.08	0.08	0
14	0.1	0.1			0.08	0.08		
15	0.1	0.1			0.08	0.08		
16	0.1	0.1	0.1	0.01	0.1	0.1	0.1	0
17	0.1	0.1			0.1	0.1		
18	0.1	0.1			0.1	0.1		
19	0.1	0.1	0.1	0	0.13	0.13	0.13	0
20	0.1	0.1			0.13	0.13		
21	0.1	0.1			0.13	0.13		
22	0.1	0.1	0.1	0	0.15	0.15	0.15	0
23	0.1	0.1			0.15	0.15		
24	0.1	0.1			0.15	0.15		
25	0.1	0.11	0.1	0	0.2	0.2	0.2	0
26	0.1	0.1			0.2	0.21		
27	0.1	0.1			0.2	0.2		
28	0.1	0.1	0.1	0	0.25	0.25	0.25	0
29	0.1	0.1			0.25	0.25		
30	0.1	0.1			0.25	0.25		

Experiment 18: Experiment performed for the mixture Fe^0+MnO_2 (X-MnO_2) at shaken intensity 75 rpm for 2 weeks.

Table A3.2.18b: Result

Exp.17	22mL	75rpm	2 weeks	Manganit
		Result		
Run	[MB] [mg/L]	mean [mg/L]	stand.dev. [mg/L]	result [mg/L]
1	8.53	8.59	0.07	8.6±0.1
2	8.67			
3	8.58			
4	7.36	7.58	0.29	7.6±0.3
5	7.49			
6	7.9			
7	4.07	4.16	0.17	4.2±0.2
8	4.04			
9	4.36			
10	4.26	4.22	0.09	4.2±0.1
11	4.29			
12	4.12			
13	4.2	4.27	0.09	4.3±0.1
14	4.37			
15	4.24			
16	4.36	4.64	0.25	4.6±0.3
17	4.71			
18	4.85			
19	4.92	4.53	0.34	4.5±0.3
20	4.32			
21	4.35			
22	4.36	4.47	0.09	4.5±0.1
23	4.54			
24	4.5			
25	4.76	4.44	0.58	4.4±0.6
26	4.78			
27	3.77			
28	4.64	4.67	0.09	4.7±0.1
29	4.6			
30	4.77			

Appendix 4.1: Column Test

Table A4.1: Height of individual material layers

Column	Fe^0 Loading	S1	RZ	S2
	(%)	(cm)	(cm)	(cm)
1	0	44	0	0
2	10	10	34	0
3	20	11	20	13
4	30	18	15	11
5	40	19	13	12
6	50	18	11	15
7	70	15	7.5	21.5
8	80	13	6.5	24.5
9	100	13	6	25
10	100	13	13	18

Table A4.2: Overview of column test 1: total input volume of MB solution (V), time difference between two measurements (Δt), cumulative time for experimental duration (Σt), unfiltered MB concentration in output solution ([MB]) and dissolved iron concentration in output solution.

Date	time	V (mL)	Δt (h)	Σt (d)	[MB] (mg/L)	[Fe] (mg/L)
25.11.2011	16:00	0	0	0	0	0
25.11.2011	20:00	60	4	0.17	0	0
27.11.2011	07:00	450	35	1.63	0	0
28.11.2011	11:20	365	28.33	2.81	0	0
01.12.2011	00:00	750	60.67	5.33	0	0
03.12.2011	21:00	870	69	8.21	0	0
06.12.2011	09:30	750	60.5	10.73	0	0
09.12.2011	14:15	950	76.75	13.93	0	0
13.12.2011	23:35	1250	105.33	18.32	0	0
18.12.2011	19:45	1420	116.17	23.16	0	0
22.12.2011	23:00	1200	99.25	27.29	0	0
27.12.2011	19:00	1350	116	32.13	0	0
01.01.2012	20:00	1400	121	37.17	0	0
06.01.2012	10:20	1300	109.67	41.74	0	0
11.01.2012	10:30	1450	120.17	46.74	0	0
16.01.2012	09:45	1400	119.75	51.73	0	0
21.01.2012	11:00	1450	121.25	56.78	0	0
26.01.2012	12:00	1400	121	61.83	0	0
31.01.2012	12:00	1410	120	66.83	0.01	0
05.02.2012	12:00	1410	120	71.83	0.02	0
10.02.2012	13:00	1460	121	76.87	0.07	0
15.02.2012	13:10	1410	120.17	81.88	0.19	0
20.02.2012	11:30	1460	118.33	86.81	0.47	0
25.02.2012	13:00	1410	121.5	91.87	0.66	0
01.03.2012	12:00	1375	119	96.83	1.32	0
06.03.2012	12:00	1375	120	101.83	1.34	0
11.03.2012	11:00	1375	119	106.78	1.35	0
16.03.2012	10:45	1425	119.75	111.77	1.42	0
21.03.2012	12:00	1425	121.25	116.83	1.49	0
26.03.2012	12:30	1375	119.5	121.81	1.75	0
31.03.2012	13:30	1425	121	126.85	1.74	0
05.04.2012	12:30	1425	119	131.81	1.78	0

Table A4.3: Overview of column test 2: total input volume of MB solution (V), time difference between two measurements (Δt), cumulative time for experimental duration (Σt), unfiltered MB concentration in output solution ([MB]) and dissolved iron concentration in output solution.

Date	time	V (mL)	Δt (h)	Σt (d)	[MB] (mg/L)	[Fe] (mg/L)
25.11.2011	16:00	0	0	0	0	0
25.11.2011	20:00	54	4	0.17	0	1.27
27.11.2011	07:00	450	35	1.63	0	1.43
28.11.2011	11:20	365	28.33	2.81	0	1.08
01.12.2011	00:00	780	60.67	5.33	0	1.33
03.12.2011	21:00	890	69	8.21	0	1.31
06.12.2011	09:30	750	60.5	10.73	0	1.09
09.12.2011	14:15	950	76.75	13.93	0	1.83
13.12.2011	23:35	1290	105.33	18.32	0	3.94
18.12.2011	19:45	1430	116.17	23.16	0	5.43
22.12.2011	23:00	1200	99.25	27.29	0.03	7.71
27.12.2011	19:00	1400	116	32.13	0.12	7.52
01.01.2012	20:00	1400	121	37.17	0.5	0.82
06.01.2012	10:20	1300	109.67	41.74	0.78	1.59
11.01.2012	10:30	1450	120.17	46.74	0.97	1.46
16.01.2012	09:45	1400	119.75	51.73	1.06	0.21
21.01.2012	11:00	1450	121.25	56.78	1.21	0.2
26.01.2012	12:00	1400	121	61.83	1.29	0.19
31.01.2012	12:00	1460	120	66.83	1.17	0.65
05.02.2012	12:00	1410	120	71.83	1.28	0.25
10.02.2012	13:00	1460	121	76.87	1.34	0.31
15.02.2012	13:10	1410	120.17	81.88	1.34	0
20.02.2012	11:30	1460	118.33	86.81	1.46	0
25.02.2012	13:00	1410	121.5	91.87	1.46	0.2
01.03.2012	12:00	1425	119	96.83	1.5	0.02
06.03.2012	12:00	1375	120	101.83	1.41	0.07
11.03.2012	11:00	1375	119	106.78	1.43	0.06
16.03.2012	10:45	1425	119.75	111.77	1.45	0.05
21.03.2012	12:00	1425	121.25	116.83	1.49	0.02
26.03.2012	12:30	1375	119.5	121.81	1.35	0
31.03.2012	13:30	1425	121	126.85	1.61	0.01
05.04.2012	12:30	1425	119	131.81	1.5	0.01

Table 4.4: Overview of column test 3: total input volume of MB solution (V), time difference between two measurements (Δt), cumulative time for experimental duration (Σt), unfiltered MB concentration in output solution ([MB]) and dissolved iron concentration in output solution.

Date	time	V (mL)	Δt (h)	Σt (d)	[MB] (mg/L)	[Fe] (mg/L)
25.11.2011	16:00	0	0	0	0	0
25.11.2011	20:00	62	4	0.17	0	0.14
27.11.2011	07:00	450	35	1.63	0	0.01
28.11.2011	11:20	355	28.33	2.81	0	0
01.12.2011	00:00	780	60.67	5.33	0	0.01
03.12.2011	21:00	860	69	8.21	0	0
06.12.2011	09:30	750	60.5	10.73	0	0
09.12.2011	14:15	950	76.75	13.93	0	0
13.12.2011	23:35	1250	105.33	18.32	0	0.05
18.12.2011	19:45	1400	116.17	23.16	0	0.19
22.12.2011	23:00	1200	99.25	27.29	0	0.34
27.12.2011	19:00	1350	116	32.13	0.04	0.7
01.01.2012	20:00	1400	121	37.17	0.38	0.25
06.01.2012	10:20	1300	109.67	41.74	0.61	0.36
11.01.2012	10:30	1450	120.17	46.74	0.73	0.2
16.01.2012	09:45	1400	119.75	51.73	0.89	0.11
21.01.2012	11:00	1450	121.25	56.78	1.04	0.05
26.01.2012	12:00	1400	121	61.83	1.17	0.07
31.01.2012	12:00	1410	120	66.83	1.25	0.1
05.02.2012	12:00	1410	120	71.83	1.21	0.19
10.02.2012	13:00	1460	121	76.87	1.31	0.05
15.02.2012	13:10	1410	120.17	81.88	1.41	0
20.02.2012	11:30	1460	118.33	86.81	1.49	0
25.02.2012	13:00	1410	121.5	91.87	1.47	0
01.03.2012	12:00	1375	119	96.83	1.59	0.05
06.03.2012	12:00	1375	120	101.83	1.59	0.04
11.03.2012	11:00	1375	119	106.78	1.61	0.05
16.03.2012	10:45	1425	119.75	111.77	1.62	0.05
21.03.2012	12:00	1425	121.25	116.83	1.49	0.04
26.03.2012	12:30	1375	119.5	121.81	1.28	0.03
31.03.2012	13:30	1425	121	126.85	1.58	0.02
05.04.2012	12:30	1425	119	131.81	1.48	0.02

Table A4.5: Overview of column test 4: total input volume of MB solution (V), time difference between two measurements (Δt), cumulative time for experimental duration (Σt), unfiltered MB concentration in output solution ([MB]) and dissolved iron concentration in output solution.

Date	time	V (mL)	Δt (h)	Σt (d)	[MB] (mg/L)	[Fe] (mg/L)
25.11.2011	16:00	0	0	0	0	0
25.11.2011	20:00	60	4	0.17	0	0.22
27.11.2011	07:00	450	35	1.63	0	0.05
28.11.2011	11:20	355	28.33	2.81	0	0.01
01.12.2011	00:00	780	60.67	5.33	0	1.11
03.12.2011	21:00	870	69	8.21	0	0.06
06.12.2011	09:30	750	60.5	10.73	0	0.01
09.12.2011	14:15	950	76.75	13.93	0	0.03
13.12.2011	23:35	1250	105.33	18.32	0	0.25
18.12.2011	19:45	1420	116.17	23.16	0	2.19
22.12.2011	23:00	1200	99.25	27.29	0	3.69
27.12.2011	19:00	1400	116	32.13	0	2.3
01.01.2012	20:00	1400	121	37.17	0	0.47
06.01.2012	10:20	1300	109.67	41.74	0.01	0.38
11.01.2012	10:30	1450	120.17	46.74	0.22	0.57
16.01.2012	09:45	1400	119.75	51.73	0.3	0.07
21.01.2012	11:00	1450	121.25	56.78	0.59	0.99
26.01.2012	12:00	1400	121	61.83	0.84	0.12
31.01.2012	12:00	1460	120	66.83	0.94	0.1
05.02.2012	12:00	1410	120	71.83	0.95	0.25
10.02.2012	13:00	1460	121	76.87	1.13	0.28
15.02.2012	13:10	1410	120.17	81.88	1.22	0
20.02.2012	11:30	1460	118.33	86.81	1.31	0
25.02.2012	13:00	1410	121.5	91.87	1.32	0.13
01.03.2012	12:00	1425	119	96.83	1.23	0.06
06.03.2012	12:00	1425	120	101.83	0.97	0.22
11.03.2012	11:00	1425	119	106.78	1.09	0.18
16.03.2012	10:45	1425	119.75	111.77	1.2	0.12
21.03.2012	12:00	1425	121.25	116.83	1.2	0.03
26.03.2012	12:30	1375	119.5	121.81	0.92	0.02
31.03.2012	13:30	1425	121	126.85	1.2	0.02
05.04.2012	12:30	1425	119	131.81	1.22	0.06

Table A4.6: Overview of column test 5: total input volume of MB solution (V), time difference between two measurements (Δt), cumulative time for experimental duration (Σt), unfiltered MB concentration in output solution ([MB]) and dissolved iron concentration in output solution.

Date	time	V (mL)	Δt (h)	Σt (d)	[MB] (mg/L)	[Fe] (mg/L)
25.11.2011	16:00	0	0	0	0	0
25.11.2011	20:00	55	4	0.17	0	0.11
27.11.2011	07:00	440	35	1.63	0	0
28.11.2011	11:20	340	28.33	2.81	0	0
01.12.2011	00:00	750	60.67	5.33	0	0
03.12.2011	21:00	840	69	8.21	0	0
06.12.2011	09:30	730	60.5	10.73	0	0.03
09.12.2011	14:15	930	76.75	13.93	0	0.17
13.12.2011	23:35	1200	105.33	18.32	0	0.51
18.12.2011	19:45	1350	116.17	23.16	0	0.37
22.12.2011	23:00	1150	99.25	27.29	0	0.34
27.12.2011	19:00	1350	116	32.13	0	1.04
01.01.2012	20:00	1350	121	37.17	0	0.2
06.01.2012	10:20	1280	109.67	41.74	0.02	0.14
11.01.2012	10:30	1350	120.17	46.74	0.17	0.19
16.01.2012	09:45	1350	119.75	51.73	0.33	0.06
21.01.2012	11:00	1400	121.25	56.78	0.49	0.05
26.01.2012	12:00	1400	121	61.83	0.72	0.24
31.01.2012	12:00	1410	120	66.83	0.92	0.09
05.02.2012	12:00	1410	120	71.83	1.03	0.15
10.02.2012	13:00	1410	121	76.87	1.15	0.07
15.02.2012	13:10	1360	120.17	81.88	1.21	0
20.02.2012	11:30	1410	118.33	86.81	1.33	0
25.02.2012	13:00	1360	121.5	91.87	1.37	0
01.03.2012	12:00	1375	119	96.83	1.41	0.1
06.03.2012	12:00	1325	120	101.83	1.22	0.13
11.03.2012	11:00	1375	119	106.78	1.33	0.1
16.03.2012	10:45	1375	119.75	111.77	1.3	0.06
21.03.2012	12:00	1375	121.25	116.83	1.32	0.11
26.03.2012	12:30	1325	119.5	121.81	1.17	0.14
31.03.2012	13:30	1375	121	126.85	1.46	0.18
05.04.2012	12:30	1375	119	#WERT!	1.38	0.21

Table A4.7: Overview of column test 6: total input volume of MB solution (V), time difference between two measurements (Δt), cumulative time for experimental duration (Σt), unfiltered MB concentration in output solution ([MB]) and dissolved iron concentration in output solution.

Date	time	V (mL)	Δt (h)	Σt (d)	[MB] (mg/L)	[Fe] (mg/L)
25.11.2011	16:00	0	0	0	0	0
25.11.2011	20:00	54	4	0.17	0	0.04
27.11.2011	07:00	435	35	1.63	0	0
28.11.2011	11:20	350	28.33	2.81	0	0
01.12.2011	00:00	760	60.67	5.33	0	0.06
03.12.2011	21:00	850	69	8.21	0	0
06.12.2011	09:30	750	60.5	10.73	0	0
09.12.2011	14:15	930	76.75	13.93	0	0
13.12.2011	23:35	1250	105.33	18.32	0	0.02
18.12.2011	19:45	1400	116.17	23.16	0	1.51
22.12.2011	23:00	1200	99.25	27.29	0	0.65
27.12.2011	19:00	1400	116	32.13	0	1.94
01.01.2012	20:00	1400	121	37.17	0	0.32
06.01.2012	10:20	1300	109.67	41.74	0.05	0.36
11.01.2012	10:30	1450	120.17	46.74	0.24	0
16.01.2012	09:45	1400	119.75	51.73	0.52	0
21.01.2012	11:00	1450	121.25	56.78	0.74	0.03
26.01.2012	12:00	1400	121	61.83	0.96	0.13
31.01.2012	12:00	1410	120	66.83	1.02	0.06
05.02.2012	12:00	1410	120	71.83	1.09	0.14
10.02.2012	13:00	1460	121	76.87	1.23	0.11
15.02.2012	13:10	1410	120.17	81.88	1.27	0
20.02.2012	11:30	1460	118.33	86.81	1.38	0
25.02.2012	13:00	1410	121.5	91.87	1.39	0
01.03.2012	12:00	1375	119	96.83	1.36	0.1
06.03.2012	12:00	1375	120	101.83	1.24	0.11
11.03.2012	11:00	1375	119	106.78	1.3	0.07
16.03.2012	10:45	1375	119.75	111.77	1.29	0.11
21.03.2012	12:00	1425	121.25	116.83	1.3	0.11
26.03.2012	12:30	1375	119.5	121.81	1.18	0.2
31.03.2012	13:30	1425	121	126.85	1.38	0.06
05.04.2012	12:30	1425	119	131.81	1.34	0.06

Table A4.8: Overview of column test 7: total input volume of MB solution (V), time difference between two measurements (Δt), cumulative time for experimental duration (Σt), unfiltered MB concentration in output solution ([MB]) and dissolved iron concentration in output solution.

Date	time	V (mL)	Δt (h)	Σt (d)	[MB] (mg/L)	[Fe] (mg/L)
25.11.2011	16:00	0	0	0	0	0
25.11.2011	20:00	53	4	0.17	0	0.1
27.11.2011	07:00	450	35	1.63	0	0.01
28.11.2011	11:20	365	28.33	2.81	0	0.03
01.12.2011	00:00	770	60.67	5.33	0	0
03.12.2011	21:00	850	69	8.21	0	0
06.12.2011	09:30	750	60.5	10.73	0	0
09.12.2011	14:15	950	76.75	13.93	0	0
13.12.2011	23:35	1270	105.33	18.32	0	0.3
18.12.2011	19:45	1400	116.17	23.16	0	0.98
22.12.2011	23:00	1200	99.25	27.29	0	2.06
27.12.2011	19:00	1400	116	32.13	0.15	0.48
01.01.2012	20:00	1400	121	37.17	0.63	0.29
06.01.2012	10:20	1300	109.67	41.74	1.03	0.15
11.01.2012	10:30	1450	120.17	46.74	1.17	0.31
16.01.2012	09:45	1400	119.75	51.73	1.2	0.07
21.01.2012	11:00	1450	121.25	56.78	1.27	0.05
26.01.2012	12:00	1400	121	61.83	1.4	0.03
31.01.2012	12:00	1410	120	66.83	1.42	0.03
05.02.2012	12:00	1410	120	71.83	1.21	0.07
10.02.2012	13:00	1460	121	76.87	1.25	0.12
15.02.2012	13:10	1410	120.17	81.88	1.3	0
20.02.2012	11:30	1460	118.33	86.81	1.51	0
25.02.2012	13:00	1410	121.5	91.87	1.39	0
01.03.2012	12:00	1375	119	96.83	1.37	0.02
06.03.2012	12:00	1375	120	101.83	1.21	0.02
11.03.2012	11:00	1375	119	106.78	1.26	0.02
16.03.2012	10:45	1425	119.75	111.77	1.25	0.02
21.03.2012	12:00	1425	121.25	116.83	1.28	0.06
26.03.2012	12:30	1375	119.5	121.81	1.66	0.02
31.03.2012	13:30	1425	121	126.85	1.45	0.08
05.04.2012	12:30	1425	119	131.81	1.4	0.08

Table A4.9: Overview of column test 8: total input volume of MB solution (V), time difference between two measurements (Δt), cumulative time for experimental duration (Σt), unfiltered MB concentration in output solution ([MB]) and dissolved iron concentration in output solution.

Date	time	V (mL)	Δt (h)	Σt (d)	[MB] (mg/L)	[Fe] (mg/L)
25.11.2011	16:00	0	0	0	0	0
25.11.2011	20:00	38	4	0.17	0	0.04
27.11.2011	07:00	445	35	1.63	0	0.01
28.11.2011	11:20	360	28.33	2.81	0	0.01
01.12.2011	00:00	760	60.67	5.33	0	0.01
03.12.2011	21:00	850	69	8.21	0	0.02
06.12.2011	09:30	750	60.5	10.73	0	0.01
09.12.2011	14:15	930	76.75	13.93	0	0.02
13.12.2011	23:35	1250	105.33	18.32	0	0
18.12.2011	19:45	1400	116.17	23.16	0	0.02
22.12.2011	23:00	1200	99.25	27.29	0.06	0.72
27.12.2011	19:00	1400	116	32.13	0.51	0.69
01.01.2012	20:00	1400	121	37.17	0.9	0.29
06.01.2012	10:20	1300	109.67	41.74	1.25	0.21
11.01.2012	10:30	1450	120.17	46.74	1.4	0.31
16.01.2012	09:45	1400	119.75	51.73	1.38	0.05
21.01.2012	11:00	1450	121.25	56.78	1.45	0.41
26.01.2012	12:00	1400	121	61.83	1.43	0.19
31.01.2012	12:00	1410	120	66.83	1.5	0.02
05.02.2012	12:00	1410	120	71.83	1.43	0.08
10.02.2012	13:00	1460	121	76.87	1.54	0.06
15.02.2012	13:10	1410	120.17	81.88	1.58	0
20.02.2012	11:30	1460	118.33	86.81	1.69	0
25.02.2012	13:00	1410	121.5	91.87	1.65	0
01.03.2012	12:00	1375	119	96.83	1.41	0.04
06.03.2012	12:00	1375	120	101.83	1.32	0.04
11.03.2012	11:00	1375	119	106.78	1.4	0.45
16.03.2012	10:45	1375	119.75	111.77	1.38	0.73
21.03.2012	12:00	1425	121.25	116.83	1.42	0.83
26.03.2012	12:30	1375	119.5	121.81	1.26	0.73
31.03.2012	13:30	1425	121	126.85	1.36	1.09
05.04.2012	12:30	1425	119	131.81	1.09	0.02

Table A4.10: Overview of column test 9: total input volume of MB solution (V), time difference between two measurements (Δt), cumulative time for experimental duration (Σt), unfiltered MB concentration in output solution ([MB]) and dissolved iron concentration in output solution.

Date	time	V (mL)	Δt (h)	Σt (d)	[MB] (mg/L)	[Fe] (mg/L)
25.11.2011	16:00	0	0	0	0	0
25.11.2011	20:00	62	4	0.17	0	0.04
27.11.2011	07:00	455	35	1.63	0	0.01
28.11.2011	11:20	370	28.33	2.81	0	0.01
01.12.2011	00:00	780	60.67	5.33	0	0
03.12.2011	21:00	870	69	8.21	0	0.12
06.12.2011	09:30	760	60.5	10.73	0	0
09.12.2011	14:15	950	76.75	13.93	0	0
13.12.2011	23:35	1300	105.33	18.32	0	0.02
18.12.2011	19:45	1450	116.17	23.16	0	1.81
22.12.2011	23:00	1200	99.25	27.29	0	1.95
27.12.2011	19:00	1400	116	32.13	0.22	0.38
01.01.2012	20:00	1400	121	37.17	0.41	0.13
06.01.2012	10:20	1300	109.67	41.74	0.84	0.14
11.01.2012	10:30	1450	120.17	46.74	0.98	0.45
16.01.2012	09:45	1400	119.75	51.73	1.09	0.07
21.01.2012	11:00	1450	121.25	56.78	1.18	0.06
26.01.2012	12:00	1400	121	61.83	1.3	0.07
31.01.2012	12:00	1460	120	66.83	1.21	0.01
05.02.2012	12:00	1460	120	71.83	1.38	0.06
10.02.2012	13:00	1460	121	76.87	1.37	0.22
15.02.2012	13:10	1460	120.17	81.88	1.36	0
20.02.2012	11:30	1460	118.33	86.81	1.56	0
25.02.2012	13:00	1410	121.5	91.87	1.43	0
01.03.2012	12:00	1425	119	96.83	1.46	0.03
06.03.2012	12:00	1425	120	101.83	1.36	0.03
11.03.2012	11:00	1425	119	106.78	1.39	0.04
16.03.2012	10:45	1425	119.75	111.77	1.37	0.05
21.03.2012	12:00	1425	121.25	116.83	1.35	0.03
26.03.2012	12:30	1375	119.5	121.81	1.13	0.02
31.03.2012	13:30	1425	121	126.85	1.36	0.04
05.04.2012	12:30	1425	119	131.81	1.37	0.08

Table A4.11: Overview of column test 10: total input volume of MB solution (V), time difference between two measurements (Δt), cumulative time for experimental duration (Σt), unfiltered MB concentration in output solution ([MB]) and dissolved iron concentration in output solution.

Date	time	V (mL)	Δt (h)	Σt (d)	[MB] (mg/L)	[Fe] (mg/L)
25.11.2011	16:00	0	0	0	0	0
25.11.2011	20:00	55	4	0.17	0	0.04
27.11.2011	07:00	455	35	1.63	0	0.01
28.11.2011	11:20	365	28.33	2.81	0	0.04
01.12.2011	00:00	780	60.67	5.33	0	0
03.12.2011	21:00	870	69	8.21	0	0
06.12.2011	09:30	750	60.5	10.73	0	0.03
09.12.2011	14:15	950	76.75	13.93	0	0.06
13.12.2011	23:35	1300	105.33	18.32	0	0.01
18.12.2011	19:45	1400	116.17	23.16	0	0.51
22.12.2011	23:00	1200	99.25	27.29	0	0.67
27.12.2011	19:00	1400	116	32.13	0	0.17
01.01.2012	20:00	1400	121	37.17	0	0.16
06.01.2012	10:20	1300	109.67	41.74	0	0.16
11.01.2012	10:30	1450	120.17	46.74	0.02	0.54
16.01.2012	09:45	1400	119.75	51.73	0.03	0.18
21.01.2012	11:00	1450	121.25	56.78	0.21	0.06
26.01.2012	12:00	1400	121	61.83	0.55	0.05
31.01.2012	12:00	1460	120	66.83	0.73	0.13
05.02.2012	12:00	1460	120	71.83	1.2	0.08
10.02.2012	13:00	1460	121	76.87	1.18	0.17
15.02.2012	13:10	1460	120.17	81.88	1.32	0
20.02.2012	11:30	1460	118.33	86.81	1.39	0
25.02.2012	13:00	1410	121.5	91.87	1.37	0
01.03.2012	12:00	1425	119	96.83	1.06	0.06
06.03.2012	12:00	1375	120	101.83	0.87	0.07
11.03.2012	11:00	1425	119	106.78	0.82	0.08
16.03.2012	10:45	1425	119.75	111.77	0.71	0.12
21.03.2012	12:00	1425	121.25	116.83	0.89	0.06
26.03.2012	12:30	1375	119.5	121.81	0.93	0.06
31.03.2012	13:30	1425	121	126.85	1.06	0.04
05.04.2012	12:30	1425	119	131.81	1.07	0.12

Appendix 4.2: Photographic Documentations of the Column Tests

Fig.1: Visual appearance of all columns at 5th day.

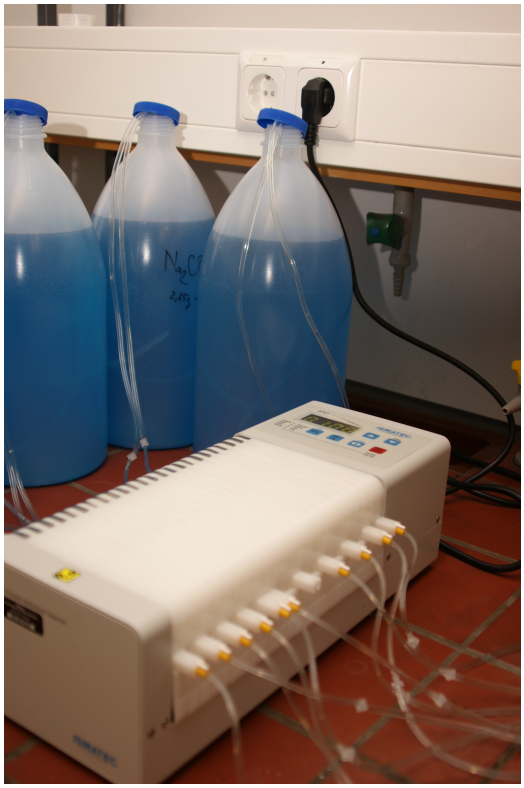

Fig.2: MB input solutions and peristaltic pump (Ismatec, ICP 24).

Fig.3: Visual appearance of all columns at 90th day.

(a) (b)

Fig.4: Differrent coloration patterns of columns at 131th day: (a) uniform coloration of sand column (column 1), (b) non- uniform coloration of Fe^0+sand columns (column6,7 and 8).

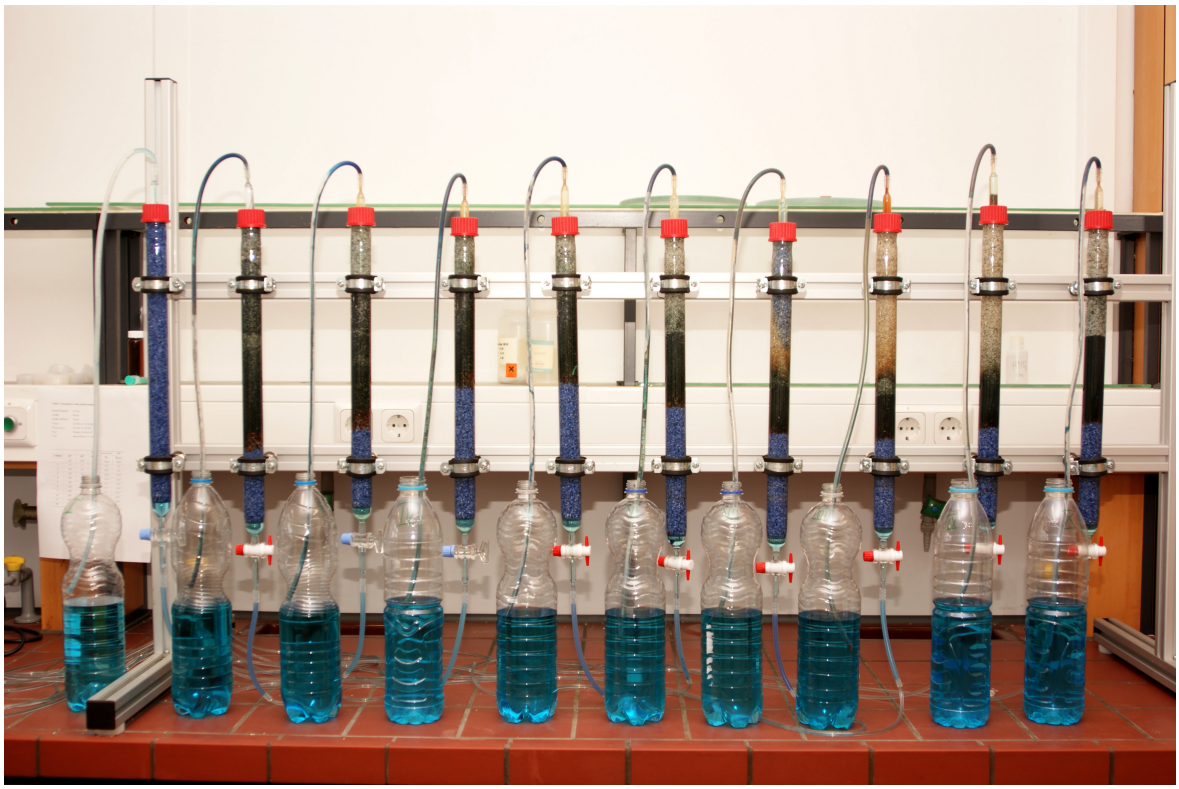

Fig.5: Visual appearance of all columns at 131th day.

Fig.6: Visual appearance of empty columns after disassembling of packed materials from columns.